RESOURCE ALLOCATION IN WIRELESS SYSTEMS WITH CONVENTIONAL AND ENERGY HARVESTING NODES

by

Imtiaz Ahmed

M.Sc. Eng., Bangladesh University of Engineering and Technology, 2008
B.Sc. Eng., Bangladesh University of Engineering and Technology, 2006

A THESIS SUBMITTED IN PARTIAL FULFILLMENT OF
THE REQUIREMENTS FOR THE DEGREE OF

DOCTOR OF PHILOSOPHY

in

The Faculty of Graduate and Postdoctoral Studies

(Electrical and Computer Engineering)

THE UNIVERSITY OF BRITISH COLUMBIA
(Vancouver)

October 2014

Abstract

High data rate, reliable communication, and low power consumption are the foremost demands for next generation of wireless communication systems. The key challenge to the design of communication systems is to combat the detrimental effects of channel fading, noise, and high power consumption. Wireless systems are often impaired by non–Gaussian noise, and the performance of systems designed for Gaussian noise can degrade if non–Gaussian noises are present but are not taken into account. Thus, it is imperative to analyze systems that are impaired by non–Gaussian noise and to manage their resources better to improve overall performance. Furthermore, there is significant interest in using renewable energy for wireless systems. However, energy harvesting (EH) is a random process and the harvested energy should be expended judiciously to maximize aggregate system throughput. In this thesis, we consider wireless systems that are impaired by Gaussian and non–Gaussian noise and powered by conventional energy sources and energy harvesters and propose appropriate resource allocation schemes for these systems.

First, we propose optimal and fair power allocation schemes for a cooperative relay network with amplify–and–forward relays that employs best and partial relay selections and is impaired by Gaussian and non–Gaussian noise. We derive closed–form expressions of asymptotic bit error rate and use this expression to allocate transmit powers for different nodes with necessary energy consumption constraints.

Second, we consider a network comprising a source, a relay, and a destination,

where the source and the relay are EH nodes. We consider conventional and buffer–aided link adaptive relaying protocols, and propose offline and online resource allocation schemes that maximize the system throughput.

Thirdly, we consider a multi–relay network with EH nodes and propose offline and online joint relay selection and power allocation schemes that maximize the system throughput.

Fourth, we consider a single source–destination link, where the source has a hybrid energy supply comprised of constant energy source and energy harvester. We propose offline and online power allocation schemes that minimize the energy consumption from the constant energy source and thereby utilize the harvested energy effectively.

Preface

The contributions in this thesis have been published in different journals and several conferences. The works in Chapters 2–5 are performed under the supervision of Prof. Robert Schober and in collaboration with Dr. Aissa Ikhlef (former post-doctoral fellow in the department of Electrical and Computer Engineering (ECE) in the University of British Columbia (UBC), Vancouver, Canada and currently with Toshiba Research Europe Limited, Bristol, UK), Dr. Amir Nasri (former post–doctoral fellow in ECE, UBC and currently with Fortinet Inc., Vancouver, Canada), Dr. Diomidis S. Michalopoulos (former post–doctoral fellow in ECE, UBC and currently with the department of ECE, University of Erlangen–Nuremberg, Germany), Dr. Derrick W. K. Ng (post–doctoral fellow in ECE, UBC and in the department of ECE, University of Erlangen-Nuremberg, Germany), and Prof. Ranjan K. Mallik (Prof. in Indian Institute of Technology (IIT), New Delhi, India). In all publications, I contributed through surveying the literature, proposing and developing the research idea, formulating and solving the problem, performing simulations, and writing the paper draft.

Two papers related to Chapter 2 have been published:

- I. Ahmed, A. Nasri, D. S. Michalopoulos, R. Schober, and R. K. Mallik, "Relay Subset Selection and Fair Power Allocation for Best and Partial Relay Selection in Generic Noise and Interference," *IEEE Trans. on Wireless Commun.*, vol. 11, pp. 1828–1839, May 2012.

- I. Ahmed, A. Nasri, D. S. Michalopoulos, R. Schober, and R. K. Mallik, "Performance Analysis and Power Allocation of AF Best Relay Selection in Generic Noise," in *Proc. of IEEE WCNC*, April 2012, Paris, France.

Two papers related to Chapter 3 have been published:

- I. Ahmed, A. Ikhlef, R. Schober, and R. K. Mallik, "Power Allocation for Conventional and Buffer-Aided Link Adaptive Relaying Systems with Energy Harvesting Nodes," *IEEE Trans. on Wireless Commun.*, vol.13, pp. 1182–1195, Mar. 2014.

- I. Ahmed, A. Ikhlef, R. Schober, and R. K. Mallik, "Power Allocation in Energy Harvesting Relay Systems," in *Proc. of IEEE VTC*, May 2012, Yokohama, Japan.

One paper related to Chapter 4 has been published:

- I. Ahmed, A. Ikhlef, R. Schober, and R. K. Mallik, "Joint Power Allocation and Relay Selection in Energy Harvesting AF Relay Systems," *IEEE Wireless Commun. Letters.*, vol. 2, pp. 239–242, Apr. 2013.

Two papers related to Chapter 5 have been published:

- I. Ahmed, A. Ikhlef, D. W. K. Ng, and R. Schober, "Power Allocation for a Hybrid Energy Harvesting Transmitter," *IEEE Trans. on Wireless Commun.*, vol. 12, pp. 6255–6267, Dec. 2013.

- I. Ahmed, A. Ikhlef, D. W. K. Ng, and R. Schober, "Optimal Power Allocation for a Hybrid Energy Harvesting Transmitter," in *Proc. of IEEE ICC*, June 2013, Hungary, Budapest.

Table of Contents

Appendices

List of Tables

List of Figures

List of Abbreviations

AF	Amplify–and–Forward
AWGN	Additive White Gaussian Noise
BER	Bit Error Rate
BICM	Bit–Interleaved Coded Modulation
BRS	Best Relay Selection
CCI	Co–Channel Interference
CLT	Central Limit Theorem
CSI	Channel State Information
DF	Decode–and–Forward
DP	Dynamic Programming
EH	Energy Harvesting
EPA	Equal Power Allocation
ESP	Equal Selection Probability
FH	Frequency Hopping
FPA	Fair Power Allocation
GGN	Generalized Gaussian Noise
GMN	Gaussian Mixture Noise
GP	Geometric Program
HR	Harvesting Rate
HSU	Harvest–Store–Use

HU	Harvest–Use
i.i.d.	Independent and Identically Distributed
i.n.d.	Independent and Non–Identically Distributed
KKT	Karush–Kuhn–Tucker
LCD	Light Emitting Diode
MGF	Moment Generating Function
MILP	Mixed Integer Linear Problem
MINLP	Mixed Integer Non–Linear Programming
NREL	National Renewable Energy Laboratory
OPA	Optimal Power Allocation
pdf	Probability Density Function
PEP	Pairwise Error Probability
PRS	Partial Relay Selection
QAM	Quadrature Amplitude Modulation
QoS	Quality of Service
RF	Radio Frequency
RFID	Radio Frequency Identification
sBB	Spatial Branch and Bound
SER	Symbol Error Rate
SNR	Signal–to–Noise Ratio
UCLA	University of California, Los Angeles
UWB	Ultra–Wide Band

Notation

$\mathcal{E}(\cdot)$	Statistical expectation
$A \doteq B$	A is asymptotically optimal to B (in the regime of high SNR unless otherwise stated)
$\Pr\{\cdot\}$	Probability of an event
$\lvert \cdot \rvert$	Absolute value of a complex number
$m_x(p)$	$2p$th order moment of x
$o(\cdot)$	Order of a function, $f(x)$ is $o(x)$ if $\lim_{x\to 0} f(x)/x = 0$
$\Gamma(\cdot)$	Gamma Function, $\Gamma(x) \triangleq \int_0^\infty e^{-t} t^{x-1} \mathrm{d}t$
$x!$	Factorial of x, $x! \triangleq 1.\ 2.\ \cdots .\ x$
$W(\cdot)$	Lambert–W function
$[x]^+$	Non–negative value of x, $[x]^+ = \max\{x, 0\}$
$\lfloor x \rfloor$	Floor operation on x, largest integer value not greater than x

Acknowledgments

First, I would like to express my invaluable gratitude to my supervisor, Prof. Robert Schober, for his relentless guidance, continuous support, high dedication, esteemed technical insights, constructive suggestions and comments, and effective advice. His energy, drive, and enthusiasm have been a great source of motivation for me since I started working with him. This thesis would have been simply impossible without him. I am extraordinarily lucky to have had the chance to work with Prof. Schober, and will be grateful forever for his support and mentorship.

I would like to thank my other supervisor, Prof. Lutz Lampe, for his overall guidance, constant support, and invaluable advice. It was very nice of him that he allowed me to join his group at the very last moment of my PhD. I am highly grateful to him, especially for his exceptional support while I was doing a MITACS internship.

I am highly grateful to Dr. Aissa Ikhlef and Dr. Derrick W. K. Ng for their constructive suggestions and advice. Special thanks go to Dr. Diomidis S. Michalopoulos, Prof. Ranjan Mallik, Dr. Ali Nezampour, and Dr. Amir Nasri for their valuable comments and suggestions. I would like to thank my friend, Shankhanaad Mallick, for his support and constructive suggestions. I am also grateful to my friends, Ghasem and Nikola and all other friends in communication lab in the department of ECE, UBC.

Last but not the least, I would like to thank my wife Sonia, my father Prof. Farruk Ahmed, my mother, my brother Imran and his family, and my in–law family

for being very patient, caring, encouraging, and believing in me during all these years. Without their love and support I would have not been the person I am.

This work was supported in part by grants from the Natural Sciences and Engineering Research Council of Canada (NSERC), the Institute for Computing, Information and Cognitive Systems (ICICS) at UBC, and TELUS.

Dedication

To My Family

Chapter 1

Introduction

Wireless communications and networking have undergone unprecedented development over the last few decades, becoming ubiquitous in a way that could hardly have been anticipated [7]. The rapid advancements of digital signal processing techniques, microprocessor technology, and radio frequency (RF) engineering have successfully placed wireless communication systems at the forefront of voice and data transmission. In general, performance evaluation of a wireless communication system is based predominantly on its achievable data rates, i.e., how many data bits can be conveyed successfully via a communication link in a given amount of time, and the bit (or symbol or packet) error rate, i.e., how many data bits are detected incorrectly at the receiver for a given number of transmitted bits. Traditionally, the error rate performance and/or throughput of wireless systems can be improved by increasing the transmit power and/or channel bandwidth. However, increased power consumption by wireless communication systems has been identified as a factor in the greenhouse effect that is known to be detrimentally impacting the environment [8]. Moreover, high transmit power creates interference that requires receivers to have increasingly complex circuitry to mitigate its impact [9]. Furthermore, the amount of channel bandwidth available for wireless communications is limited and thus cannot be exploited lavishly. A feasible response to these issues is much coveted by academics and industry leaders. Ideally, a better system design would be obtained by optimizing the available limited resources, e.g., the transmit power and the channel bandwidth.

Because of the limited resources and the nature of the systems, an efficient system design will require formulating and solving different optimization problems and, from there, proposing different resource allocation schemes. For instance, a transmit power allocation scheme in a system with a constant energy source is significantly different from a system whose available energy is a random variable. In this chapter, we will describe resource allocation schemes for wireless communication systems and provide a brief overview on different communication systems powered by both constant and random energy sources, and impaired by Gaussian and non–Gaussian noises.

Chapter 1 is organized as follows. Section 1.1 provides a brief overview of resource allocation and corresponding optimization frameworks for wireless communication systems. Gaussian and different non–Gaussian noises present in wireless communication systems are discussed in Section 1.2. Section 1.3 describes energy harvesting (EH) methods in communication systems. Section 1.4 summarizes the contributions of this thesis, while Section 1.5 describes its structure.

1.1 Resource Allocation in Wireless Communication Systems

The evolving next generation wireless communication systems are expected to overcome the fundamental challenges of existing systems and thus provide a dependable and precise quality of service (QoS) for users. This is quite a challenging task to accomplish, especially for the emerging high data rate wireless applications. As a first step, careful allocation of all available communication resources is required such that the system capacity is increased and the error rate performance is improved. Achieving certain specific goals for wireless communication systems demands that

the participating entities are managed efficiently and the communication resources are utilized effectively. One of the vital factors in improving the system throughput and operational efficiency is the development of appropriate resource allocation schemes.

1.1.1 Optimization Framework

In general, resource allocation schemes are formulated as constrained optimization problems. A typical constrained optimization problem consists of a utility function used as an objective/fitness function, a set of constraints used to confine a feasible solution set, and a set of optimization variables. The elements of an optimization problem are described in detail in the subsections that follow.

Objective Function: An objective function in an optimization problem maps the satisfaction of users into a real number and provides a tangible performance metric. Different objective functions are used in different communication systems as follows:

- In most wireless communication systems, an aggregate end–to–end system throughput is a figure of merit integral to evaluation of the system's performance [10]. Considering a single link non–cooperative communication system with channel signal–to–noise ratio (SNR) γ, bandwidth B, and transmit power P, the system throughput C is calculated by Shannon's channel capacity formula [11],

$$C = B \log_2(1 + \gamma P). \tag{1.1}$$

  In general, an ergodic capacity/system throughput is used as the objective function for an infinite horizon optimization (maximization) problem, whereas for a finite horizon problem, the system throughput aggregated over the considered

transmission time interval is adopted.

- From a green communication standpoint, it is desirable that energy sources be tapped into as little as possible to transmit a given number of data bits [12]. Therefore, optimization problems are often formulated with the aim of minimizing the energy consumption [13].

- Another important figure of merit is the average error rate or the outage probability of a system. The quality of data transmission is often evaluated based on closed–form expressions for the error rate and outage probability. Minimizing the error rate (outage probability) while limiting the use of the available resources (e.g., transmit power) improves the operational efficiency and ensures a better quality of signal reception [14].

Set of Constraints: In general, the QoS requirements are represented in an optimization problem by a set of constraints that are defined according to the physical limitations of the system. For example, there is always a maximum limit on how much power is available for the purpose of transmission. This maximum limit depends on the type of the energy source. For a constant energy source, this limit is always constant across the transmission time intervals. However, in case of a random energy source (e.g., EH node) the maximum limit on the available energy changes over time. Moreover, there is a maximum power budget for a cellular communication system, to limit the amount of interference inflicted on other users [15]. On the other hand, in power minimization problems, we generally use a constraint to satisfy the minimum data rate requirement. The minimum data rate requirement is usually imposed in the problem formulation when there is a trade–off between the objective function and the system throughput.

1.1.2 Key Features of Resource Allocation Schemes

In real–world wireless communication systems, there are several important limitations on the transmitter that might vary according to the application. One of these limitations arises from the energy source of the communication node, which is captured by the long–term or short–term power constraints in the optimization problem. A long–term power constraint can be stated as follows:

$$\lim_{K\to\infty} \frac{1}{K} \sum_{k=1}^{K} P_k \leq \bar{P}, \tag{1.2}$$

where K is the number of transmission time intervals, P_k is the transmit power in interval $k \in \{1, 2, \cdots, K\}$, and $\bar{P}$ is the available average power. This power constraint is meaningful if the node is supplied by a constant energy source or equipped with a battery that can be charged periodically at a constant rate. Furthermore, it is appropriate to use long–term utility functions if the performance is evaluated in a probabilistic manner, e.g., based on the average error rate, ergodic capacity, average outage probability, and so on. In some cases, it is relevant to derive the analytical expression of the average error probability and hence to adopt long–term utility functions and constraints, cf. [16] to optimize the system's performance.

In some practical situations, we consider short–term utility functions and constraints instead of the long–term utility functions and constraints. Batteries, for example, might not have the capacity for getting charged fully in a periodic manner. Beside, in EH systems, the incoming energy is a random variable and therefore the availability of energy supply is not guaranteed in every transmission interval. In such systems, the input power is subject to hard power constraints, i.e., the amount of energy consumed in each interval cannot exceed the amount of energy available in

the battery. In EH systems, the long–term power constraint in (1.2) cannot capture the optimal use of the harvested energy in each time interval and hence short–term power constraints are adopted as follows:

$$P_k \leq B_k, \ \forall k, \tag{1.3}$$

where P_k and B_k represent the transmit power and the available energy in the battery, respectively, in time interval $k \in \{1, 2, \cdots, K\}$. However, B_k is updated in each interval by[1]

$$B_k = B_{k-1} - P_{k-1} + H_k, \tag{1.4}$$

where H_k is the amount of energy harvested from the renewable sources. As P_k depends on both the immediate and the past energy arrivals in (1.4), optimization problems for EH communication systems cannot be formulated in probabilistic manner[2] or over a single time interval, and hence we have to formulate the optimization problem for EH systems with short–term utility function and constraints. For convenience, we denote the optimization problem with long–term utility function and constraints as "long–term optimization" and the problem with short–term utility function and constraints as "short–term optimization".

In this thesis, we consider both long–term and short–term optimization. In Chapter 2, we incorporate the effect of Gaussian and non–Gaussian noises in relay systems and formulate a long–term optimization problem with the derived analytical expression for average error rate. In Chapters 3–5, we examine EH systems and discuss

[1] We use the linear model for the battery, as is well–established in the literature [17, 18].

[2] By the term "probabilistic manner", here we refer to an optimization problem with ergodic system throughput and average power consumption constraints.

short–term optimization for them.

In general, finding resource allocation policies is more challenging for EH systems than for systems with constant energy supply because of the randomness of the arrival times and the randomness of the amounts of harvested energy. Some of the existing literature on wireless sensor networks with EH, e.g., [19, 20, 21, 22], considers long–term utility, analyzes the error rate performance, or proposes probabilistic power management and scheduling policies. In particular, a large, possibly infinite number of transmission time slots is considered, and thus the average error rate or the average throughput is calculated. This is in contrast to the contributions made in Chapters 3–5, where we optimize power allocation as well as relay and link selection policies over a finite number of time slots, which leads to more practical designs for realistic transmission scenarios. In this thesis, we consider two types of resource allocation scheme for EH systems, namely offline schemes and online schemes [17, 18].

- In offline schemes, we assume that the non–causal information regarding the channel SNR, the harvested energy, the number of incoming data bits, etc. are known a priori. We formulate a single optimization problem considering the causal and non–causal information over all the transmission time intervals, and solve the optimization problem optimally. In general, offline schemes provide useful performance upper bounds for the more practical online schemes. Moreover, these schemes can provide design insights that can help us to design an efficient online scheme.

- In practice, the amount of harvested energy, the channel SNR, and the number of incoming data bits are random in nature and cannot be predicted in advance. Therefore, in this case, online resource allocation schemes have to be employed taking into account the available information regarding the channel SNR, the

harvested energy, and the incoming data bits. In general, an optimal online resource allocation scheme is formulated by computationally intensive stochastic dynamic programming (DP) [23]. To alleviate the computational cost of the optimal online scheme, we propose suboptimal but low–complexity online schemes.

1.2 Noise in Wireless Communication Systems

Most contemporary wireless communication systems are designed with the assumption that the underlying noise is Gaussian distributed. This assumption is mainly based on the analytical tractability and simple design of communication systems in Gaussian noise and is often well justified by the central limit theorem (CLT). Nevertheless, in practice, wireless systems are also impaired by non–Gaussian noise and interference[3]. The commonly observed non–Gaussian noises are man–made impulsive noise, Gaussian mixture noise (GMN), generalized Gaussian noise (GGN), co–channel interference (CCI), and ultra–wideband (UWB) interference, cf. [24]–[30] and references therein. For example, non–Gaussian platform noise is present if wireless chips are implemented close to high–frequency central processors [31], and partial discharge and switching effects cause impulsive noise in smart grid communication systems [32]. It is acknowledged in the literature, cf. e.g. [29], that the performance of systems designed for Gaussian noise degrades alarmingly in non–Gaussian noise. Therefore, the inherent non–Gaussian noise in many wireless communication systems should be taken into account in the design process to achieve reliable performance and high data rates. However, another reason for assuming Gaussian noise in conventional system

[3]To simplify our notation, in this thesis, "noise" refers to any additive impairment of the received signal, i.e., our definition of noise also includes what is commonly referred to as "interference".

design is that the noise distribution usually changes rapidly and cannot be estimated easily. Nevertheless, it is important to investigate and study the performance of wireless communication systems in non–Gaussian noise and interference.

In general, the mathematical models for non–Gaussian noise can be divided into two broad categories, namely, noise models with exponentially–tailed probability density functions (pdfs) and with algebraically–tailed pdfs [33]. A random variable X is said to have an exponentially–tailed pdf, $f_X(x)$, if there exist $c > 0$ and $a > 0$ such that

$$\lim_{x\to\infty} \exp\left(x^a\right) f_X(x) = c. \tag{1.5}$$

Similarly, X is said to have an algebraically–tailed pdf, if there exist $c > 0$ and $a > 0$ such that

$$\lim_{x\to\infty} x^a\, f_X(x) = c. \tag{1.6}$$

It can be easily shown from (1.6) that for noises with algebraically–tailed pdfs, the nth absolute moment $M_n(X) \triangleq \mathcal{E}\left\{|X|^n\right\}$, for any $n \geq a$ does not exist, i.e., is infinity. This is in contrast to the exponentially–tailed noises for which the moments for all values of $n \geq 0$ are finite. Examples of noises with exponentially–tailed distributions include Gaussian noise, GGN, Middleton's Class A noise, GMN, and CCI. On the other hand, Middleton's Class B and Class C [25], Generalized–t [34], and α–stable noise [33, 35] are noises with algebraically–tailed pdfs. In Chapter 2, we analyze the error rate performance of a relay system that is impaired by Gaussian and non–Gaussian noise and interference. The analysis presented in Chapter 2 assumes that all noise moments are finite and hence it is applicable only in the case

of exponentially–tailed type of noises. Note that exponentially–tailed noises include the most common types of noise in communication systems and for this reason we limit our focus to them in Chapter 2. Analysis of the performance of a system impaired by the noise with algebraically–tailed pdf is beyond the scope of this thesis and is presented instead in Chapter 6 as a potential subject for future research. It is worth mentioning that few algebraically–tailed noises, e.g., underwater acoustic noise, etc. can be approximated by exponentially–tailed noise (e.g., GGN), and hence we can analyze their performance by our developed methods in Chapter 2. However, this kind of approximation and analysis show suboptimal performance, in general.

Mathematical Modeling of Gaussian and Non–Gaussian Noise: In Chapters 3–5, we use Shannon's capacity formula, which is valid for Gaussian noise and Gaussian input signals[4] to evaluate the system throughput [11]. However, Chapter 2 studies the performance for both Gaussian and different non–Gaussian noises. Therefore, we briefly review the properties of Gaussian and non–Gaussian noises in the following:

- *Gaussian noise*: As mentioned earlier, the Gaussianity property of noise is usually justified by the CLT. Other important reasons for the popularity of Gaussian noise in communication system analysis are the preservation of the distribution under linear transformations and well–developed mathematical analysis tools such as the Gaussian Q–function [36] and Turin's formula [37]. The Gaussian pdf for a scalar (complex) random variable X with zero–mean and variance σ^2 is given by

$$f_X(x) = \frac{1}{\pi\sigma^2} \exp\left(-\frac{|x|^2}{\sigma^2}\right). \tag{1.7}$$

[4]In practice, the input signals do not follow Gaussian distribution. Instead, the input signals are modulated into symbols having finite alphabet and also coded, if required. Note that the practical modulation and coding schemes can be accommodated in the Shannon's capacity formula by multiplying all transmit powers by a constant.

Note that the maximum–likelihood (ML) receiver for Gaussian noise minimizes the average Euclidean distance (ED) between the decoded symbol and the received signal. Unfortunately, the ED metric is not optimal for non–Gaussian noise [33].

- *Laplacian noise*: Laplacian noise is a non–Gaussian impulsive noise model. Generally, a noise is said to be impulsive if it is absent or possesses a low amplitude most of the time but once in a while generates high amplitude spikes, i.e., impulses. The pdf of Laplacian noise is given by

$$f_X(x) = \frac{1}{2\sigma_M} \exp\left(-\frac{|x|}{\sigma_M}\right), \tag{1.8}$$

where σ_M is a scale parameter analogous to the variance in the Gaussian pdf. It can be shown that the ML receiver in Laplacian noise applies a median filter on the received signal [33]. Note that there is no strong evidence for the existence of Laplacian noise in practical communication systems [33].

- *GGN*: A generalization of both the Gaussian and Laplacian noise models is known as GGN, which is described by the pdf

$$f_X(x) = \frac{\beta\,\Gamma(4/\beta)}{2\pi\,\sigma^2\,(\Gamma(2/\beta))^2} \exp\left(-\frac{|x|^\beta}{c}\right), \tag{1.9}$$

where $\beta > 0$ is a parameter that controls the shape of the pdf, σ^2 is the variance of the noise, $c \triangleq \left(\sigma^2 \frac{\Gamma(2/\beta)}{\Gamma(4/\beta)}\right)^{\beta/2}$, and $\Gamma(\cdot)$ represents the Gamma function [38]. Note that $\beta = 1$ and $\beta = 2$ correspond to the Laplacian and Gaussian pdfs, respectively. Fig. 1.1 shows the pdf of GGN for different values of β. It is worth mentioning that the lower the value of β, the more impulsive the noise will be.

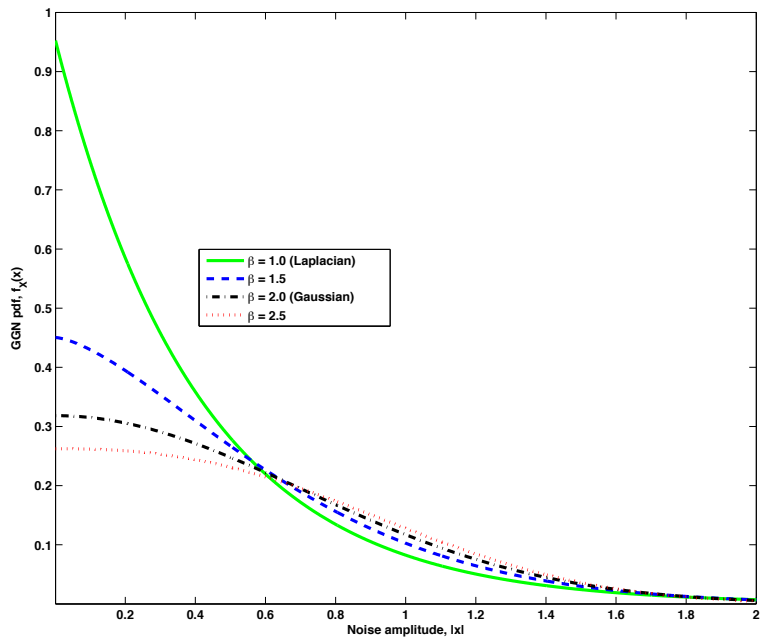

Figure 1.1: The pdf of GGN. $\sigma^2 = 1$ and different β have been considered.

- *GMN*: This model is a generalized version of Middleton's Class–A noise model [25], in which the number of interference sources is variable and their arrival time is not necessarily Poisson distributed [33]. The pdf of GMN is given by

$$f_X(x) = \sum_{i=1}^{I} \frac{c_i}{\pi\sigma_i^2} \exp\left(-\frac{|x|^2}{\sigma_i^2}\right), \tag{1.10}$$

where $c_i > 0, \sum_{i=1}^{I} c_i = 1$, and $\sigma_i^2, 1 \leq i \leq I$, are noise parameters and the total variance is given by $\sigma^2 = \sum_{i=1}^{I} c_i\sigma_i^2$. The pdf in (1.10) indicates that at any time, a specific noise state $i \in \{1, 2, \ldots, I\}$ is present with probability c_i and then a Gaussian random variable with variance σ_i^2 is generated. Therefore, conditioned on the state of the noise, GMN is Gaussian distributed. GMN is a popular model for impulsive non–Gaussian noise in systems with receive

antenna diversity [27], bit-interleaved coded modulation (BICM) [39, 40], and for partial band interference in frequency hopping (FH) systems [41], etc.

- *ϵ–mixture noise*: For $I = 2$, GMN with variance σ^2 and $c_1 = 1-\epsilon$, $c_2 = \epsilon$, $\sigma_2^2 = \kappa\sigma_1^2 = \kappa\sigma^2/(1-\epsilon+\kappa\epsilon)$ simplifies to the well–known ϵ–mixture noise. In this noise model, the pdf of the noise can be characterized by only two parameters, namely, $0 < \epsilon < 1$ and $\kappa \gg 1$. The physical interpretation of these parameters is as follows. The prevalent type of noise (i.e., the noise in $(1-\epsilon)$ fraction of time) is a Gaussian background noise with variance $\sigma_1^2 = \sigma^2/(1-\epsilon+\kappa\epsilon)$, whereas in ϵ fraction of the time (i.e., on average once every $\frac{1}{\epsilon}$ seconds), a strong Gaussian interference with variance $\sigma_2^2 = \kappa\sigma_1^2$ appears. Therefore, the smaller the value of ϵ and the larger the value of κ, the more impulsive the noise will be.

- *CCI*: One of the most common types of interference is CCI, particularly in cellular systems due to frequency re–use by different cells [42]–[43]. In fact, the capacity of cellular systems is mainly limited by CCI rather than the background noise [44]. Mathematically, CCI from a single source of interference can be expressed as

$$x = a\,z, \quad z \triangleq \sum_{k=k_l}^{k_u} g[k]\,i[k], \tag{1.11}$$

where a represents the fading gain of the channel between the interferer and the desired user and k_l, k_u, $g[k]$, and $i[k]$ denote the lower limit, the upper limit, fixed (in general complex) coefficients, and the independent, identically distributed (i.i.d.) interference symbols taken from an M_i–ary alphabet. Eq. (1.11) can be used to model multiple synchronous, a single asynchronous, or multiple asynchronous co–channel interferers. For example, for I synchronous interferers

we have $k_l = 1$, $k_u = I$, and $g[k]$ and $i[k]$ denote the gain and the transmitted symbol of the kth interferer, respectively.

Table 1.1: Examples of different EH sources and their performances; data collected from [1] and [2].

EH source	Performance
Ambient light (direct sunlight)	100mW/cm^2
Ambient light (illuminated office)	100μW/cm^2
Thermal (5 K gradient)	60μW/cm^2
Thermal (10 K gradient)	135μW/cm^2
Vibrational microgenerator (human motion)	4μW/cm^3
Vibrational microgenerator (machines)	800μW/cm^3
Ambient airflow	1mW/cm^2
Push buttons	50μJ/N
Hand generators	30W/Kg
Isotropic RF transmitter with 4W transmission (902–928 MHz)	5.5μW at 15m
TX91501 Powercast transmitter with 3W transmission (915 MHz)	189μW at 5m

1.3 Energy Harvesting in Wireless Communication Systems

In wireless communication systems, the transceiver nodes expend their energy for processing and transmitting data. For some applications, connecting the transceiver nodes to the power grid is cumbersome or may not even be possible. Pre–charged batteries can be a viable solution to this problem. In practice, the limited storage capacity of batteries and high transmit powers may result in quick drainage of the batteries. As a result, the batteries need to be replaced/recharged periodically, which can be sometimes impractical. An alternative solution is the deployment of EH nodes. EH nodes harvest energy from their surrounding environment, convert it to electrical energy, and store the electrical energy in batteries to carry out their functions. In

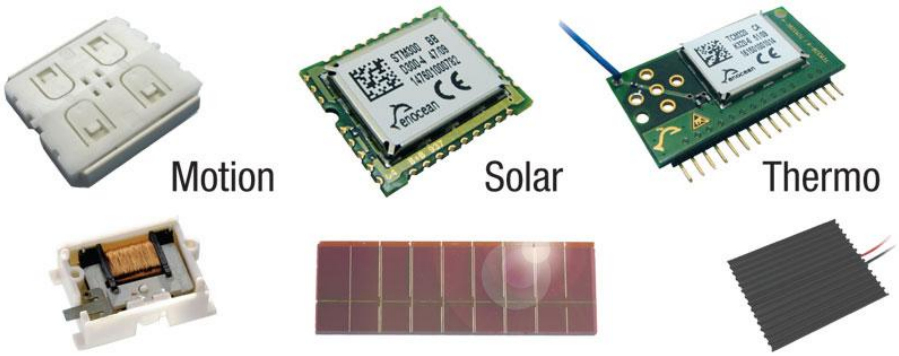

Figure 1.2: EH modules for wireless communication systems. Source: [4].

general, the energy can be harvested from unused ambient renewable energy sources using solar, thermoelectric, and motion effects, or through other physical phenomena [19]. A list of various EH sources and their performances is provided in Table 1.1.

EH nodes can be regarded as a promising option for deployment as they ensure a long system lifetime without the need for periodic battery replacements. In EH systems, the energy can be independently harvested by the transceiver nodes during the course of data transmission at random times and in random amounts. For data transmission (and for other signal processing tasks), EH nodes expend the energy from their storage and only the unused energy remains in the batteries. In particular, in each transmission time interval, the EH nodes are constrained to use, at most, only the energy available in their storage. These constraints necessitate the design of new transmission strategies for the EH nodes, to ensure optimum performance in an EH environment.

1.3.1 EH Methods

As mentioned earlier, numerous EH methods are available in practice. Among them, a few EH modules are shown in Fig. 1.2. We describe some of these methods in the

Figure 1.3: Solar EH system. Researchers at the University of California, Los Angeles (UCLA), used liquid-crystal display (LCD) screens to work as photovoltaic cells for harvesting solar energy. Source: [5].

following:

- *Solar EH systems*: Solar energy is a convenient EH source and hence there exist many implementations of solar EH nodes in the literature of sensor networks and communication systems [45, 46]. The power density of solar energy at midday is approximately 100mW/cm^2, i.e., 100mW/cm^2 of eletrical power can be harvested from the sun using polycrystalline solar cells, which have an efficiency of 16%–17%. Conversely, the power density in an indoor environment (e.g., in an illuminated office) is approximately 100μW/cm^2. Solar energy is captured in a solar cell and then converted into electrical energy by exploiting the photovoltaic effect. When the sunlight is incident upon a material surface on a solar panel, the electrons present in the material's valence band absorb energy and, being energized, jump to the conduction band of the material and become free. These highly energized, non–thermal electrons diffuse, and reach

Figure 1.4: EH roller sneaker which produces electricity from human motion. Source: [6].

a junction where they are accelerated into a different material by a built–in potential. This effect, referred to as the photovoltaic effect, generates an electromotive force, and thus some of the light energy is converted into electrical energy. In Fig. 1.3, we show the experimentation on a new technology that turns LCD screens into photovoltaic cells, which would allow laptops and smart phones to harvest solar energy while they are in use [5].

- *Thermal EH systems*: Several approaches, e.g., the Seebeck effect and the piezothermal effect, among others, are exploited to convert the thermal energy into electrical energy [47]. The efficiencies of these approaches are evaluated by Carnot's law. For example, for a thermal gradient of 5K with respect to the normal ambient temperature of 300K, the thermal EH efficiency is approximately 1.67% [1]. A commercial application of thermal EH systems is the Seiko

Thermal wristwatch, which is powered by the heat generated by the human body [47].

- *Vibrational EH systems*: Mechanical vibration is a potential EH source that occurs in human activities and industrial machinery, for example. Electricity can be generated from the vibration by many methods, e.g., piezoelectric materials, electromagnetic systems, and electrostatic systems. Piezoelectric materials exploit the ability of some materials, such as ceramics or crystals, to generate an electric potential difference between two nodes of a material in response to an implied mechanical stress. For electromagnetic converters, a coil oscillates in a static magnetic field and an electric potential is induced. In the case of electrostatic converters, electric charges on a set of flexible capacitor plates create an electric potential once the plates are moved. Prominent examples of vibrational EH sources include the vibration–based wristwatch, piezoelectric–powered radio–frequency identification (RFID) systems for shoes, and vibration–based micro–generators for intelligent sensor systems [47]. Fig. 1.4 shows an example of exploitation of the piezoelectric effect from human movement in a roller sneaker.

- *Wind EH systems*: Harvesting energy from wind is widely researched and is popular for high power application. Large wind turbine–generators are used for supplying power to remote loads, grids, and cellular base stations. According to a research conducted by the National Renewable Energy Laboratory (NREL), wind energy is considered the fastest growing electricity generation technology in the world [48]. Expanding on the continuing success of large–scale wind EH systems, attempts have been made to develop small–scale systems by considering miniatured size and high portability.

- *RF EH systems*: Recently, it has been shown in [49]–[52] that background RF electromagnetic waves from ambient transmitters are also viable sources of energy. RF electromagnetic waves ranging from 3 KHz to 300 GHz are used as a medium to carry energy. RF EH can be regarded as a far–field energy transfer technique. Therefore, the amount of energy that can be harvested depends on the transmit power, the wavelength of the RF signal, and most importantly, the distance between the RF energy source and the harvesting node. Moreover, the RF–to–DC energy conversion efficiency has a vital impact on the amount of usable harvested energy. Although the development of RF EH systems is still in its infancy, there are already a few companies that sell products for practical implementations. The Powercast transmitter, which can transmit upto 3 W in the 915 MHz band, is an example of a commercial RF source [2]. An important advantage of RF EH systems is that RF signals can carry energy and information at the same time [49, 50]. Therefore, energy–constrained nodes can harvest energy and process the information simultaneously. This simultaneous wireless information and power transfer requires a careful design of the receiver so as to extract the correct information and harvest energy successfully [53, 54]. Note that simultaneous information and power transfer is beyond the scope of this thesis and discussed in Chapter 6 as a potential future direction of research.

1.3.2 EH Architectures

Communication with the EH nodes strongly depends on the characteristics of the storage capacity of the battery. For example, the storage capacity of a base station is entirely different from the storage capacity of a small sensor node. A small sensor node may not have a battery at all, and hence can rely only on the energy har-

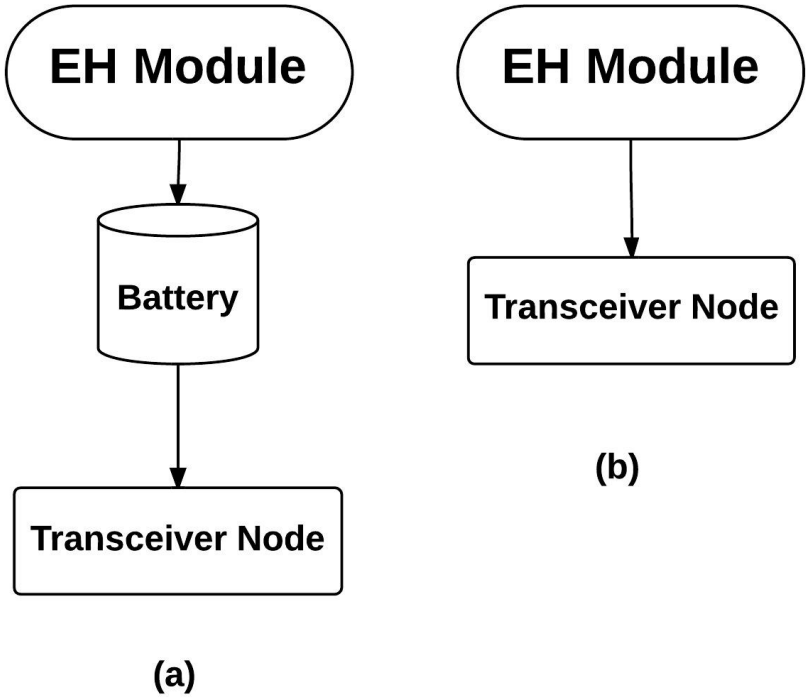

Figure 1.5: EH architectures: (a) HSU architecture and (b) HU architecture.

vested immediately before its operation [55]. On the other hand, a base station can have ample storage capacity of the battery in comparison to the sensor nodes [56]. Therefore, the resource allocation policy for EH nodes highly depends on the battery management algorithm to minimize the deleterious impact of energy outage[5]. We classify the EH architectures for wireless communications into two main categories, harvest–store–use (HSU) architecture and harvest–use (HU) architecture, as shown in Fig. 1.5.

- *HSU architecture*: In this architecture, the energy is harvested from renewable

[5]An energy outage is defined by a state when the transmitter is ready to transmit data bits, but cannot do so due to an insufficient amount of energy supply.

sources and then stored in a battery for immediate and/or future use. EH is a random process and there is no guarantee that the energy will be available in future. Therefore, depending on the size of the battery, it is better to store as much extra energy as possible and thus reduce the randomness of the energy availability. There is a large body of literature on resource allocation for EH systems using the HSU architercture [17, 18, 57, 58, 59]. However, scheduling and optimizing the available resources for an HSU architecture is more involved and strongly depends on the considered time horizon (finite or infinite). For example, the random energy arrival and management policy for EH systems forms a Markov decision process [23], and hence the optimization problem for resource allocation cannot be formulated for a single time interval. Instead, in a given time interval, we have to incorporate the dependency of the resource allocation policy on the factors of other time intervals. These considerations result in more complicated formulations of the optimization problem than the HU architecture, which is described next.

- *HU architecture*: In an HU architecture, the harvested energy is not stored and hence powers the communication nodes directly [60]. Typically, a sensor node of miniature size does not contain a battery and thus its operation relies solely on immediately–harvested energy. Examples of EH nodes with HU architecture include sensor nodes used for monitoring by bursty short message and push–button controllers [61]. The resource allocation policy for HU architecture is different from that for HSU architecture. For example, it is sufficient to formulate the optimization problem for the given time interval, and not to consider the effect of the factors of other time intervals. There are a few contributions in the literature on the design of EH systems with HU architecture, cf., [60, 62].

1.4 Contributions and Results

In this thesis, we consider resource allocation algorithm designs for different wireless communication systems with constant energy sources (Chapter 2), energy harvesters (Chapters 3 and 4), and a hybrid supply of energy (Chapter 5). A hybrid supply consists of a constant energy source and an energy harvester. The main contributions of this thesis are as follows:

1. We introduce a fair and flexible power allocation scheme for two amplify–and–forward (AF) relay selection systems, impaired by Gaussian and different non–Gaussian noises and powered by constant energy sources. The two AF relay selection schemes are denoted as best relay selection (BRS) and partial relay selection (PRS) in this thesis. To formulate the objective function for the optimization problem, we analyze the average error rate in the asymptotic regime of high SNR for the considered systems. The derived analytical results are valid for Gaussian and non–Gaussian noises with finite moments, independent and non–identically distributed (i.n.d.) Rayleigh fading, and arbitrary linear modulation schemes. Our formulated power allocation schemes ensure the fairness with energy consumption constraints, which does not affect the achievable diversity gain. In order to reduce the signaling overhead required for channel state information (CSI) acquisition, we propose a relay subset selection scheme for BRS and PRS. Simulation results confirm the accuracy of the proposed error rate analysis, and optimal power allocation (OPA) was shown to outperform competing approaches to enforce fairness in energy consumption.

2. We propose optimal resource allocation schemes for EH relay systems, where an EH source communicates with the destination via an EH decode–and–forward

(DF) relay over fading channels. We consider two relaying protocols, namely, conventional relaying and buffer–aided link adaptive relaying protocols. Our objective is to maximize the system throughput over a finite number of transmission time slots for both relaying protocols. In the case of conventional relaying, we propose optimal offline, optimal online, and several low–complexity but suboptimal online joint source and relay transmit power allocation schemes. For buffer–aided link adaptive relaying, we propose an optimal offline and efficient but suboptimal online schemes, which jointly optimize source and relay transmit powers along with the link selection. Simulation results show that buffer–aided link adaptive relaying provides significant performance gains compared to conventional relaying but requires a higher complexity for computation of the resource allocation solution.

3. We propose joint relay selection and power allocation schemes for maximization of the throughput of an AF cooperative communication system, where the source and the relays are EH nodes. We formulate an offline optimization problem which can be solved optimally by Generalized Bender's Decomposition (GBD) method. For real–time implementation with low computational cost, we propose two suboptimal online power allocation schemes. The performance of the proposed schemes is evaluated via simulations.

4. We consider a point–to–point communication link, where the transmitter has a hybrid energy supply comprised of a constant energy source and an energy harvester. We minimize the power consumed by the constant energy source for transmission of a given amount of data in a given number of time intervals. Two scenarios are considered for packet arrival. In the first scenario, we assume that all data packets have arrived before transmission begins, whereas

in the second scenario, we assume that data packets are arriving during the course of data transmission. For both scenarios, we propose optimal offline, optimal online, and low–complexity but suboptimal online transmit power allocation schemes. Simulation results reveal that the offline scheme performs best among all considered schemes and the suboptimal online scheme provides a good performance–complexity tradeoff.

1.5 Organization of the Thesis

In the following, we provide a brief overview of the remainder of this thesis:

In Chapter 2, we derive accurate high SNR approximations for the error probability and propose power allocation schemes for a cooperative network employing AF relays and BRS or PRS. Since we do not assume that the noise distributions at the various network nodes are known at the destination, BRS and PRS are performed based on the end–to–end and source–relay (relay–destination) SNRs, respectively, and the signals received via the relayed link and the direct link are combined with the additive white Gaussian noise (AWGN) ML combining rule. We formulate an OPA problem for minimization of the asymptotic error probability under energy consumption constraints to enable fair energy consumption across relays. Furthermore, to reduce the amount of instantaneous CSI required for relay selection and the associated signaling overhead, we propose to pre–select a subset of relays based on the developed error rate expressions which depend only on the average CSI.

In Chapter 3, we propose offline and online power allocation schemes for conventional and buffer–aided link adaptive EH relay systems for a three–node cooperative communication system, where the source and the relay are assumed as EH nodes. In the case of conventional relaying, we formulate a convex optimization problem for

the offline power allocation, whereas for the online case, we propose a stochastic DP approach to compute the optimal online transmit power. To alleviate the complexity inherent to DP, we also propose several suboptimal online power allocation schemes. For buffer–aided link adaptive relaying, we show that the joint offline optimization of the source and relay transmit powers along with the link selection results in a non–convex mixed integer non–linear problem (MINLP), which we solve optimally using the spatial branch–and–bound (sBB) method. However, we do not formulate an optimal online scheme by DP for buffer–aided relaying, as otherwise, the formulation would lead to a very high complexity and might not be implementable in practice.

In Chapter 4, we consider AF relay selection where the source and the relays are EH nodes and thus the optimal relay selection depends on both the channel SNR and the amount of harvested energy stored by the nodes. We propose offline and online joint relay selection and source and relay transmit power allocation schemes that maximize the end–to–end system throughput over a finite number of transmission intervals. The offline scheme results in a convex MINLP, which is solved by the GBD. However, as in Chapter 3, we do not formulate an optimal online scheme by DP, because such a formulation would lead to a very high complexity even greater than that of buffer–aided relaying for more than two relays. Instead, we formulate a suboptimal but low–complexity scheme, which exploits the statistical properties of EH and relay selection.

In Chapter 5, we consider a single communication link where the transmitter is equipped with a hybrid energy source, comprised of a constant energy source and an energy harvester. Our aim is to minimize the amount of energy drawn from the constant energy source, such that the harvested energy is efficiently utilized for transmitting a given number of data packets over a finite number of transmission

intervals. We propose optimal offline, optimal online, and low–complexity but sub-optimal online power allocation schemes for the considered system with two data arrival scenarios. The solution of the optimization problem considered in Chapter 5 provides insights regarding the optimal power allocation policy for communication systems with hybrid energy sources and thereby facilitates the design of reliable green communication systems.

Finally, Chapter 6 summarizes the contributions of this thesis and provides directions for future research.

Appendices A and B contain the proofs of error rate expressions used in Chapter 2. In Appendix C, we enlist some related contributions that were accomplished during my PhD, but are not included in this thesis.

Chapter 2

Relay Subset Selection and Fair Power Allocation for Best and Partial Relay Selection in Generic Noise and Interference

2.1 Introduction

BRS is an efficient approach to achieve full diversity in multi–relay systems [63, 64]. Synchronization requirements are relaxed and spectral efficiency is increased compared to other cooperative diversity schemes where all relays transmit concurrently [65] and sequentially over orthogonal channels [66], respectively. Thus, the analysis of BRS has received considerable attention in the literature, cf. e.g. [63, 64, 67]. However, since BRS is typically based on the instantaneous end–to–end SNR, a significant signaling overhead is required for CSI acquisition and feedback. To reduce the required amount of CSI for relay selection, PRS has been proposed. PRS uses only the CSI of the source–relay or the relay–destination channels for relay selection, which reduces the estimation and signaling overhead at the expense of a loss in diversity [68, 69]. In both BRS and PRS relays with favorable channel conditions are

selected more frequently, which drains their energy resources compared to relays with weaker channels. To overcome this problem, equal selection probability (ESP) BRS has been proposed in [3], where the end–to–end SNRs are biased such that all relays are selected with equal probability. While this approach achieves fairness in energy consumption among the relays, it may not yield high performance since relays with strong channels and relays with weak channels transmit with identical powers and for equal amounts of time.

We mentioned in Chapter 1 that practical wireless communication systems are often impaired not only by AWGN but also by non–Gaussian noise and interference. In this chapter, we derive asymptotic error probability of a cooperative network employing AF relays and BRS or PRS. The developed framework is applicable to all types of noise with finite moments and different network nodes may be impaired by different types of noise. Furthermore, we propose a relay subset selection scheme to reduce the requirement of instantaneous CSI and signaling overhead. BRS is performed for the relays in the pre–selected subset, i.e., instantaneous CSI is required only for the links of these relays.[6] In addition, we exploit the derived error rate expression and formulate an OPA problem with energy consumption constraints. It is shown that BRS/PRS with OPA achieves significant performance gains compared to BRS/PRS with ESP and equal power allocation (EPA), respectively, since different relays may transmit with different powers and for different amounts of time. However, the dependence of the energy consumption on the relay selection probability makes the resulting OPA problem non–convex and more difficult to solve than the convex OPA problem for cooperative networks with orthogonal relay channels [16, 72, 73].

The remainder of this chapter is organized as follows. In Section 2.2, the system

[6] We note that rate–maximizing relay subset selection schemes have been proposed in [70, 71] for systems impaired by AWGN. However, BRS and PRS are not considered in [70, 71] and the proposed relay subset selection schemes are not motivated by reducing the CSI estimation overhead.

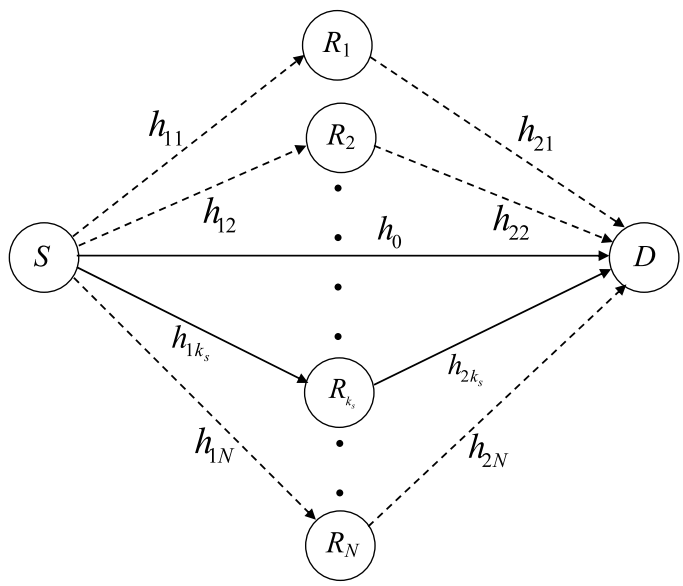

Figure 2.1: Block diagram of the considered AF relay system with BRS and PRS. Solid lines indicate the direct S–D link and the selected relay link.

model for BRS and PRS is presented. The asymptotic bit error rate (BER) and symbol error rate (SER) are analyzed in Section 2.3. In Section 2.4, the proposed schemes for relay subset selection and OPA with energy consumption constraints are developed. The effectiveness of these schemes and the accuracy of the developed analytical error rate expressions are evaluated based on computer simulations in Section 2.5. Section 2.6 concludes this chapter.

2.2 System Model

In this section, we introduce the considered signal and channel models.

Channel Model: We consider a cooperative network with one source terminal, S, N half–duplex AF relays, R_k, $k = 1, \ldots, N$, and one destination terminal, D, cf. Fig. 2.1. Transmission is organized in two phases. In the first phase, the source

transmits and the relays and the destination receive. In the second phase, one relay is selected for transmission and the destination receives. The fading gains of the S–D, S–R_k, and R_k–D links are denoted by h_0, h_{1k}, and h_{2k}, respectively. We assume independent Rayleigh fading in all links, i.e., $h_0 \triangleq a_0 e^{j\theta_0}$, $h_{1k} \triangleq a_{1k} e^{j\theta_{1k}}$, and $h_{2k} \triangleq a_{2k} e^{j\theta_{2k}}$ are independent complex Gaussian random variables with zero mean and variances $\Omega_0 \triangleq \mathcal{E}\left\{|h_0|^2\right\}$, $\Omega_{1k} \triangleq \mathcal{E}\left\{|h_{1k}|^2\right\}$, and $\Omega_{2k} \triangleq \mathcal{E}\left\{|h_{2k}|^2\right\}$, respectively, where $\mathcal{E}\{\cdot\}$ denotes statistical expectation. Here, the channel amplitudes, a_0, a_{1k}, and a_{2k} are Rayleigh distributed, whereas the channel phases, θ_0, θ_{1k}, and θ_{2k} are uniformly distributed in $[-\pi, \pi)$. The channel amplitudes are statistically independent of the channel phases.

n_0, n_{1k}, and n_{2k} denote the (possibly) non–Gaussian noise samples at the destination in the first phase of transmission, at relay k, and at the destination in the second phase of transmission, respectively. Due to the distributed nature of relay networks, the noise samples at different relays are statistically independent and not necessarily identically distributed. For the proposed analysis we require all moments of all the noises to exist. This is a mild assumption which is fulfilled by most types of noise and interference of practical interest including AWGN, GMN, GGN, CCI, and UWB interference (with α–stable noise being the only notable exception) [24].

The instantaneous SNRs of the S–D, S–R_k, and R_k–D links are given by $\gamma_0 \triangleq P_0 a_0^2/\sigma_{n_0}^2$, $\gamma_{1k} \triangleq P_0 a_{1k}^2/\sigma_{n_{1k}}^2$, and $\gamma_{2k} \triangleq P_k a_{2k}^2/\sigma_{n_{2k}}^2$, respectively, where $\sigma_{n_0}^2 \triangleq \mathcal{E}\{|n_0|^2\}$, $\sigma_{n_{1k}}^2 \triangleq \mathcal{E}\{|n_{1k}|^2\}$, $\sigma_{n_{2k}}^2 \triangleq \mathcal{E}\{|n_{2k}|^2\}$, and P_0 and P_k are the average transmit powers of the source and relay k, respectively. In this chapter, we assume that S and R_k nodes are powered by constant energy sources. The corresponding average SNRs are given by $\bar{\gamma}_0 \triangleq P_0\Omega_0/\sigma_{n_0}^2$, $\bar{\gamma}_{1k} \triangleq P_0\Omega_{1k}/\sigma_{n_{1k}}^2$, and $\bar{\gamma}_{2k} \triangleq P_k\Omega_{2k}/\sigma_{n_{2k}}^2$. For future reference, we also introduce the normalized noise samples as $\bar{n}_0 \triangleq n_0/\sigma_{n_0}$, $\bar{n}_{1k} \triangleq n_{1k}/\sigma_{n_{1k}}$, and

$\bar{n}_{2k} \triangleq n_{2k}/\sigma_{n_{2k}}$.

BRS: As customary in the literature, best relay selection is based on the maximum bottleneck link SNR, which constitutes a tight upper bound for the end–to–end SNR [63]. The selected relay, R_{k_s}, is thus determined by

$$k_s = \underset{k\in\{1,\ldots,N\}}{\arg\max}\{\min\{\gamma_{1k}, \gamma_{2k}\}\}. \tag{2.1}$$

For BRS, we assume that the destination acquires the CSI of all links (which requires CSI feedback from the source or the relays), determines the best relay according to (2.1), and feeds k_s back to the relays. Only the selected relay participates in the second phase of transmission.

PRS: In PRS, relay selection is performed either by the source, based on the source–relay SNRs or by the destination, based on the relay–destination SNRs. The best relay, R_{k_s}, is obtained as [68, 69]

$$k_s = \underset{k\in\{1,\ldots,N\}}{\arg\max}\, \gamma_{jk}, \tag{2.2}$$

where $j = 1$ and $j = 2$ if the source and the destination select the relay, respectively. We refer to these relay selection schemes as PRS–S and PRS–D, respectively. In PRS–S and PRS–D, the source and the destination can directly estimate the required CSI based on pilots sent by the relays, respectively. Thus, compared to BRS the signaling overhead is reduced.

Signal Model: The received signals at the destination in the first and second phase of transmission are given by

$$r_0 = \sqrt{P_0} h_0 x + n_0 \tag{2.3}$$

and

$$r_{k_s} = A_{k_s} h_{2k_s} u_{k_s} + n_{2k_s} = A_{k_s} \sqrt{P_0} h_{2k_s} h_{1k_s} x + \tilde{n}_{k_s}, \tag{2.4}$$

respectively, where $u_{k_s} = \sqrt{P_0} h_{1k_s} x + n_{1k_s}$ is the signal received at the selected relay, A_{k_s} is an amplification gain, and $\tilde{n}_{k_s} \triangleq A_{k_s} h_{2k_s} n_{1k_s} + n_{2k_s}$ is the effective noise. The transmitted symbol x is taken from an M–ary alphabet, $\mathcal{A}$, with $\mathcal{E}\{|x|^2\} = 1$, such as M–ary quadrature amplitude modulation (QAM) or M–ary phase–shift keying (PSK). The amplification gain is given by [74]

$$A_{k_s} = \sqrt{P_{k_s}/(P_0 a_{1k_s}^2 + b)}, \tag{2.5}$$

where $b = \sigma_{n_{1k_s}}^2$ is used for normalization of the average relay output power to P_{k_s}. Thus, for the simulation results shown in Section 2.5, $b = \sigma_{n_{1k_s}}^2$ is adopted. However, in our performance analysis in Section 2.3, $b = 0$ is assumed to make the problem tractable as is customary in the literature [74]. Using $b = 0$ instead of $b = \sigma_{n_{1k_s}}^2$ leads to a very tight performance upper bound, especially at high SNR, cf. Section 2.5.

Processing at Destination: We assume the destination does not know the distribution of the noise at the different nodes of the network, which is a realistic assumption in practice. Therefore, the destination employs L_2–norm combining [75] (which is optimal in the maximum likelihood sense for AWGN but suboptimal for non–Gaussian noise) to combine the signals received in the first and second phase of transmission, yielding

$$L(\tilde{x}) = \frac{|r_0 - \sqrt{P_0} h_0 \tilde{x}|^2}{\sigma_{n_0}^2} + \frac{|r_{k_s} - \sqrt{P_0} A_{k_s} h_{2k_s} h_{1k_s} \tilde{x}|^2}{\sigma_{\tilde{n}_{k_s}}^2}, \tag{2.6}$$

where $\tilde{x} \in \mathcal{A}$ is a trial symbol and $\sigma_{\tilde{n}_{k_s}}^2 \triangleq \sigma_{n_{2k_s}}^2 + A_{k_s}^2 a_{2k_s}^2 \sigma_{n_{1k_s}}^2$. The detected symbol,

$\hat{x} \in \mathcal{A}$, is obtained from $\hat{x} = \arg\min_{\tilde{x}\in\mathcal{A}} L(\tilde{x})$[7].

2.3 Asymptotic Error Rate Analysis

In this section, we derive the asymptotic error rate performances of BRS, PRS–S, and PRS–D in i.n.d. Rayleigh fading and generic, possibly non–Gaussian noise. We first note that for sufficiently high SNR[8], the SER and BER can be approximated by those terms of the truncated union bound which dominate at high SNR [30, 36]. For the SER and BER of the considered linear modulation schemes thus leads to

$$P_s^X \doteq \bar{\zeta} P_e^X(d_{\min}) \qquad \text{and} \qquad P_b^X \doteq \frac{\bar{\zeta}}{\log_2 M} P_e^X(d_{\min}), \tag{2.7}$$

respectively, where $A \doteq B$ means that A and B are asymptotically (i.e., for high SNR) equal, $P_e^X(d)$ denotes the asymptotic pairwise error probability (PEP) of two distinct signal points $\hat{x}, x \in \mathcal{A}$ having an Euclidean distance of $d \triangleq |e|$, $e \triangleq x - \hat{x}$, from each other, $d_{\min}$ denotes the minimum Euclidean distance of constellation $\mathcal{A}$, $\bar{\zeta}$ is the average number of minimum–distance neighbors of each element of $\mathcal{A}$. In (2.7), X is used to specify the considered relay selection scheme and $X = B$, $X = PS$, and $X = PD$ stand for BRS, PRS–S, and PRS–D, respectively.

Exploiting (2.3) and (2.6), the PEP of the considered relay selection schemes can

[7] It is worth noting that an L_p–norm detector can be used to optimally detect the signals impaired by non–Gaussian noise [24]. For this detector, a tunable parameter p is adjusted offline for different noise distributions, and hence the detector can be implemented online. However, we need to know the noise distribution beforehand to implement the L_p–norm detector. This consideration is in contrast to the assumptions made in this chapter.

[8] At what SNR values the analytical SER and BER approximations derived in this section become tight depends on the relay selection scheme, the number of relays, the type of fading, and the type of noise. Typical SNR values where our analytical results become accurate lie between 20 dB and 40 dB, cf. Section 2.5. For example, for BRS with $N = 4$ relays and independent and identically distributed Rayleigh fading, Fig. 2.2 reveals that the derived asymptotic BER expressions are tight for SNRs larger than 25 dB.

be expressed as

$$P_e^X(d) = \Pr\left\{L(\hat{x}) < L(x)\right\} = \Pr\left\{\Delta_0 + \Delta_{k_s} < 0\right\}, \tag{2.8}$$

where $\Pr\{A\}$ denotes the probability of event A, x is the transmitted symbol, and $\Delta_0 \triangleq (|\sqrt{P_0}h_0e+n_0|^2-|n_0|^2)/\sigma_{n_0}^2$ and $\Delta_{k_s} \triangleq (|\sqrt{P_0}A_{k_s}h_{2k_s}h_{1k_s}e+\tilde{n}_{k_s}|^2-|\tilde{n}_{k_s}|^2)/\sigma_{\tilde{n}_{k_s}}^2$. Furthermore, defining the moment generating functions (MGFs) of Δ_0 and Δ_{k_s} as $\Phi_{\Delta_0}(s) \triangleq \mathcal{E}_{a_0,\theta_0}\left\{e^{-s\Delta_0}\right\}$ and $\Phi_{\Delta_{k_s}}^X(s) \triangleq \mathcal{E}_{a_{k_s},\theta_{k_s}}\left\{e^{-s\Delta_{k_s}}\right\}$, respectively, (2.8) can be rewritten as

$$P_e^X(d) = \frac{1}{2\pi j}\int_{c-j\infty}^{c+j\infty} \Phi_\Delta^X(s)\,\frac{ds}{s}, \tag{2.9}$$

where $\Phi_\Delta^X(s) \triangleq \Phi_{\Delta_0}(s)\Phi_{\Delta_{k_s}}^X(s)$ and constant $c > 0$ lies in the region of convergence of the integral. Since $\Phi_{\Delta_0}(s)$ and $\Phi_{\Delta_{k_s}}^X(s)$ correspond to the direct S–D and the relayed links, respectively, the former MGF is identical for BRS and PRS, whereas the latter MGF depends on the selection scheme used. The asymptotic MGF of Δ_0 can be obtained by averaging [16, Eq. (11)] with respect to the noise

$$\Phi_{\Delta_0}(s) = \frac{1}{d^2 s\bar{\gamma}_0}\sum_{\xi=0}^{\infty}\frac{1}{\xi}s^\xi m_0(\xi) + o\left(\bar{\gamma}_0^{-1}\right), \tag{2.10}$$

where a function $f(y)$ is $o(y)$ if $\lim_{y\to 0} f(y)/y = 0$ and $m_0(\xi) \triangleq \mathcal{E}\{|\bar{n}_0|^{2\xi}\}$ denotes the 2ξ–th moment of $\bar{n}_0$. In the following subsections, we derive $\Phi_{\Delta_{k_s}}^X(s)$ and the asymptotic PEPs for the three considered relay selection schemes.

2.3.1 Asymptotic PEP of Best Relay Selection

For BRS, we show in Appendix A that the asymptotic MGF of Δ_{k_s} can be expressed as $\Phi^B_{\Delta_{k_s}}(s) =$

$$\sum_{k=1}^{N} \frac{1}{\prod\limits_{m=1,m\neq k}^{N} \left(\frac{\bar{\gamma}_{1m}\bar{\gamma}_{2m}}{\bar{\gamma}_{1m}+\bar{\gamma}_{2m}}\right)(d^2 s)^N} \sum_{\xi=0}^{\infty} \frac{(\xi+N-1)!s^{\xi}}{(\xi!)^2} \left(\frac{m_{1k}(\xi)}{\bar{\gamma}_{1k}} + \frac{m_{2k}(\xi)}{\bar{\gamma}_{2k}}\right) + o\left(\bar{\gamma}_c^{-1}\right), \quad (2.11)$$

where $m_{1k}(\xi) \triangleq \mathcal{E}\{|\bar{n}_{1k}|^{2\xi}\}$ and $m_{2k}(\xi) \triangleq \mathcal{E}\{|\bar{n}_{2k}|^{2\xi}\}$ denote the noise moments of $\bar{n}_{1k}$ and $\bar{n}_{2k}$, respectively, and $\bar{\gamma}_c \triangleq \prod_{k=1}^{N} \min\{\bar{\gamma}_{1k}, \bar{\gamma}_{2k}\}$. We note that the assumption that all noise moments exist is necessary for (2.10) and (2.11) to be valid since higher order noise terms were absorbed into the respective $o(\cdot)$ terms. Combining (2.10) and (2.11) and assuming $\bar{\gamma}_0, \bar{\gamma}_{1k}, \bar{\gamma}_{2k} \to \infty$, we obtain the asymptotic MGF

$$\Phi^B_{\Delta}(s) \doteq \sum_{k=1}^{N} \frac{1}{\prod\limits_{m=1,m\neq k}^{N} \left(\frac{\bar{\gamma}_{1m}\bar{\gamma}_{2m}}{\bar{\gamma}_{1m}+\bar{\gamma}_{2m}}\right)(d^2 s)^{N+1}\bar{\gamma}_0} \times \sum_{\xi=0}^{\infty} \sum_{i+j=\xi} \frac{s^{\xi}(i+N-1)!m_0(j)}{(i!)^2 j!} \left(\frac{m_{1k}(i)}{\bar{\gamma}_{1k}} + \frac{m_{2k}(i)}{\bar{\gamma}_{2k}}\right), \quad (2.12)$$

where $\sum\limits_{i+j=\xi}$ represents the summation over all possible combinations of non–negative integers i and j with $i+j=\xi$. Considering (2.9), the PEP, $P_e^B(d)$, is given by the sum of the residues of $\Phi^B_{\Delta}(s)/s$ in the left hand side of the complex s–plain. Using d'Alembert's convergence test [76, 0.222] it can be shown that the right hand side of (2.12) is convergent for $s \neq 0$, i.e., the only singularity of $\Phi^B_{\Delta}(s)/s$ is at $s=0$. Thus, the asymptotic PEP is given by the residue of $\Phi^B_{\Delta}(s)/s$ at $s=0$ or equivalently by the coefficient associated with s^0 in the series expansion of the right hand side of (2.12). Based on this observation, for high SNR, we only consider the term in the sum over

$i+j$ with $\xi = N+1$ in (2.12) to obtain the asymptotic PEP for BRS $P_e^B(d) \doteq$

$$\frac{1}{d^{2(N+1)}} \sum_{k=1}^{N} \sum_{i+j=N+1} \frac{(i+N-1)!m_0(j)}{(i!)^2 j! \bar{\gamma}_0 \prod_{m=1,m\neq k}^{N} \left(\frac{\bar{\gamma}_{1m}\bar{\gamma}_{2m}}{\bar{\gamma}_{1m}+\bar{\gamma}_{2m}}\right)} \left(\frac{m_{1k}(i)}{\bar{\gamma}_{1k}} + \frac{m_{2k}(i)}{\bar{\gamma}_{2k}}\right). \tag{2.13}$$

Combining (2.7) and (2.13) yields closed–form expressions for the SER and BER of AF BRS in generic, possibly non–Gaussian noise. The noise moments required in (2.13) can be found in [24, Tables I and II] for many types of noise of practical interest including AWGN, GGN, GMN, and CCI.

No S–D Link: In some applications, the direct S–D link is negligible or cannot be used. In this case, the PEP can still be obtained from (2.9) if we let $\Phi_{\Delta_0}(s) = 1$. Thus, $\Phi_{\Delta}^B(s) = \Phi_{\Delta_{k_s}}^B(s)$ holds and using a similar approach as before, we obtain for the asymptotic PEP

$$P_e^B(d) \doteq \sum_{k=1}^{N} \frac{\Gamma(2N)}{d^{2N}(\Gamma(N+1))^2 \prod_{m=1,m\neq k}^{N} \left(\frac{\bar{\gamma}_{1m}\bar{\gamma}_{2m}}{\bar{\gamma}_{1m}+\bar{\gamma}_{2m}}\right)} \left(\frac{m_{1k}(N)}{\bar{\gamma}_{1k}} + \frac{m_{2k}(N)}{\bar{\gamma}_{2k}}\right). \tag{2.14}$$

DF Relays: The asymptotic PEP of BRS with DF relays (without S–D link) in generic noise is also given by (2.14). A proof for this result can be found in [77, Appendix C] and corresponding numerical results are shown in Section 2.5.

2.3.2 Asymptotic PEP for Partial Relay Selection

We show in Appendix B that the MGF of Δ_{k_s} for PRS–S can be written as

$$\Phi_{\Delta_{k_s}}^{PS}(s) = \sum_{k=1}^{N} \sum_{\xi=0}^{\infty} \sum_{\substack{u_1=0 \\ k\neq 1}}^{1} \cdots \sum_{\substack{u_N=0 \\ k\neq N}}^{1} \frac{s^{\xi}(-1)^{\sum_{\substack{\nu=1 \\ \nu\neq k}}^{N} u_\nu}}{\xi! s d^2} \times \left(\frac{m_{1k}(\xi)}{\bar{\gamma}_{1k}} + \frac{m_{2k}(\xi)}{\bar{\gamma}_{PS}} \right) + o\left(\bar{\gamma}_{1k}^{-1}\right) + o\left(\bar{\gamma}_{PS}^{-1}\right), \quad (2.15)$$

where $\bar{\gamma}_{PS} \triangleq \bar{\gamma}_{1k}\bar{\gamma}_{2k}(1/\bar{\gamma}_{1k} + \sum_{i=1, i\neq k}^{N} u_i/\bar{\gamma}_{1i})$. For high SNR, combining (2.10) and (2.15) we obtain the asymptotic MGF of Δ for PRS–S as

$$\Phi_{\Delta}^{PS}(s) \doteq \sum_{k=1}^{N} \frac{1}{(sd^2)^2 \bar{\gamma}_0} \sum_{\xi=0}^{\infty} \sum_{i+j=\xi} \sum_{\substack{u_1=0 \\ k\neq 1}}^{1} \cdots \sum_{\substack{u_N=0 \\ k\neq N}}^{1} \frac{s^{\xi} m_0(i)}{i! j!} \times (-1)^{\sum_{\substack{\nu=1 \\ \nu\neq k}}^{N} u_\nu} \left(\frac{m_{1k}(j)}{\bar{\gamma}_{1k}} + \frac{m_{2k}(j)}{\bar{\gamma}_{PS}} \right). \quad (2.16)$$

Using again d'Alembert's convergence test [76, 0.222], it can be shown that the right hand side of (2.16) is convergent for $s \neq 0$. Thus, the asymptotic PEP can be expressed by the residue of $\Phi_{\Delta}^{PS}(s)/s$ at $s = 0$ or equivalently by the coefficient associated with s^0 in the series expansion of the right hand side of (2.16). Hence, for the asymptotic PEP, in (2.16) only the term with $\xi = 2$ is relevant and we obtain

$$P_e^{PS}(d) \doteq \frac{1}{d^4 \bar{\gamma}_0} \sum_{k=1}^{N} \sum_{i+j=2} \frac{m_0(i)}{i! j!} \sum_{\substack{u_1=0 \\ k\neq 1}}^{1} \sum_{\substack{u_2=0 \\ k\neq 2}}^{1} \cdots \sum_{\substack{u_N=0 \\ k\neq N}}^{1} (-1)^{\sum_{\substack{\nu=1 \\ \nu\neq k}}^{N} u_\nu} \times \left(\frac{m_{1k}(j)}{\bar{\gamma}_{1k}} + \frac{m_{2k}(j)}{\bar{\gamma}_{PS}} \right). \quad (2.17)$$

Combining (2.7) and (2.17) yields closed–form expressions for the SER and BER of PRS–S in generic, possibly non–Gaussian noise.

The asymptotic PEP of PRS–D, P_e^{PD}, can be obtained in a similar fashion as that of PRS–S and is given by $P_e^{PD}(d) \doteq$

$$\frac{1}{d^4\bar{\gamma}_0}\sum_{k=1}^{N}\sum_{i+j=2}\frac{m_0(i)}{i!j!}\sum_{\substack{u_1=0\\k\neq 1}}^{1}\sum_{\substack{u_2=0\\k\neq 2}}^{1}\cdots\sum_{\substack{u_N=0\\k\neq N}}^{1}(-1)^{\sum\limits_{\substack{\nu=1\\\nu\neq k}}^{N}u_\nu}\left(\frac{m_{1k}(j)}{\bar{\gamma}_{PD}}+\frac{m_{2k}(j)}{\bar{\gamma}_{2k}}\right), \tag{2.18}$$

where $\bar{\gamma}_{PD} \triangleq \bar{\gamma}_{1k}\bar{\gamma}_{2k}(1/\bar{\gamma}_{2k} + \sum\limits_{i=1,i\neq k}^{N} u_i/\bar{\gamma}_{2i})$.

Remark 1: For $N = 1$ (no selection), BRS, PRS–S, and PRS–D are equivalent and (2.13), (2.17), and (2.18) give identical results. Furthermore, for $N > 1$, all terms in (2.17) involving noise moments $m_{1k}(j)$ cancel, i.e., the asymptotic PEP of PRS–S is independent of the type of noise that impairs the relays. Similarly, for $N > 1$, all terms in (2.18) involving noise moments $m_{2k}(j)$ cancel and the asymptotic PEP of PRS–D is independent of the type of noise that impairs the destination in the second hop. In contrast, for the case $N = 1$ (no selection), the asymptotic PEPs of BRS and PRS depend on both the relay noise moments and the destination noise moments.

Remark 2: For the special case of i.i.d. Rayleigh fading in the S–R and the R–D links, respectively, i.e., $\bar{\gamma}_{1k} = \bar{\gamma}_1$ and $\bar{\gamma}_{2k} = \bar{\gamma}_2$, $1 \leq k \leq K$, for $N > 1$ the asymptotic error rate of PRS–S (PRS–D) only depends on the relay–destination SNR, $\bar{\gamma}_2$ (source–relay SNR, $\bar{\gamma}_1$), but not on the source–relay SNR, $\bar{\gamma}_1$ (relay–destination SNR, $\bar{\gamma}_2$). In contrast, for $N = 1$ (no selection), the asymptotic error rate performance of PRS depends on both $\bar{\gamma}_1$ and $\bar{\gamma}_2$. For the special case that all nodes are impaired by AWGN, similar observations have been made before in [68]. Here, we have extended this result

to non–Gaussian noise. However, we emphasize that for general i.n.d. Rayleigh fading channels (not considered in [68]), regardless of the type of noise, the error rate of PRS depends on the SNRs of all links also for $N > 1$.

2.3.3 Diversity and SNR Gain

It is convenient to express the SER (or BER) in terms of the diversity gain G_d and the SNR gain G_c, i.e., $P_s^X \doteq (G_c\bar{\gamma})^{-G_d}$, where $\bar{\gamma}_{11} = \ldots = \bar{\gamma}_{1N} = \bar{\gamma}_{21} = \ldots = \bar{\gamma}_{2N} = \bar{\gamma}_0 = \bar{\gamma}$ is assumed. Based on (2.7) and (2.13) we conclude that the diversity gain of AF BRS is given by $G_d = N + 1$, irrespective of the type of noise. In contrast, the diversity gain of both PRS–S and PRS–D is $G_d = 2$, regardless of N and the type of noise, cf. (2.7), (2.17) and (2.7), (2.18), i.e., full diversity is not achieved. On the other hand, the SNR gains of all considered relay selection schemes depend on the type of noise via the noise moments.

2.4 Optimization of BRS and PRS in Generic Noise

In this section, we exploit the asymptotic error rate expressions from the previous section for a reduction of the required signaling overhead via relay subset selection and for optimization of the transmit powers of the source and the relays under energy consumption constraints.

2.4.1 Relay Subset Selection

In systems with large numbers of relays, the overhead required for collection of the instantaneous CSI of all links may be excessive. On the other hand, acquisition of the average CSI of all links in the form of average link SNRs and noise moments at

the relays and the destination may be possible since these parameters change much more slowly with time than the instantaneous CSI (i.e., the channel gains). The main idea of relay subset selection is to pre–select K out of the N available relays based on their average CSI and noise moments. Out of these K relays one relay is then selected based on the corresponding instantaneous CSI of the involved links and the BRS criterion (2.1). The same idea can be applied to PRS.

Let us denote all possible subsets of K out of N relays by $\mathcal{S}_k$, $1 \leq k \leq N!/((N-K)!K!)$. We define the best subset for BRS, $\hat{\mathcal{S}}$, as that subset which minimizes the derived asymptotic PEP, $P_e^B(d)$, in (2.14). As mentioned before, since the average CSI changes very slowly with time, the best subset has to be updated relatively infrequently. However, the best relay within the subset is updated relatively frequently based on the instantaneous CSI and (2.1).

We note that subset selection reduces the achievable diversity order to $G_d = K+1$. However, if the average end–to–end SNRs and noise moments of the relays that are not included in the selected subset are much worse than those of the relays included in the subset, this loss in diversity will have a noticeable effect on performance only for very high SNRs, cf. Section 2.5.

2.4.2 Power Allocation with Energy Consumption Constraints

In this subsection, we impose energy consumption constraints on the relays and the source in order to limit the amount of energy consumed by each node. Throughout this section we assume that the average CSI, i.e., the link SNRs and the relevant noise moments, is known for power allocation. However, knowledge of the exact distribution of the noise is not required.

Based on the error rate expression developed in the previous section, we formulate the following optimization problem for BRS, PRS–S, and PRS–D:

$$\min_{\boldsymbol{P}\succeq 0} \quad J_X(\boldsymbol{P}) \tag{2.19}$$

$$\text{s.t.} \quad P_0 + \sum_{k=1}^{N} P_k f_k^X(\boldsymbol{P}) \leq E_T, \tag{2.20}$$

$$E_{\min,k} \leq f_k^X(\boldsymbol{P}) P_k \leq E_{\max,k}, \quad 0 \leq k \leq N, \tag{2.21}$$

where $X \in \{B, PS, PD\}$, $J_X(\boldsymbol{P})$ is the objective function which is proportional to the PEP $P_e^X(d)$, $\boldsymbol{P} \triangleq [P_0\, P_1 \ldots P_N]$, $f_0^X(\boldsymbol{P}) \triangleq 1$, $f_k^X(\boldsymbol{P})$ denotes the probability that relay k is selected, $E_{\min,k}$ and $E_{\max,k}$ denote, respectively, the normalized (to a certain interval of time) minimum and maximum energy that can be allocated to node k, and E_T denotes the normalized total available energy. The normalized energy consumed by node k is given by $f_k^X(\boldsymbol{P})P_k$.

We note that problem (2.19)–(2.21) encompasses many practical design problems. For example, in systems where the source and the relays are connected to the power grid (constant energy source), we may only restrict the total consumed energy E_T and set $E_{\min,k} = 0$ and $E_{\max,k} = \infty$, $k = 0, 1, \ldots, N$. On the other hand, for applications where the relays have their own power supply (e.g. a battery), we may select appropriate finite values for $E_{\max,k}$, $k = 0, 1, \ldots, N$, to avoid that relays with favorable channel conditions drain their energy resources prematurely. We note that (2.19)–(2.21) is more difficult to solve than related power allocation problems in [16, 72, 73] for orthogonal relay channels, since $f_k^X(\boldsymbol{P})$ is in general not a posynomial[9], and thus, (2.19) is in general not a geometric program (GP). In the following, we will

[9] A posynomial is a function $f(x_1, \cdots, x_n) = \sum_{k=1}^{N} c_k x_1^{\alpha_{1k}} \cdots x_n^{\alpha_{nk}}$, where the variables x_i and coefficients c_k are positive real numbers, and the exponents α_{ik} are real numbers [78].

specify $J_X(\boldsymbol{P})$ and $f_k^X(\boldsymbol{P})$ for the considered relay selection schemes and discuss the resulting optimization problems.

Power Allocation for BRS

Based on the asymptotic PEP in (2.13), the objective function for BRS is defined as

$$J_B(\boldsymbol{P}) \triangleq \sum_{k=1}^{N} \sum_{i+j=N+1} \frac{m_0(j)(i+N-1)!}{(i!)^2 j! P_0 \prod\limits_{m=1,m\neq k}^{N} \left(\frac{P_0\xi_{1m}P_m\xi_{2m}}{P_0\xi_{1m}+P_m\xi_{2m}}\right)} \times \left(\frac{m_{1k}(i)}{P_0\xi_{1k}} + \frac{m_{2k}(i)}{P_k\xi_{2k}}\right), \quad (2.22)$$

where $\xi_{1k} \triangleq \Omega_{1k}/\sigma_{n_{1k}}^2$ and $\xi_{2k} \triangleq \Omega_{2k}/\sigma_{n_{2k}}^2$. On the other hand, the selection probability of relay k is given by

$$f_k^B(\boldsymbol{P}) = \int_0^\infty p_{z_k}(z_k) \prod_{\substack{n=1\\n\neq k}}^{N} P_{z_n}(z_k) dz_k = \sum_{\substack{u_1=0\\k\neq 1}}^{1} \cdots \sum_{\substack{u_N=0\\k\neq N}}^{1} \frac{(-1)^{\sum\limits_{\substack{i=1\\i\neq k}}^{N} u_i} (P_0\xi_{1k} + P_k\xi_{2k})}{P_0\xi_{1k} + P_k\xi_{2k} + P_k\xi_{1k}\xi_{2k} \sum\limits_{\substack{i=1\\i\neq k}}^{N} \frac{u_i(P_0\xi_{1i}+P_i\xi_{2i})}{P_i\xi_{1i}\xi_{2i}}}, \quad (2.23)$$

where $p_{z_k}(z) = \frac{\bar{\gamma}_{1k}+\bar{\gamma}_{2k}}{\bar{\gamma}_{1k}\bar{\gamma}_{2k}} e^{-\frac{z}{\bar{\gamma}_{1k}\bar{\gamma}_{2k}/(\bar{\gamma}_{1k}+\bar{\gamma}_{2k})}}$ and $P_{z_k}(z) = 1 - e^{-\frac{z}{\bar{\gamma}_{1k}\bar{\gamma}_{2k}/(\bar{\gamma}_{1k}+\bar{\gamma}_{2k})}}$ denote the pdf and the cumulative distribution function (cdf) of random variable $z_k = \min\{\gamma_{1k}, \gamma_{2k}\}$, respectively. For any given N, $f_k^B(\boldsymbol{P})$ in (2.23) can be written as a single fraction where both the numerator and the denominator, $\lambda(\boldsymbol{P})$, are sums of positive terms. For example, for $N = 2$, we have

$$f_1^B(\boldsymbol{P}) = P_1\xi_{11}\xi_{21}\left(P_0\xi_{12} + P_2\xi_{22}\right)/\lambda(\boldsymbol{P}) \quad (2.24)$$

and

$$f_2^B(\boldsymbol{P}) = P_2\xi_{12}\xi_{22}\,(P_0\xi_{11} + P_1\xi_{21})/\lambda(\boldsymbol{P}), \tag{2.25}$$

where $\lambda(\boldsymbol{P}) \triangleq$

$$P_1\xi_{11}\xi_{21}\,(P_0\xi_{12} + P_2\xi_{22}) + P_2\xi_{12}\xi_{22}\,(P_0\xi_{11} + P_1\xi_{21}). \tag{2.26}$$

However, since $\lambda(\boldsymbol{P})$ is a sum of products of the elements of $\boldsymbol{P}$, $f_k^B(\boldsymbol{P})$ is not a posynomial and (2.22) is not a GP [78]. Thus, it is very difficult to solve (2.22) exactly. Hence, we follow the monomial fitting approach proposed in [78, Section 8] for this class of problems to find an approximate solution for (2.22) by solving a series of GPs. In particular, in the neighborhood of a given vector $\boldsymbol{P}_i \triangleq [P_{0i}\, P_{1i} \ldots P_{Ni}]$, $\lambda(\boldsymbol{P})$ can be approximated as a monomial

$$\lambda(\boldsymbol{P}) \approx c_i {P_0}^{\alpha_{0i}} {P_1}^{\alpha_{1i}} \cdots {P_N}^{\alpha_{Ni}}, \tag{2.27}$$

where the monomial parameters are given by [78]

$$\alpha_{ki} = \frac{P_{k(i)}}{\lambda(\boldsymbol{P}_i)} \frac{\partial \lambda(\boldsymbol{P}_i)}{\partial P_{ki}} \quad \text{and} \quad c_i = \frac{\lambda(\boldsymbol{P}_i)}{P_{0i}^{\alpha_{0i}} P_{1i}^{\alpha_{1i}} \cdots P_{Ni}^{\alpha_{Ni}}}, \tag{2.28}$$

where $k = 1, 2, \ldots, N$. Once we have replaced the denominator of $f_k(\boldsymbol{P})$ by the approximation in (2.27), $f_k(\boldsymbol{P})$, $J_B(\boldsymbol{P})$, and all polynomials in (2.19) are posynomials. Hence, (2.19) is a GP and can be efficiently solved using standard software [79]. This yields a new power allocation vector $\boldsymbol{P}_{i+1}$ and $\lambda(\boldsymbol{P})$ can be approximated in the neighborhood of $\boldsymbol{P}_{i+1}$ as shown in (2.27) but with i replaced by $i+1$. This leads to a new GP. This procedure is repeated until the power allocation vector $\boldsymbol{P}_i$ does not change noticeably between iterations, i.e., $||\boldsymbol{P}_{i+1} - \boldsymbol{P}_i|| < \epsilon$, where ϵ is a small

constant (e.g. $\epsilon = 10^{-4}$). For initialization, a suitable $\boldsymbol{P}_0$ which satisfies all constraints in (2.19) is chosen.

We note that for the adopted monomial fitting approach, convergence to the global optimal solution cannot be guaranteed in general [78]. However, in agreement with the findings reported in [78], we were not able to find better power allocations using a (very complex and time consuming) numerical search, which suggests that the solution obtained with the proposed iterative algorithm is close to optimal.

Power Allocation for PRS

Based on the asymptotic PEPs in (2.17) and (2.18), it is straightforward to define for PRS–S and PRS–D objective functions $J_{PS}(\boldsymbol{P}) \propto P_e^{PS}(d)$ and $J_{PD}(\boldsymbol{P}) \propto P_e^{PD}(d)$, similar to the BRS case. We omit the expressions for $J_{PS}(\boldsymbol{P})$ and $J_{PD}(\boldsymbol{P})$ because of space limitation. The selection probabilities of relay k for PRS–S and PRS–D are obtained as

$$f_k^{PS}(\boldsymbol{P}) = \int_0^\infty p_{\gamma_{1k}}(x) \prod_{i=1, i\neq k}^{N} P_{\gamma_{1i}}(x)dx = \sum_{\substack{u_1=0\\k\neq 1}}^{1} \cdots \sum_{\substack{u_N=0\\k\neq N}}^{1} \frac{(-1)^{\sum_{i=1,i\neq k}^{N} u_i}}{1 + \sum_{i=1,i\neq k}^{N} \frac{u_i \xi_{1k}}{\xi_{1i}}} \tag{2.29}$$

and

$$f_k^{PD}(\boldsymbol{P}) = \int_0^\infty p_{\gamma_{2k}}(x) \prod_{i=1, i\neq k}^{N} P_{\gamma_{2i}}(x)dx \sum_{\substack{u_1=0\\k\neq 1}}^{1} \cdots \sum_{\substack{u_N=0\\k\neq N}}^{1} \frac{(-1)^{\sum_{i=1,i\neq k}^{N} u_i}}{1 + \sum_{i=1,i\neq k}^{N} \frac{u_i P_k \xi_{2k}}{P_i \xi_{2i}}}, \tag{2.30}$$

respectively, where $p_{\gamma_{jk}}(x)$ and $P_{\gamma_{jk}}(x)$ denote the pdf and cdf of γ_{jk}, $j = \{1, 2\}$, $1 \leq k \leq N$, respectively. Since for PRS–S the source–relay SNRs determine which relay is selected, $f_k^{PS}(\boldsymbol{P})$ is independent of P_i, $i \in \{0, 1, \cdots, N\}$. Furthermore,

$J_{PS}(\boldsymbol{P})$ is a posynomial. Therefore, for PRS–S the power optimization problem in (2.19) is a GP and can be solved exactly. In contrast, for PRS–D, neither $f_k^{PD}(\boldsymbol{P})$ nor $J_{PD}(\boldsymbol{P})$ are posynomials. Thus, for PRS–D, the resulting power optimization problem in (2.19) has to be solved using a monomial fitting approach similar to the one used for BRS.

2.5 Numerical Results

In this section, we verify the analytical results derived in Section 2.3 with simulations. The asymptotic results shown in Figs. 2.2–2.6 were obtained by combining (2.7) with (2.13), (2.17), and (2.18). The considered noise models include ϵ–noise with parameters $\epsilon = 0.25$ and $\kappa = 50$ (ϵ and κ denote the fraction of time where the impulsive component is present and the ratio of the variances of the impulsive and the Gaussian components, respectively), GGN with parameter $\beta = 1$ (i.e., Laplacian noise), unfaded and Ricean (Ricean factor two) faded synchronous CCI, and AWGN. More details about the adopted noise models can be found in [24].

In Fig. 2.2, we show the BER of AF BRS for 4–PSK and $N = 4$ relays. I.i.d. Rayleigh fading is assumed, i.e., the average SNR in all links is $\bar{\gamma}$. Three different noise scenarios are considered, cf. caption of figure. For all three noise scenarios, the derived asymptotic error rate expressions accurately predict the performance for sufficiently high SNR. Furthermore, as expected from Section 2.3, for all noise scenarios, BRS yields the maximum diversity gain of $G_d = N + 1 = 5$. However, since the SNR gain is noise dependent, the BER curves have different SNR offsets for the different scenarios. For the considered example, Scenario 1, where all nodes are impaired by AWGN, yields the best performance since for the other two scenarios at least one node is affected by impulsive ϵ–mixture noise which has a negative effect on performance. For

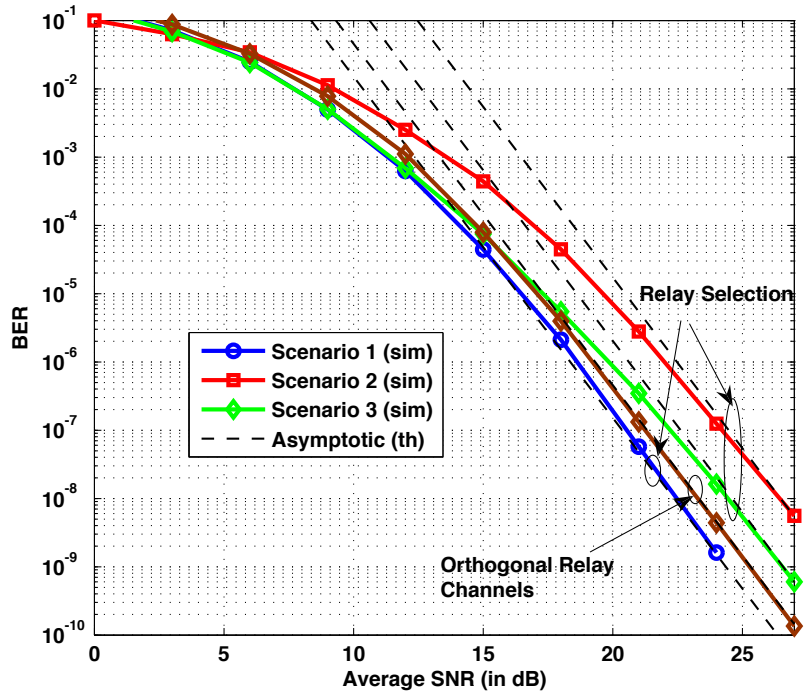

Figure 2.2: BER vs. average SNR, $\bar{\gamma}$, for BRS with $N = 4$ AF relays and 4–PSK. I.i.d. Rayleigh fading and equal transmit powers for the source and the relays. Scenario 1: All relays and the destination are corrupted by AWGN. Scenario 2: All relays and the destination are corrupted by ϵ–mixture noise. Scenario 3: R_1 and R_3 are corrupted by ϵ–mixture noise and unfaded synchronous CCI, respectively, and the other relays and the destination are corrupted by AWGN. Solid lines with markers: Simulated BER. Dashed lines: Asymptotic BER obtained with (2.7) and (2.13).

Scenario 3, we have also included the BER of cooperative relaying with orthogonal relay channels, which was considered in [16]. As expected we notice that although the scheme with orthogonal relay channels outperforms BRS, both schemes achieve the same diversity gain. More importantly, relay selection requires only two orthogonal channels as compared to five for the scheme with orthogonal relay channels, i.e., relay selection is 2.5 times more bandwidth efficient.

In Fig. 2.3, we compare BRS with AF and DF relays, respectively, assuming that

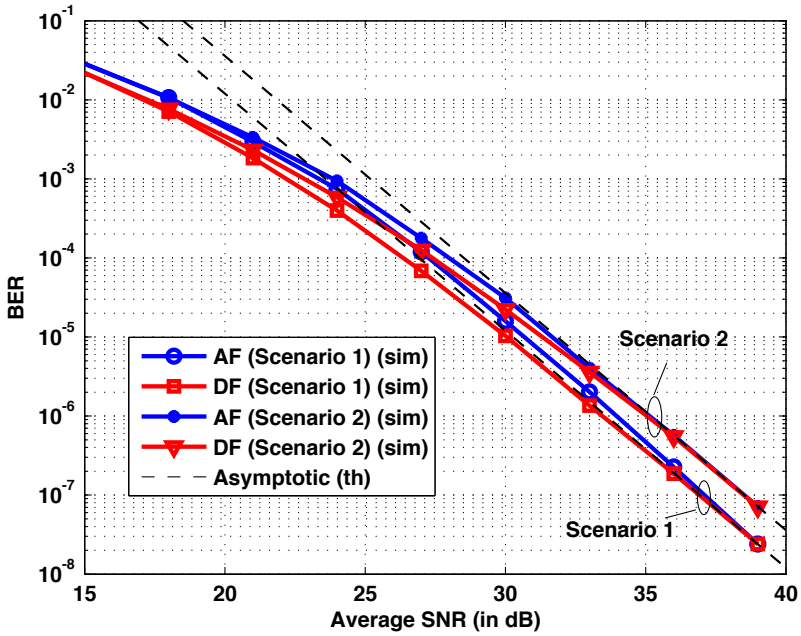

Figure 2.3: BER vs. average SNR, $\bar{\gamma}$, for BRS with $N = 3$ AF and DF relays, respectively, and 4–PSK. The direct link is not used. $\bar{\gamma}_{11} = \bar{\gamma}_{21} = \bar{\gamma}$, $\bar{\gamma}_{12} = \bar{\gamma}_{22} = \bar{\gamma} - 10\,\text{dB}$, and $\bar{\gamma}_{13} = \bar{\gamma}_{23} = \bar{\gamma} - 13\,\text{dB}$. Scenario 1: All relays and the destination are corrupted by AWGN. Scenario 2: R_2 and R_3 are corrupted by ϵ–mixture noise and Rician faded synchronous CCI, respectively, and the other relay and the destination are corrupted by AWGN. Solid lines with markers: Simulated BER. Dashed lines: Asymptotic BER obtained with (2.7) and (2.14).

the direct S–D link cannot be exploited. I.n.d. Rayleigh fading and two different noise scenarios are considered, cf. caption of figure. As expected from Section 2.3, for both noise scenarios AF and DF relays yield the same BER at sufficiently high SNR. This result was already known for the special case of impairment by AWGN, cf. [80], but is new for non–Gaussian types of noise and interference.

Fig. 2.4 shows the performance of PRS–S under i.n.d. Rayleigh fading and two different noise scenarios. For both scenarios, the destination is impaired by AWGN, whereas for Scenarios 1 and 2 the relays are corrupted by AWGN and ϵ–mixture noise, respectively. For $N = 1$ (no selection) there exists a 1–dB performance gap

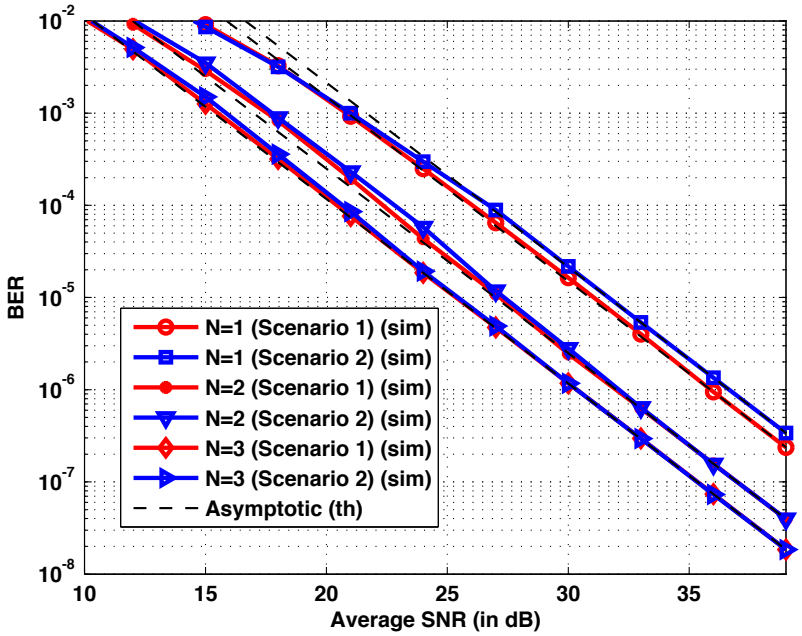

Figure 2.4: BER vs. average SNR, γ, for 4–PSK PRS–S with $N = 1, 2, 3$. For $N = 1$, $\bar{\gamma}_0 = \bar{\gamma}$ and $\bar{\gamma}_{11} = \bar{\gamma}_{21} = \bar{\gamma} - 10\,\text{dB}$. For $N = 2$, $\bar{\gamma}_0 = \bar{\gamma}$, $\bar{\gamma}_{11} = \bar{\gamma}_{21} = \bar{\gamma} - 3\,\text{dB}$, and $\bar{\gamma}_{12} = \bar{\gamma}_{22} = \bar{\gamma} - 10\,\text{dB}$. For $N = 3$, $\bar{\gamma}_0 = \bar{\gamma}_{11} = \bar{\gamma}_{21} = \bar{\gamma}$, $\bar{\gamma}_{12} = \bar{\gamma}_{22} = \bar{\gamma} - 3\,\text{dB}$, and $\bar{\gamma}_{13} = \bar{\gamma}_{23} = \bar{\gamma} - 10\text{dB}$. Scenario 1: All relays and the destination are corrupted by AWGN. Scenario 2: All relays are subject to ϵ–mixture noise and the destination is corrupted by AWGN. Solid lines with markers: Simulated BER. Dashed lines: Asymptotic BER obtained with (2.7) and (2.17).

between both scenarios. On the contrary, for $N > 1$ both scenarios show identical performance as expected from Remark 1. Thus, for $N > 1$ the performance of PRS–S is not affected by the type of noise that impairs the relays.

In Fig. 2.5, we investigate the effectiveness of the considered relay subset selection scheme. We assume i.n.d. Rayleigh fading channels and i.n.d. noise. Out of $N = 3$ available relays, a subset of $K = 2$ relays is selected. From the two remaining relays the best one is selected using BRS. The BERs for all $3!/2! = 3$ possible subsets are shown in Fig. 2.5. The subset consisting of relays R_1 and R_2 yields the best performance as accurately predicted by our asymptotic analysis. Thus, the subset selection

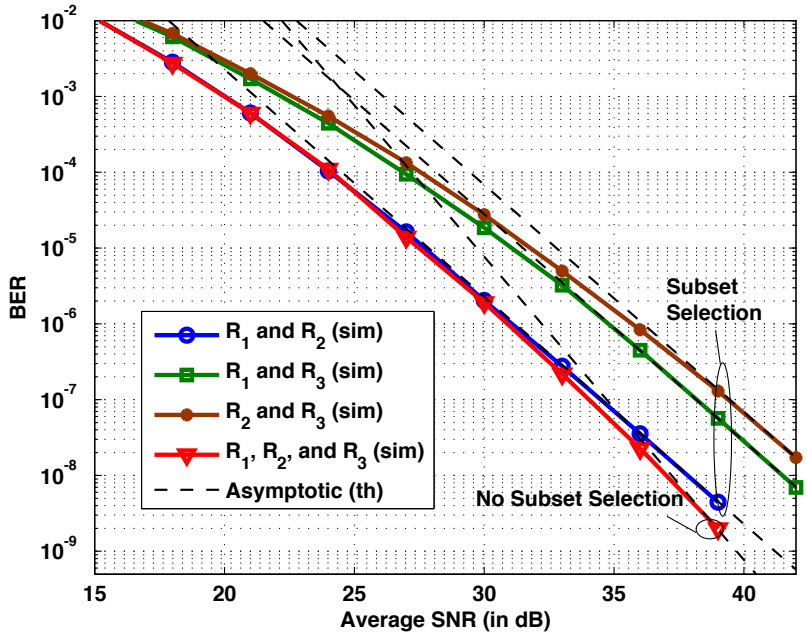

Figure 2.5: BER vs. average SNR, $\bar{\gamma}$, for BRS with relay subset selection and 16–QAM. $K = 2$ of $N = 3$ relays are selected. $\bar{\gamma}_0 = \bar{\gamma}_{11} = \bar{\gamma}_{21} = \bar{\gamma}_{12} = \bar{\gamma}_{22} = \bar{\gamma}$, $\bar{\gamma}_{13} = \bar{\gamma} - 17\,\text{dB}$, and $\bar{\gamma}_{23} = \bar{\gamma} - 10\,\text{dB}$. R_2 is impaired by ϵ–mixture noise and all other nodes are corrupted by AWGN. Solid lines with markers: Simulated BER. Dashed lines: Asymptotic BER obtained with (2.7) and (2.13).

can be based on the asymptotic error rate expression in (2.13). For comparison, we have also included the BER for BRS without subset selection. Although the latter case results in a higher diversity gain, a noticeable performance gain compared to the subset consisting of relays R_1 and R_2 is achieved only for SNRs higher than 30 dB because of the comparably poor average channel conditions of R_3. Thus, in this case, relay subset selection enables a significant reduction in signaling overhead at the expense of a small performance loss.

In Fig. 2.6, we investigate the performance of the proposed power allocation scheme for BRS with $N = 3$ AF relays and i.n.d. Rayleigh fading. In the considered scenario, relays R_1 and R_3 experience the best and worst channel conditions,

Table 2.1: Power and energy constraints for OPA, FPA–1, FPA–2, EPA, and ESP [3], cf. Fig. 2.6. For all schemes $P_0 + P_1 f_1^X + P_2 f_2^X + P_3 f_3^X \leq E_T$ is valid.

	OPA	EPA	FPA-1	FPA-2	ESP [3]
P_0	$0 \leq P_0 < \infty$	$P_0 = E_T/2$	$0 \leq P_0 \leq E_T/4$	$0 \leq P_0 < \infty$	$P_0 = E_T/4$
P_1	$0 \leq P_1 f_1^X < \infty$	$P_1 = E_T/2$	$0 \leq P_1 f_1^X \leq E_T/4$	$0 \leq P_1 f_1^X \leq E_T/3$	$P_1 f_1^X = E_T/4$
P_2	$0 \leq P_2 f_2^X < \infty$	$P_2 = E_T/2$	$0 \leq P_2 f_2^X \leq E_T/4$	$0 \leq P_2 f_2^X \leq E_T/3$	$P_2 f_2^X = E_T/4$
P_3	$0 \leq P_3 f_3^X < \infty$	$P_3 = E_T/2$	$0 \leq P_3 f_3^X \leq E_T/4$	$0 \leq P_3 f_3^X \leq E_T/3$	$P_3 f_3^X = E_T/4$

respectively. We consider five different power allocation/selection schemes: OPA, two fair power allocation (FPA) schemes, EPA, and ESP [3]. OPA, FPA–1, and FPA–2 are obtained by optimizing the transmit powers based on (2.19) under different energy consumption constraints, while EPA and ESP serve as benchmarks. EPA allocates equal powers to the source and all relays, and ESP selects all relays with equal probability while all nodes transmit with equal powers. The power allocation/energy consumption of all considered schemes is summarized in Table 2.1. OPA and EPA do not constrain the energy consumed by individual nodes and will drain the energy resources of the source and R_1 more quickly than those of the other relays since the source always transmits and R_1 is selected more often because of its favorable channel conditions. Both FPA–1 and ESP force the source and all relays to consume the same amounts of energy on average. For FPA–2, these stringent constraints are relaxed. Fig. 2.6 reveals that OPA achieves a 1 dB performance gain compared to EPA. The price to be paid for the fairness enforced by FPA–1 is an SNR loss of 2.5 dB compared to OPA. However, FPA–1 achieves a 2.5 dB gain compared to the fair benchmark scheme ESP. The relatively poor performance of ESP is due to the fact that all relays are used for the same amounts of time and transmit with the same powers, while FPA–1 is more flexible and uses relays with good channels more fre-

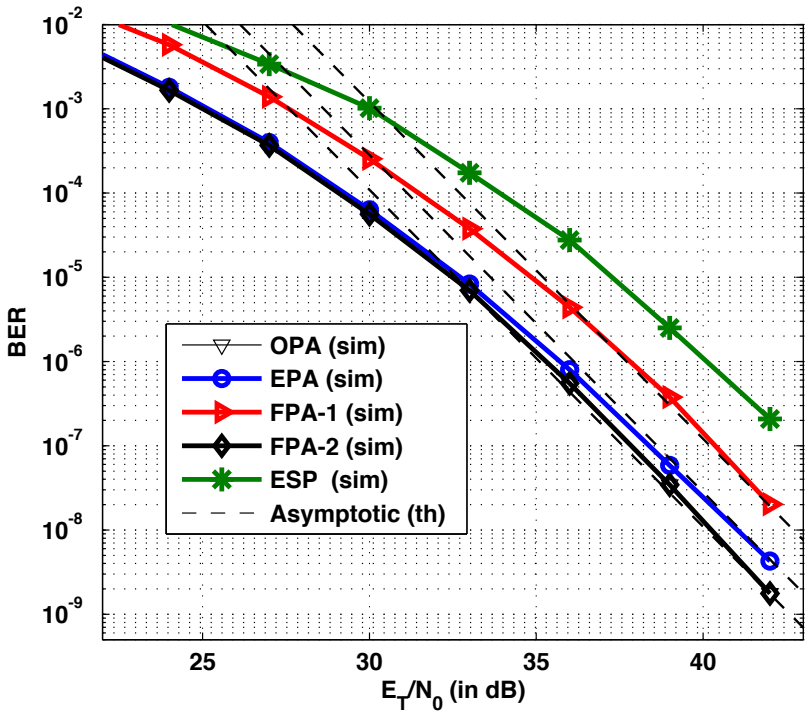

Figure 2.6: BER vs. E_T/N_0 for BRS with $N = 3$ AF relays and 16–QAM. $\Omega_0 = \Omega_{11} = \Omega_{21} = 1$, $\Omega_{12} = \Omega_{22} = 0.1$, $\Omega_{13} = \Omega_{23} = 0.05$. All noise variances are equal to N_0. R_1 and R_2 are impaired by GGN and unfaded synchronous CCI, respectively, and R_3 and the destination are impaired by AWGN. Solid lines with markers: Simulated BER. Dashed lines: Asymptotic BER obtained with (2.7) and (2.13).

quently while allocating higher powers to relays with poor channels. FPA–2 achieves practically the same performance as OPA while still limiting the energy consumption of the nodes.

2.6 Conclusions

In this chapter, we derived closed–form expressions for the asymptotic BER and SER of BRS and PRS with AF relays in i.n.d. Rayleigh fading and generic, possibly non–Gaussian i.n.d. noise. The developed analytical results reveal that the diversity

gains of BRS and PRS are independent of the type of noise but their SNR gains do depend on the type of noise via certain noise moments. With the derived error rate expressions, we developed OPA scheme with energy consumption constraints to avoid premature drainage of the energy resources of nodes with favorable channel conditions. Furthermore, to reduce the CSI feedback overhead, we considered schemes for relay subset selection. Simulation results confirmed the accuracy of the proposed asymptotic analysis and OPA was shown to outperform competing approaches to enforce fairness in energy consumption.

Chapter 3

Resource Allocation for Conventional and Buffer-Aided Link Adaptive Relaying Systems with Energy Harvesting Nodes

3.1 Introduction

As mentioned in Chapter 1, EH nodes can operate autonomously over long periods of time, as they are capable of harvesting energy from the surrounding environment. Therefore, EH nodes can be employed in different communication systems.

Recently, transmission strategies for and performance analyses of EH nodes in wireless communication systems have been provided in [17, 18, 20, 81, 57, 58, 82]. In [17], a single source–destination non–cooperative link with an EH source was considered and an optimal offline along with an optimal and several sub–optimal online transmission policies were provided for allocating transmit power to the source according to the random variations of the channel and the energy storage conditions. In [18], a similar system model was considered, where DP was employed to allocate the source transmit power for the case when causal CSI was available. In [20], explicit

throughput–optimal and delay–optimal policies were developed for a single link point–to–point communication system. Several higher layer issues such as transmission time minimization and transmission packet scheduling in EH systems were investigated in [57, 58, 82]. The use of EH relays in cooperative communication was introduced in [81], where a comprehensive performance analysis was performed for relay selection in a cooperative network employing EH relays. A deterministic EH model (assuming a priori knowledge of the energy arrival times and the amount of harvested energy) for the Gaussian relay channel was considered in [59], [83], where delay and no–delay constrained traffics were studied. In [84], cooperative communication with EH nodes using an energy sharing strategy was studied. The concept of energy transfer in EH relay systems was considered in [85], where an offline power allocation scheme was proposed. The deployment of EH sensors in sensor networks has been extensively discussed in the literature [19, 20, 21, 22].

In this chapter, we consider a simple single link cooperative system where the source communicates with the destination via a DF relay and both the source and the relay are EH nodes. We assume that each node stores the harvested energy in a battery having finite capacity and the relay operates in the half–duplex mode. In most of the existing literature on half duplex relaying [81, 59, 86, 87], it is assumed that relays receive a packet in one time slot from the source and forward it in the next time slot to the destination. We refer to this approach as "conventional" relaying throughout this chapter. Recently, it has been shown in [88, 89, 90] that equipping relays with buffers can improve the performance of cooperative communication systems. In fact, using buffers at the relays allows temporary storage of packets at the relay when the relay–destination channel quality is poor until the quality of the channel has sufficiently improved. In [89], a buffer–aided adaptive link selection protocol

was proposed for the case where both source and relay have a constant energy supply. This protocol gives the relay the freedom to decide in which time slot to receive and in which time slot to transmit. We note that both conventional and buffer–aided relaying are important and deserve consideration since their applicability depends on the system requirements. For example, conventional relaying is suitable for delay sensitive systems, e.g., voice communications, because it entails the minimum possible delay. On the other hand, buffer–aided relaying is suitable for delay non–sensitive systems, e.g., data communications, where a certain amount of delay is tolerable, but a high average throughput is needed.

In this chapter, we consider both conventional and buffer–aided link adaptive relaying protocols. For both protocols, we propose offline and online (real–time) power allocation schemes that maximize the end–to–end system throughput over a finite number of transmission slots. For conventional relaying, we propose an optimal online power allocation scheme which is based on a stochastic DP approach. To avoid the high complexity inherent to DP, we also propose several sub–optimal online algorithms. In case of buffer–aided link adaptive relaying, we formulate an offline optimization problem that jointly optimizes the source and the relay transmit powers along with the link selection variable. Thereby, the link selection variable indicates whether the source or the relay is selected for transmission in a given time slot. The optimization problem is shown to be a non–convex MINLP. We propose to use the sBB method to solve the offline MINLP problem optimally [91, 92, 93]. We also propose a practical online power allocation scheme for the buffer–aided link adaptive relaying protocol.

The buffer–aided link adaptive protocol considered in this chapter is different from the no–delay constrained protocol in [59]. Firstly, [59] considers the Gaussian

relay channel whereas the source–relay and relay–destination links in this chapter are impaired by time–varying fading. Secondly, [59] only considers offline power allocation for delay and no–delay constrained relaying protocols, whereas we consider both offline and online power allocation schemes for conventional and buffer–aided link adaptive relaying. Thirdly, although the no–delay constrained relaying protocol in [59] also employs a buffer, unlike the protocol in this chapter, it does not perform adaptive link selection. Moreover, it was shown in [89] that optimizing power allocation and link selection for buffer–aided relaying over an infinite number of time slots and for a constant energy supply always leads to an online solution, i.e., only knowledge of the current channel state is required and any additional knowledge about past or future channel states cannot further improve the solution obtained in [89]. In other words, for the problem considered in [89] the solution to the offline optimization problem can be implemented online. In contrast, since the optimization in this chapter is performed over a finite number of time slots and the amount of energy available for transmission is random, offline power allocation and link selection policies outperform online policies, i.e., knowledge about past or future channel and EH states can further improve performance.

The rest of this chapter is organized as follows. Section 3.2 describes the system model. The proposed resource allocation schemes for buffer–aided link adaptive relaying and conventional relaying are discussed in Sections 3.3 and 3.4, respectively. In Section 3.5, we show the simulation results and Section 3.6 concludes this chapter.

3.2 System Model

We consider an EH relay system, where the source, S, communicates with the destination, D, via a cooperative relay, R, as shown in Fig. 3.1. Both S and R are EH

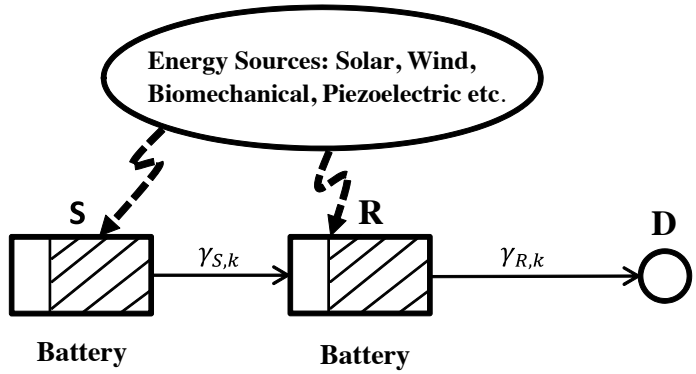

Figure 3.1: System model for a single link S–R–D system where S and R are EH devices. S and R have batteries with finite storage which can store the energies harvested from the energy sources. The rectangle boxes in S and R represent the batteries and the hashed areas represent the amount of energy stored.

devices and are equipped with batteries, which have limited storage capacity and store the harvested energy for future use. In particular, the batteries of S and R can store at most $B_{S,max}$ and $B_{R,max}$ Joules of energy, respectively. The participation of S and R in signal transmission depends on the amount of harvested energy stored in their batteries. The harvested energy can be of any form, e.g. solar, wind, or electro–mechanical energy. We assume that the data transmission is packet based and organized in time slots of duration T. In the following, without loss of generality, we set $T = 1$s, and the system transmits for K time slots. Throughout this chapter, we assume that S is the central node. In particular, S acquires knowledge about the channel SNRs and the harvested energies, executes the power allocation algorithms, and conveys the optimal transmit power for R and the link selection policy (for link adaptive relaying) to R in each time slot. We assume that S has perfect knowledge of the channel SNRs and the energy harvested at R[10]. In the next two subsections,

[10]In practice, the channel SNRs may not be perfectly known to the source node due to different sources of errors in the estimation process, e.g., background noise, quantization errors, and outdated estimates. Furthermore, feedback errors and delay impair the quality of the estimates of the harvested energy at the relay node at the source node. However, studying the effect of imperfect channel and energy knowledge is beyond the scope of this chapter and is an interesting topic for

we discuss the signal model, the system throughput, and the battery dynamics for conventional and buffer–aided link adaptive relaying.

3.2.1 Conventional Relaying

Signal Model: In conventional relaying, during the first time slot, S transmits and R receives, and during the second time slot, R transmits and D receives. This sequential process continues for K time slots, where K is assumed to be an even number. The received packet at R in the $(2k-1)$th time slot is modelled as

$$y_{R,2k-1} = h_{S,2k-1}x_{2k-1} + n_{R,2k-1}, \quad k \in \{1, 2, \cdots, K/2\}, \tag{3.1}$$

where $h_{S,2k-1}$ is the fading gain of the S–R link and $n_{R,2k-1}$ denotes the noise sample at R. The transmitted packet x_{2k-1} contains Gaussian–distributed symbols[11]. Assuming DF relaying, the detected packet, $\hat{x}_{2k}$, is transmitted from R during time slot $2k$. Thus, the received packet at D is given by

$$y_{D,2k} = h_{R,2k}\hat{x}_{2k} + n_{D,2k}, \tag{3.2}$$

where $h_{R,2k}$ and $n_{D,2k}$ denote the fading gain of the R–D link and the noise sample at D, respectively. $h_{S,2k-1}$ and $h_{R,2k}$ can follow any fading distribution, e.g. Rayleigh, Rician, Nakagami–q, or Nakagami–m fading. $n_{R,2k-1}$ and $n_{D,2k}$ are AWGN samples having zero mean and unit variance. We assume the channels are quasi–static within each time slot and the channel SNRs of the S–R and the R–D links are denoted by $\gamma_{S,2k-1}$ and $\gamma_{R,2k}$, respectively, where $\gamma_{S,2k-1} = |h_{S,2k-1}|^2$ and $\gamma_{R,2k} = |h_{R,2k}|^2$. We

future work.

[11]We note that practical modulation and coding schemes can be accommodated in the later analysis by multiplying all transmit powers by a constant $\chi > 1$, which represents performance gap between the practical scheme and optimal one.

assume $\gamma_{S,2k-1}$ and $\gamma_{R,2k}$ are i.i.d. over the time slots. Furthermore, $\gamma_{S,2k-1}$ and $\gamma_{R,2k}$ are mutually i.n.d. For future reference, we introduce the average SNRs of the S–R and the R–D links as $\bar{\gamma}_S$ and $\bar{\gamma}_R$, respectively.

System Throughput: If x_{2k-1} is transmitted from S with transmit power $P_{S,2k-1}$ during time slot $2k-1$,

$$\xi_{S,2k-1} \triangleq \log_2\left(1+\gamma_{S,2k-1}P_{S,2k-1}\right) \tag{3.3}$$

bits of data can be received error–free at R. Similarly, if $\hat{x}_{2k}$ is transmitted from R with transmit power $P_{R,2k}$,

$$\xi_{R,2k} \triangleq \log_2\left(1+\gamma_{R,2k}P_{R,2k}\right) \tag{3.4}$$

bits of data can be received error–free at D. During the $2k$th and the $(2k-1)$th time slots, S and R, respectively, do not transmit any data, i.e., $P_{S,2k}=0$ and $P_{R,2k-1}=0$. We assume that R ensures error–free detection by employing an appropriate error correction coding scheme and hence $\hat{x}_{2k}=x_{2k-1}$[12]. Therefore, the end–to–end (S–D) system throughput is given by $\frac{1}{2}\min\{\xi_{S,2k-1},\xi_{R,2k}\}$ bits/s/Hz where the factor $\frac{1}{2}$ is due to the half–duplex constraint. Throughout this thesis, we assume that the number of transmitted packets is fixed in each time slot. On the contrary, the number of transmitted data bits (contained within data packets) per time slot, which is calculated using Shannon's capacity formula [11], is not fixed and changes over the time slots depending on the channel SNR and the harvested energy. This type of data transmission protocol is referred to as "adaptive rate transmission" in the literature [94].

[12]To ensure an error–free detection, capacity achieving codes, e.g., turbo code and low–density parity–check (LDPC) code are usually employed in practical wireless communication systems [11].

Battery Dynamics: The energies stored in the batteries of S and R in time slot k are denoted by $B_{S,k}$ and $B_{R,k}$, respectively. The transmit powers of S and R are limited by the battery energies, i.e., $0 \leq P_{S,2k-1} \leq B_{S,2k-1}$ and $0 \leq P_{R,2k} \leq B_{R,2k}$. We assume throughout this chapter that the energy consumed by the internal circuitry of S and R is negligible compared to the transmit power [18][13]. The energy harvester at S harvests $H_{S,m} \leq B_{S,max}$ Joules of energy for transmission purpose during the mth time slot, where $m \in \{1, 2, \cdots, K\}$. Similarly, the energy harvester at R collects $H_{R,m} \leq B_{R,max}$ Joules of energy during the mth time slot. It is worth noting that energies are harvested during every time slot m at S and R. In general, the commonly used model for the harvested energy is the Markovian model [18]. For example, solar energy is usually modeled by a stationary Markov model. However, we did not use any specific model for EH process to develop the resource allocation algorithms throughout this thesis. Rather, any stationary model can be accommodated for the developed algorithms. Let $H_S \triangleq \mathcal{E}\{H_{S,m}\}$ and $H_R \triangleq \mathcal{E}\{H_{R,m}\}$ denote the average EH rate of S and R over the time slots, respectively. Because of the spatial separation of S and R, we assume $H_{S,m}$ and $H_{R,m}$ are independent of each other and i.i.d. over the time slots[14]. Similar to [18], we assume the stored energies at S and R increase and decrease linearly provided the maximum storage capacities, $B_{S,max}$ and $B_{R,max}$, are not exceeded, i.e.,

$$B_{S,m+1} = \min\{(B_{S,m} - P_{S,m} + H_{S,m}), B_{S,max}\}, \quad \forall m \tag{3.5}$$

[13]If the energy consumed by the internal circuitry is not negligible, our problem formulations in Sections 3.3 and 3.4 have to be changed accordingly. Problem formulations for EH systems accounting for the energy consumed by the internal circuitry can be found in e.g. [95, 96]. Alternatively, the energy consumed by the internal circuitry may be supplied by a pre–charged battery and only the transmitted energy is generated via EH.

[14]The EH process at different nodes can be correlated as well, e.g., when S and R are exposed to sunlight, their EH processes can be correlated. The algorithms developed in this chapter are also valid for the mutually correlated EH processes.

$$B_{R,m+1} = \min\{(B_{R,m} - P_{R,m} + H_{R,m}), B_{R,max}\}, \ \ \forall m. \tag{3.6}$$

Furthermore, $B_{S,1} = H_{S,0} \geq 0$ and $B_{R,1} = H_{R,0} \geq 0$, respectively, denote the available energies at S and R before transmission starts.

3.2.2 Buffer–Aided Adaptive Link Selection

Signal Model: For buffer–aided link adaptive relaying, relay R is equipped with a buffer in which it can temporarily store the packets received from S. In this case, S decides whether S or R should transmit in a given time slot, $k \in \{1, 2, \cdots, K\}$ [89]. Therefore, unlike conventional relaying, in any time slot k, S or R can transmit packets. Let $d_k \in \{0, 1\}$ denote a binary link selection variable, where $d_k = 0$ ($d_k = 1$) if the S–R (R–D) link is selected for transmission. When $d_k = 0$, the received packet at R is given by

$$y_{R,k} = h_{S,k} x_k + n_{R,k}. \tag{3.7}$$

On the other hand, when $d_k = 1$, the received packet at D is given by

$$y_{D,k} = h_{R,k} \hat{x}_k + n_{D,k}. \tag{3.8}$$

System Throughput: When $d_k = 0$, S is selected for transmission and $\xi_{S,k}$ bits of data can be transmitted error–free via the S–R link. Hence, R receives $\xi_{S,k}$ data bits from S and appends them to the queue in its buffer. Therefore, the number of bits in the buffer at R at the end of the kth time slot is denoted as Q_k and given by $Q_k = Q_{k-1} + \xi_{S,k}$. However, when $d_k = 1$, R transmits and the number of bits transmitted via the R–D link is given by $\min\{\xi_{R,k}, Q_{k-1}\}$, i.e., the maximal number

of bits that can be sent by R is limited by the number of bits in the buffer and the instantaneous capacity of the R–D link [89]. The number of bits remaining in the buffer at the end of the kth time slot is given by $Q_k = Q_{k-1} - \min\{\xi_{R,k}, Q_{k-1}\}$. We assume that S has always data to transmit and the buffer at R has very large (possibly infinite) capacity to store them. Therefore, a total of $\sum_{k=1}^{K} \min\{d_k \xi_{R,k}, Q_{k-1}\}$ bits are transmitted from S to D during the entire transmission time.

Battery Dynamics: The battery dynamics for the link adaptive transmission protocol are identical to those for conventional relaying.

3.3 Power Allocation and Link Selection for Buffer–Aided Relaying

In this section, we propose offline and online joint link selection and power allocation schemes for EH systems employing buffer–aided relaying. Buffer–aided relaying is preferable over conventional relaying for applications which can tolerate delays but require high throughput.

3.3.1 Offline Power Allocation

Our goal is to maximize the total number of transmitted bits (from S to D) delivered by a deadline of K time slots for the link adaptive transmission protocol. The offline (prior) information about the full CSI and the energy arrivals at S and R in each time slot are assumed to be known in advance. The resulting maximization problem is subject to a causality constraint on the harvested energy and the (maximum) storage constraint for the batteries at both S and R. The offline optimization problem for

the link adaptive transmission protocol can be formulated as follows:

$$\max_{\mathcal{T}\succeq 0,\,\{d_k|\forall k\}} \quad \sum_{k=1}^{K} d_k \log_2(1+\gamma_{R,k}P_{R,k}) \tag{3.9}$$

$$\text{s.t.} \quad \sum_{k=1}^{q}((1-d_k)P_{S,k}+\lambda_{S,k}) \leq \sum_{k=0}^{q-1} H_{S,k}, \;\; \forall q \tag{3.10}$$

$$\sum_{k=1}^{q}(d_k P_{R,k}+\lambda_{R,k}) \leq \sum_{k=0}^{q-1} H_{R,k}, \;\; \forall q \tag{3.11}$$

$$\sum_{k=0}^{v} H_{S,k} - \sum_{k=1}^{v}((1-d_k)P_{S,k}+\lambda_{S,k}) \leq B_{S,max}, \;\; \forall v \tag{3.12}$$

$$\sum_{k=1}^{v} H_{R,k} - \sum_{k=1}^{v}(d_k P_{R,k}+\lambda_{R,k}) \leq B_{R,max}, \;\; \forall v \tag{3.13}$$

$$\sum_{k=1}^{q}(1-d_k)\log_2\left(1+\gamma_{S,k}P_{S,k}\right) \geq \sum_{k=1}^{q} d_k \log_2\left(1+\gamma_{R,k}P_{R,k}\right), \;\; \forall q \tag{3.14}$$

$$d_k(1-d_k)=0, \;\; \forall k, \tag{3.15}$$

where $\mathcal{T} \triangleq \{P_{S,k},\, P_{R,k},\, \lambda_{S,k},\, \lambda_{R,k}|k \in \{1,2,\cdots,K\}\}$. Also, $\forall q$, $\forall k$, and $\forall v$ stand for $q \in \{1,2,\cdots,K\}$, $k \in \{1,2,\cdots,K\}$, and $v \in \{1,2,\cdots,K-1\}$, respectively. The slack variables $\lambda_{S,k}$ and $\lambda_{R,k}$ ensure that constraints (3.12)–(3.14) can be met for all realizations of $\gamma_{S,k}$, $\gamma_{R,k}$, $H_{S,k}$, and $H_{R,k}$. In particular, these slack variables represent the power (possibly) wasted in each transmission interval[15]. Constraints (3.10) and (3.11) stem from the causality requirement on the energy harvested at S and R, respectively. Moreover, (3.12) and (3.13) ensure that the harvested energy does not exceed the limited storage capacity of the batteries at S and R, respectively. Constraint (3.14) ensures that R cannot transmit more bits than it has in its buffer.

[15]For example, if $H_{S,k}$ and $H_{R,k}$ are large values ($H_{S,k}$ and $H_{R,k}$ are random variables and cannot be controlled in the optimization problem) and $B_{S,max}$ and $B_{R,max}$ are small, then if $\lambda_{S,k}$ and $\lambda_{R,k}$ were omitted, constraints (3.12) and (3.13) would not be satisfied and problem (3.9)–(3.15) would become infeasible. Therefore, slack variables $\lambda_{S,k}$ and $\lambda_{R,k}$ ensure that problem (3.9)–(3.15) is always feasible.

Moreover, (3.15) ensures that d_k can only be 0 or 1, i.e., either S or R transmits in a given time slot, $k \in \{1, 2, \cdots, K\}$. We note that, in this optimization problem, although we are maximizing the throughput of the R–D link, using constraint (3.14) incorporates the effect of the throughput of the S–R link. As $\xi_{S,k}$ and $\xi_{R,k}$ are increasing functions of $P_{S,k}$ and $P_{R,k}$, respectively, the optimization problem in (3.9)–(3.15) can be restated as follows:

$$\max_{\mathcal{T}' \geq 0,\, \{d_k | \forall k\}} \quad \sum_{k=1}^{K} d_k \xi_{R,k} \tag{3.16}$$

$$\text{s.t.} \quad \sum_{k=1}^{q} \left(\frac{(1-d_k)(2^{\xi_{S,k}}-1)}{\gamma_{S,k}} + \lambda_{S,k} \right) \leq \sum_{k=0}^{q-1} H_{S,k}, \;\; \forall q \tag{3.17}$$

$$\sum_{k=1}^{q} \left(\frac{d_k(2^{\xi_{R,k}}-1)}{\gamma_{R,k}} + \lambda_{R,k} \right) \leq \sum_{k=0}^{q-1} H_{R,k}, \;\; \forall q \tag{3.18}$$

$$\sum_{k=0}^{v} H_{S,k} - \sum_{k=1}^{v} \left(\frac{(1-d_k)(2^{\xi_{S,k}}-1)}{\gamma_{S,k}} + \lambda_{S,k} \right) \leq B_{S,max}, \;\; \forall v \tag{3.19}$$

$$\sum_{k=1}^{v} H_{R,k} - \sum_{k=1}^{v} \left(\frac{d_k(2^{\xi_{R,k}}-1)}{\gamma_{R,k}} + \lambda_{R,k} \right) \leq B_{R,max}, \;\; \forall v \tag{3.20}$$

$$\sum_{k=1}^{q} (1-d_k)\xi_{S,k} \geq \sum_{k=1}^{q} d_k \xi_{R,k}, \;\; \forall q \tag{3.21}$$

$$d_k(1-d_k) = 0, \;\; \forall k, \tag{3.22}$$

where $\mathcal{T}' \triangleq \{\xi_{S,k}, \xi_{R,k}, \lambda_{S,k}, \lambda_{R,k} | k \in \{1, 2, \cdots, K\}\}$. The problem in (3.16)–(3.22) is a non–convex MINLP due to the binary variables d_k and the non–convex and non–linear constraints (3.17)–(3.22). In the following, we propose two optimal methods to solve the buffer–aided link adaptive offline optimization problem.

Exhaustive Search

For given d_k, $k \in \{1, 2, \cdots, K\}$, the optimization problem in (3.16)–(3.22) is con-

vex. Therefore, we can optimize $\xi_{S,k}$ and $\xi_{R,k}$ for given $d_k \in \{0, 1\}$ very efficiently. In this method, we optimize $\xi_{S,k}$ and $\xi_{R,k}$ for all possible combinations of d_k, $k \in \{1, 2, \cdots, K\}$, and select from all the solutions that combination of d_k, $k \in \{1, 2, \cdots, K\}$, which maximizes the cost function. This exhaustive search method provides the global optimal solution but with an exponential complexity. For instance, for K time slots we have 2^{K-2} possible combinations of d_k and hence to optimize $\xi_{S,k}$ and $\xi_{R,k}$, we need to solve 2^{K-2} optimization problems. Therefore, in practice, this approach cannot be adopted in general, especially for large K. However, the exhaustive search scheme can be effective for small K.

Spatial Branch-and-Bound (sBB)

As mentioned before, our problem is a non–convex MINLP. One of the recent advances in (globally) solving MINLP problems is the sBB method [91, 92]. The sBB method sequentially solves subproblems of problem (3.16)–(3.22). These subproblems are obtained by partitioning the original solution space. For each subproblem, the sBB method relies on the generation of rigorous lower and upper bounds of the problem over any given variable sub–domain. The feasible lower bounds are chosen to be the local minimizers of the (sub)problems whereas the upper bounds are obtained from convex relaxations. Interestingly, MINLP problems can be solved by using the widely available open source solver Couenne [93, 92]. Couenne provides the global optimal solution for both convex and non–convex MINLP problems. It implements linearization, bound reduction, and branching methods within a branch and bound framework. The convergence of the sBB method in a finite number of iterations is guaranteed [93]. However, the worst–case computational cost of sBB is exponential in the size of the optimization variables [92].

3.3.2 Online Power Allocation

In practice, only causal information about channels and harvested energies is available for power allocation. Therefore, the offline power allocation scheme is not readily applicable as, at a given time slot, the future CSI and the upcoming harvested energy are not known in advance. To this end, we could formulate an optimal online scheme using stochastic DP. Unfortunately, this approach leads to a very high computational cost because of the adaptive link selection in every time slot and may not be implementable in practice. Therefore, we propose two efficient suboptimal online schemes which have low complexity.

Suboptimal Harvesting Rate (HR) Assisted Online Power Allocation

We propose an efficient online power allocation scheme referred to as "HR Assisted". To this end, we formulate an optimization problem which is based on the average data rate, the average energy causality constraints at S and R, and the average buffering constraint for $K \to \infty$ as follows:

$$\max_{\{P_{S,k}\geq 0,\, P_{R,k}\geq 0,\, d_k|\forall k\}} \quad \frac{1}{K}\sum_{k=1}^{K} d_k \log_2(1+\gamma_{R,k}P_{R,k}) \tag{3.23}$$

$$\text{s.t.} \quad \frac{1}{K}\sum_{k=1}^{K}(1-d_k)P_{S,k} \leq \frac{1}{K}\sum_{k=0}^{K-1} H_{S,k} \tag{3.24}$$

$$\frac{1}{K}\sum_{k=1}^{K} d_k P_{R,k} \leq \frac{1}{K}\sum_{k=0}^{K-1} H_{R,k} \tag{3.25}$$

$$\frac{1}{K}\sum_{k=1}^{K}(1-d_k)\log_2\left(1+\gamma_{S,k}P_{S,k}\right) = \frac{1}{K}\sum_{k=1}^{K} d_k \log_2\left(1+\gamma_{R,k}P_{R,k}\right) \tag{3.26}$$

$$\frac{1}{K}d_k(1-d_k) = 0, \;\; \forall k \tag{3.27}$$

The Lagrangian of (3.23)–(3.27) is given by

$$\begin{aligned}\mathcal{L} = &\frac{1}{K}\sum_{k=1}^{K} d_k \log_2(1+\gamma_{R,k}P_{R,k}) - \frac{\psi_S}{K}\left(\sum_{k=1}^{K}(1-d_k)P_{S,k} - H_{S,k-1}\right)\\ &- \frac{\psi_R}{K}\left(\sum_{k=1}^{K} d_k P_{R,k} - H_{R,k-1}\right) - \frac{1}{K}\sum_{k=1}^{K}\beta_k d_k(1-d_k)\\ &- \frac{\varrho}{K}\left(\sum_{k=1}^{K} d_k \log_2(1+\gamma_{R,k}P_{R,k}) - (1-d_k)\log_2(1+\gamma_{S,k}P_{S,k})\right),\end{aligned} \tag{3.28}$$

where ψ_S, ψ_R, ϱ, and β_k are Lagrange multipliers. Differentiating (3.28) with respect to $P_{S,k}$, $P_{R,k}$, and d_k and equating each of the differentiated expressions to zero leads to the following optimum values of $P_{S,k}$, $P_{R,k}$, and d_k:

$$P^*_{S,k} = \begin{cases} \frac{\vartheta}{\nu_S} - \frac{1}{\gamma_{S,k}}, & \text{if } \gamma_{S,k} > \frac{\nu_S}{\vartheta} \text{ AND } d_k = 0,\\ 0, & \text{otherwise,}\end{cases} \tag{3.29}$$

$$P^*_{R,k} = \begin{cases} \frac{1}{\nu_R} - \frac{1}{\gamma_{R,k}}, & \text{if } \gamma_{R,k} > \nu_R \text{ AND } d_k = 1,\\ 0, & \text{otherwise,}\end{cases} \tag{3.30}$$

$$d^*_k = \begin{cases} 1, & \text{if } (\mathcal{C}_R > \mathcal{C}_S) \text{ OR } \left(\gamma_{R,k} > \nu_R \text{ AND } \gamma_{S,k} < \frac{\nu_S}{\vartheta}\right),\\ 0, & \text{if } (\mathcal{C}_R < \mathcal{C}_S) \text{ OR } \left(\gamma_{R,k} < \nu_R \text{ AND } \gamma_{S,k} > \frac{\nu_S}{\vartheta}\right),\end{cases} \tag{3.31}$$

where $\mathcal{C}_R = \ln\left(\frac{\gamma_{R,k}}{\nu_R}\right) + \frac{\nu_R}{\gamma_{R,k}} - 1$, $\mathcal{C}_S = \vartheta \ln\left(\frac{\vartheta\gamma_{S,k}}{\nu_S}\right) + \frac{\nu_S}{\gamma_{S,k}} - \vartheta$, $\vartheta = \varrho/(1-\varrho)$, $\nu_S = \psi_S \ln(2)/(1-\varrho)$, and $\nu_R = \psi_R \ln(2)/(1-\varrho)$. We observe that the optimal $P_{S,k}$, $P_{R,k}$, and d_k depend on the instantaneous channel SNRs and Lagrange multipliers. The Lagrange multipliers can be solved efficiently, as shown in the next part of this section, without requiring any non–causal knowledge. Therefore, the optimal $P_{S,k}$, $P_{R,k}$, and d_k are readily applicable in a real–time (online) environment with low implementation complexity.

Finding the Lagrange Multipliers: Combining (3.29)–(3.31) and (3.24)–(3.26) yields the following conditions for $K \to \infty$:

$$\int_0^{\nu_R} \left[\int_{\frac{\nu_S}{\vartheta}}^{\infty} \left(\frac{\vartheta}{\nu_S} - \frac{1}{\gamma_{S,k}} \right) f_{\gamma_{S,k}}(\gamma_{S,k}) \mathrm{d}\gamma_{S,k} \right] f_{\gamma_{R,k}}(\gamma_{R,k}) \mathrm{d}\gamma_{R,k}$$
$$+ \int_{\nu_R}^{\infty} \left[\int_{L_1}^{\infty} \left(\frac{\vartheta}{\nu_S} - \frac{1}{\gamma_{S,k}} \right) f_{\gamma_{S,k}}(\gamma_{S,k}) \mathrm{d}\gamma_{S,k} \right] f_{\gamma_{R,k}}(\gamma_{R,k}) \mathrm{d}\gamma_{R,k} = H_{S,E}, \quad (3.32)$$

$$\int_0^{\frac{\nu_S}{\vartheta}} \left[\int_{\nu_R}^{\infty} \left(\frac{1}{\nu_R} - \frac{1}{\gamma_{R,k}} \right) f_{\gamma_{R,k}}(\gamma_{R,k}) \mathrm{d}\gamma_{R,k} \right] f_{\gamma_{S,k}}(\gamma_{S,k}) \mathrm{d}\gamma_{S,k}$$
$$+ \int_{\frac{\nu_S}{\vartheta}}^{\infty} \left[\int_{L_2}^{\infty} \left(\frac{1}{\nu_R} - \frac{1}{\gamma_{R,k}} \right) f_{\gamma_{R,k}}(\gamma_{R,k}) \mathrm{d}\gamma_{R,k} \right] f_{\gamma_{S,k}}(\gamma_{S,k}) \mathrm{d}\gamma_{S,k} = H_{R,E}, \quad (3.33)$$

$$\int_0^{\nu_R} \left[\int_{\frac{\nu_S}{\vartheta}}^{\infty} \log_2 \left(\frac{\vartheta \gamma_{S,k}}{\nu_S} \right) f_{\gamma_{S,k}}(\gamma_{S,k}) \mathrm{d}\gamma_{S,k} \right] f_{\gamma_{R,k}}(\gamma_{R,k}) \mathrm{d}\gamma_{R,k}$$
$$+ \int_{\nu_R}^{\infty} \left[\int_{L_1}^{\infty} \log_2 \left(\frac{\vartheta \gamma_{S,k}}{\nu_S} \right) f_{\gamma_{S,k}}(\gamma_{S,k}) \mathrm{d}\gamma_{S,k} \right] f_{\gamma_{R,k}}(\gamma_{R,k}) \mathrm{d}\gamma_{R,k}$$
$$= \int_0^{\frac{\nu_S}{\vartheta}} \left[\int_{\nu_R}^{\infty} \log_2 \left(\frac{\gamma_{R,k}}{\nu_R} \right) f_{\gamma_{R,k}}(\gamma_{R,k}) \mathrm{d}\gamma_{R,k} \right] f_{\gamma_{S,k}}(\gamma_{S,k}) \mathrm{d}\gamma_{S,k}$$
$$+ \int_{\frac{\nu_S}{\vartheta}}^{\infty} \left[\int_{L_2}^{\infty} \log_2 \left(\frac{\gamma_{R,k}}{\nu_R} \right) f_{\gamma_{R,k}}(\gamma_{R,k}) \mathrm{d}\gamma_{R,k} \right] f_{\gamma_{S,k}}(\gamma_{S,k}) \mathrm{d}\gamma_{S,k}, \quad (3.34)$$

where $L_1 = -\frac{\nu_S}{\vartheta \mathrm{W}\left(-e^{\frac{\gamma_{R,k}-\nu_R}{\vartheta\gamma_{R,k}}-1}\left(\frac{\nu_R}{\gamma_{R,k}}\right)^{\frac{1}{\vartheta}}\right)}$ and $L_2 = -\frac{\nu_R}{\mathrm{W}\left(-e^{\vartheta-\frac{\nu_S}{\gamma_{S,k}}-1}\left(\frac{\nu_S}{\vartheta\gamma_{S,k}}\right)^{\vartheta}\right)}$. Here, $W(\cdot)$ is the Lambert W–function [97]. For Rayleigh fading, $f_{\gamma_{S,k}}(\gamma_{S,2k-1}) = (1/\bar{\gamma}_S)$ $e^{-\gamma_{S,2k-1}/\bar{\gamma}_S}$ and $f_{\gamma_{R,k}}(\gamma_{R,2k}) = (1/\bar{\gamma}_R)e^{-\gamma_{R,2k}/\bar{\gamma}_R}$. We need to solve (3.32)–(3.34) to find the optimal ν_S, ν_R, and ϑ. The solution can be obtained by using the built–in root–finding function in Mathematica. We note that the optimal ν_S, ν_R, and ϑ are computed offline before transmission starts. When transmission begins, $P^*_{S,k}$, $P^*_{R,k}$, and d^*_k are calculated based on offline parameters ϑ, ν_S, and ν_R and online variables $\gamma_{S,k}$ and $\gamma_{R,k}$.

Algorithm 3.1 HR Assisted Online Scheme For Buffer–Aided Link Adaptive Relaying

```
Initialize the buffer status, Q_0 = 0 bits;
for k = 1 to K do
    Calculate B_{S,k} and B_{R,k} using (3.5) and (3.6), respectively.
    Calculate P*_{S,k}, P*_{R,k}, and d*_k using (3.29)–(3.31) and (3.24)–(3.26).
    if d*_k = 0 then
        if P*_{S,k} > B_{S,k} then
            P*_{S,k} = B_{S,k};
        end if
        Q_k = Q_{k-1} + log_2(1 + γ_{S,k} P*_{S,k});
    else
        if P*_{R,k} > B_{R,k} then
            P*_{R,k} = B_{R,k};
        end if
        if log_2(1 + γ_{R,k} P*_{R,k}) > Q_k then
            P*_{R,k} = (2^{Q_k} - 1)/γ_{R,k};
        end if
        Q_k = Q_{k-1} - log_2(1 + γ_{R,k} P*_{R,k});
    end if
end for
Obtain throughput = Σ_{k=1}^{K} d_k log_2(1 + γ_{R,k} P*_{R,k}).
```

The solution of problem (3.23)–(3.27) provides an upper bound for the practical case where the storage capacity of the batteries is limited. Moreover, the problem

may yield $P_{R,k} \neq 0$ even if the buffer is empty at R. To avoid this undesirable behavior, we propose a practical but suboptimal online algorithm which is summarized in Algorithm 3.1. At first, we calculate $B_{S,k}$ and $B_{R,k}$ using (3.5) and (3.6), respectively. We then calculate $P^*_{S,k}$, $P^*_{R,k}$, and d^*_k from (3.29)–(3.31) and (3.24)–(3.26). To ensure that $P^*_{S,k}$ and $P^*_{R,k}$ do not exceed the storage limits, we perform steps 6 to 8 and 11 to 13, respectively. Steps 9 and 17 keep track of the arrival of data bits into and the departure of data bits out of the buffer, respectively. Steps 14 to 16 are adopted to ensure that R transmits only if there is data in the buffer.

Suboptimal Naive Online Power Allocation

In the suboptimal naive power allocation scheme for link adaptive relaying, at each time slot, k, S and R consider the amount of energy stored in their batteries as their transmit powers. Based on the transmit powers, S and R compute their capacities. Note that the buffer status should be taken into account in the computation of the capacity of R. The S–R (R–D) link is selected if the capacity of S is greater (smaller) than that of R.

3.3.3 Complexity

The overhead of buffer–aided link adaptive relaying includes both the computational cost and the required feedback of the corresponding power allocation schemes. The worst–case computational cost of the sBB algorithm used to solve the offline power allocation scheme for link adaptive relaying is exponential in K [92], whereas the computational cost of the exhaustive search algorithm is always exponential in K. Moreover, the worst–case complexity of the sBB algorithm is not likely to occur as is evident from the execution time results shown in Section V. Determining the exact and/or average complexity of the sBB algorithm is quite involved and beyond the

scope of this thesis. The complexities of the proposed suboptimal online schemes for link adaptive relaying are linear in K.

Furthermore, for buffer–aided link adaptive relaying, S needs to know the instantaneous values of $\gamma_{S,k}$, $\gamma_{R,k}$, $H_{S,k}$, and $H_{R,k}$ along with the averages $\bar{\gamma}_S$, $\bar{\gamma}_R$, H_S, and H_R for execution of the online power allocation algorithms. Moreover, S also has to track the status of the relay buffer. After calculating the optimal power and link selection policies, S has to convey $P^*_{R,k}$ as well as information regrading which link is selected to R.

3.4 Power Allocation for Conventional Relaying

In this section, we propose an offline and several online power allocation schemes for the considered EH system with conventional relaying. We note that conventional relaying is preferable over buffer–aided relaying if small end–to–end delays are required.

3.4.1 Optimal Offline Power Allocation

Like for buffer–aided relaying, for conventional relaying, our objective is to maximize the total number of transmitted bits (from S to D) delivered by a deadline of K time slots over a fading channel. We assume offline knowledge of the full CSI and the energy arrivals at S and R in each time slot. The offline optimization problem for maximization of the throughput of the considered system for K time slots can be

formulated as follows:

$$\max_{\mathcal{T}''\succeq 0} \quad \sum_{k=1}^{K/2} \min\{\xi_{S,2k-1}, \xi_{R,2k}\} \tag{3.35}$$

$$\text{s.t.} \quad \text{Constraints (3.10)} - \text{(3.13) with } d_{2k-1}=0 \text{ and } d_{2k}=1,\ \forall k, \tag{3.36}$$

$$\gamma_{S,2k-1}P_{S,2k-1} = \gamma_{R,2k}P_{R,2k},\ \ \forall k, \tag{3.37}$$

where $\mathcal{T}'' \triangleq \{P_{S,2k-1}, P_{R,2k}, \lambda_{S,2k-1}, \lambda_{R,2k} | k \in \{1,2,\cdots,K/2\}\}$ and $\forall k$ stands for $k \in \{1,2,\cdots,K/2\}$. Like for buffer–aided relaying, constraints (3.36) ensure the energy causality and limited energy conditions for conventional relaying. Constraint (3.37) ensures that the amount of information transmitted from S to R is identical to that transmitted from R to D so as to avoid data loss at R. Constraint (3.37) is required since we assume individual power constraints for S and R. This is a reasonable assumption since S and R have independent power supplies.

Using (3.37) in (3.35) and (3.36), the considered offline optimization problem can be rewritten as

$$\max_{\mathcal{T}'''\succeq 0} \quad \sum_{k=1}^{K/2} \xi_{S,2k-1} \tag{3.38}$$

$$\text{s.t.} \quad \sum_{k=1}^{l}\left(\frac{\gamma_{S,2k-1}P_{S,2k-1}}{\gamma_{R,2k}} + \lambda_{R,2k}\right) \le \sum_{k=0}^{2l-1} H_{R,k},\ \ \forall l \tag{3.39}$$

$$\sum_{k=0}^{2m} H_{R,k} - \sum_{k=1}^{m}\left(\frac{\gamma_{S,2k-1}P_{S,2k-1}}{\gamma_{R,2k}} + \lambda_{R,2k}\right) \le B_{R,max},\ \ \forall m \tag{3.40}$$

$$\text{Constraints (3.11) and (3.13) with } d_{2k-1}=0 \text{ and } d_{2k}=1,\ \forall k, \tag{3.41}$$

where $\mathcal{T}''' \triangleq \mathcal{T}'' \setminus \{P_{R,2k}|\forall k\}$, and $\forall l$ and $\forall m$ stand for $l \in \{1,2,\cdots,K/2\}$ and $m \in \{1,2,\cdots,K/2-1\}$, respectively. Problem (3.38)–(3.41) forms a convex optimization problem and the optimum solution can be obtained either in closed form by using

the Karush–Kuhn–Tucker (KKT) conditions or by using any standard technique for solving convex optimization problems [75], [79]. Let $P^*_{S,2k-1}$ denote the optimum solution of the considered optimization problem. Then, the optimum $P_{R,2k}$ can be obtained as

$$P^*_{R,2k} = \frac{\gamma_{S,2k-1} P^*_{S,2k-1}}{\gamma_{R,2k}}. \tag{3.42}$$

3.4.2 Optimal Online Power Allocation by DP

Unlike buffer–aided link adaptive relaying, the link selection policy is pre-defined for conventional relaying, i.e., $d_{2k-1} = 0$ and $d_{2k} = 1$, $k \in \{1, 2, \cdots, K\}$. This feature of conventional relaying reduces the complexity of stochastic DP compared to link adaptive relaying. Therefore, for conventional relaying, we consider a stochastic DP approach for optimum online power allocation [18, 23]. Let $\boldsymbol{c}_{2k-1,2k} \triangleq (\gamma_{S,2k-1}, \gamma_{R,2k}, (H_{S,2(k-1)} + H_{S,2k-3}), (H_{R,2k-1} + H_{R,2(k-1)}), B_{S,2k-1}, B_{R,2k})$ denote the state for time slots $2k-1$ and $2k$. We note that $H_{S,k} = 0$ for $k < 0$. Our aim is to maximize the total throughput over K time slots. We assume the initial state $\boldsymbol{c}_{1,2} = (\gamma_{S,1}, \gamma_{R,2}, H_{S,0}, (H_{R,0} + H_{R,1}), B_{S,1}, B_{R,2})$ is always known. We define a policy $p = \{(P_{S,2k-1}(\boldsymbol{c}_{2k-1,2k}), P_{R,2k}(\boldsymbol{c}_{2k-1,2k})), \forall \boldsymbol{c}_{2k-1,2k}, k = 1, 2, \cdots, K/2\}$ as feasible if the EH constraints $0 \leq P_{S,2k-1}(\boldsymbol{c}_{2k-1,2k}) \leq B_{S,2k-1}$ and $0 \leq P_{R,2k}(\boldsymbol{c}_{2k-1,2k}) \leq B_{R,2k}$ are satisfied for all k. Hence, the objective function to be maximized can be reformulated as [18]

$$R(p) = \sum_{k=1}^{K/2} \mathcal{E}\{\min\{\xi'_{S,2k-1}, \xi'_{R,2k}\} | \boldsymbol{c}_{1,2}, p\}, \tag{3.43}$$

where we used the definitions $\xi'_{S,2k-1} \triangleq \log_2\left(1+\gamma_{S,2k-1}P_{S,2k-1}(\boldsymbol{c}_{2k-1,2k})\right)$ and $\xi'_{R,2k} \triangleq \log_2(1+\gamma_{R,2k}P_{R,2k}\ (\boldsymbol{c}_{2k-1,2k}))$. The expectation is with respect to the SNRs of the channels and the harvested energies. In particular, for a given $\boldsymbol{c}_{1,2}$, the maximum throughput can be obtained as

$$R^* = \max_{p\in\mathcal{P}} R(p), \tag{3.44}$$

where $\mathcal{P}$ denotes the space of all feasible policies.

The maximum throughput during time slots $2k-1$ and $2k$ is denoted by $J_{2k-1,2k}$ $(B_{S,2k-1}, B_{R,2k})$. For a given $\boldsymbol{c}_{1,2}$, the maximum throughput, $J_{1,2}(B_{S,1}, B_{R,2})$, can be recursively obtained from $J_{K-1,K}(B_{S,K-1}, B_{R,K})$, $J_{K-3,K-2}(B_{S,K-3}, B_{R,K-2})$, $\cdots$, $J_{3,4}(B_{S,3}, B_{R,4})$ [18]. For the last two time slots $K-1$ and K, we have

$$J_{K-1,K}(B_{S,K-1}, B_{R,K}) = \max_{\substack{0\le P_{S,K-1}\le B_{S,K-1}\\ 0\le P_{R,K}\le B_{R,K}\\ \gamma_{S,K-1}P_{S,K-1}=\gamma_{R,K}P_{R,K}}} \frac{1}{2}\min\left\{\xi_{S,K-1}, \xi_{R,K}\right\} \tag{3.45}$$

and for time slots $2k-1$ and $2k$, we obtain

$$\begin{aligned} J_{2k-1,2k}(B_{S,2k-1}, B_{R,2k}) = \max_{\substack{0\le P_{S,2k-1}\le B_{S,2k-1}\\ 0\le P_{R,2k}\le B_{R,2k}\\ \gamma_{S,2k-1}P_{S,2k-1}=\gamma_{R,2k}P_{R,2k}}} & \frac{1}{2}\min\left\{\xi_{S,2k-1}, \xi_{R,2k}\right\} \\ & +\bar{J}_{2k+1,2k+2}(B_{S,2k-1}-P_{S,2k-1}, B_{R,2k}-P_{R,2k}), \end{aligned} \tag{3.46}$$

where $\bar{J}_{2k+1,2k+2}(B'_{S,2k+1}, B'_{R,2k+2}) =$

$$\begin{aligned} \mathcal{E}_{\tilde{\gamma}_{S,2k+1},\tilde{\gamma}_{R,2k+2},\tilde{H}_{S,2k-1},\tilde{H}_{R,2k}}\{J_{2k+1,2k+2}(&\min\{B'_{S,2k+1}+\tilde{H}_{S,2k-1}, B_{S,max}\}, \\ &\min\{B'_{R,2k+2}+\tilde{H}_{R,2k}, B_{R,max}\})\}. \end{aligned} \tag{3.47}$$

Here, $B'_{S,2k+1} \triangleq B_{S,2k-1} - P_{S,2k-1}$, $B'_{R,2k+2} \triangleq B_{R,2k} - P_{R,2k}$, $\tilde{\gamma}_{S,2k+1}$ ($\tilde{\gamma}_{R,2k+2}$) represents the SNR of the S–R (R–D) link in the $(2k+1)$th ($(2k+2)$th) slot given the SNR $\gamma_{S,2k-1}$ ($\gamma_{R,2k}$) in the $(2k-1)$th ($2k$th) slot, and $\tilde{H}_{S,2k-1}$ ($\tilde{H}_{R,2k}$) denotes the harvested energy at S (R) in the $(2k-1)$th ($2k$th) slot given the harvested energy $H_{S,2k-2}$ ($H_{R,2k-1}$) in the $(2k-2)$th ($(2k-1)$th) slot. It can be shown that the cost functions in (3.45) and (3.46) are concave in $P_{S,2k-1}$ and $P_{R,2k}$. Thus, (3.45) and (3.46) are convex optimization problems and can be solved very efficiently [75]. Further simplification of (3.45) yields

$$J_{K-1,K}(B_{S,K-1}, B_{R,K}) = \frac{1}{2}\log_2\left(1 + \gamma_{S,K-1}\rho_{K-1}\right), \tag{3.48}$$

where $\rho_{K-1} = \min\{B_{S,K-1}, \gamma_{R,K}B_{R,K}/\gamma_{S,K-1}\}$. Therefore, $P^*_{S,K-1} = \min\{B_{S,K-1}, \frac{\gamma_{R,K}B_{R,K}}{\gamma_{S,K-1}}\}$, and $P^*_{R,K}$ follows from (3.42). Similarly, (3.46) can be simplified as

$$\begin{aligned} J_{2k-1,2k}(B_{S,2k-1}, B_{R,2k}) = & \max_{0 \le P_{S,2k-1} \le \min\left\{B_{S,2k-1}, \gamma_{R,2k}B_{R,2k}/\gamma_{S,2k-1}\right\}} \frac{1}{2}\xi_{S,2k-1} \\ & + \bar{J}_{2k+1,2k+2}(B_{S,2k-1} - P_{S,2k-1}, B_{R,2k} - \gamma_{S,2k-1}P_{S,2k-1}/\gamma_{R,2k}). \end{aligned} \tag{3.49}$$

Using (3.48) and (3.49), $P^*_{S,2k-1}$ and $P^*_{R,2k}$, $k \in \{1, 2, \cdots, K/2\}$, can be obtained for different possible values of $\gamma_{S,k}$, $\gamma_{R,k}$, $B_{S,k}$, and $B_{R,k}$ and can be stored in a look–up table. This is done before transmission starts. When transmission starts, for given realizations of $\gamma_{S,2k-1}$, $\gamma_{R,2k}$, $B_{S,2k-1}$, and $B_{R,2k}$ in time slots $2k-1$ and $2k$, the values of $P^*_{S,2k-1}$ and $P^*_{R,2k}$ corresponding to these realizations are taken from the look–up table.

3.4.3 Suboptimal Online Power Allocation

In the proposed DP–based optimal online power allocation scheme, for a certain

transmission time slot, we consider the average effect of all succeeding time slots, c.f. (3.47). Due to the recursive nature of DP, the computational cost of this approach increases alarmingly with increasing K. For this reason, in the following, we propose three different suboptimal online power allocation schemes, which perform close to the optimal DP approach but have reduced complexity.

Suboptimal Simplified DP Power Allocation ("DP–I_2" and "DP–I_1" Schemes)

In this scheme, we use the average effect of only 2 (or 4) following time slots to allocate the transmit power in each time slot. In particular, we assume for the current time slot that all energies have to be spent over the following 2 (or 4) time slots. Moreover, in the last two time slots, either S or R uses up all of its stored energy. This scheme reduces the computational cost at the expense of a performance degradation. We refer to the suboptimal DP schemes taking into account 4 and 2 time slots as "DP–I_2" and "DP–I_1", respectively.

Suboptimal HR Assisted Power Allocation ("HR Assisted" Scheme)

As for link adaptive relaying, we also propose an efficient "HR Assisted" online power allocation scheme for conventional relaying. To this end, we first formulate an optimization problem which is based on the average data rate and the average energy causality constraints at S and R for $K \to \infty$. Then, we revise the optimal solutions taking into account the energy storage constraints in (3.5) and (3.6). The optimiza-

tion problem for $K \to \infty$ can be formulated as

$$\max_{\{P_{S,2k-1}\geq 0,\, P_{R,2k}\geq 0, |\forall k\}} \quad \frac{1}{K}\sum_{k=1}^{K/2} \min\{\log_2(1+\gamma_{S,2k-1}P_{S,2k-1}), \log_2(1+\gamma_{R,2k}P_{R,2k})\} \tag{3.50}$$

$$\text{s.t.} \quad \text{Constraints (3.24) and (3.25) with } d_{2k-1}=0 \text{ and } d_{2k}=1,\ \forall k, \tag{3.51}$$

$$\gamma_{S,2k-1}P_{S,2k-1} = \gamma_{R,2k}P_{R,2k}. \tag{3.52}$$

Incorporating (3.52) into (3.50) and (3.51) yields

$$\max_{\{P_{S,2k-1}\geq 0|\forall k\}} \quad \frac{1}{K}\sum_{k=1}^{K/2} \log_2(1+\gamma_{S,2k-1}P_{S,2k-1}) \tag{3.53}$$

$$\text{s.t.} \quad \frac{1}{K}\sum_{k=1}^{K/2} P_{S,2k-1} \leq \frac{1}{K}\sum_{k=0}^{K-1} H_{S,k} \tag{3.54}$$

$$\frac{1}{K}\sum_{k=1}^{K/2} \frac{\gamma_{S,2k-1}}{\gamma_{R,2k}} P_{S,2k-1} \leq \frac{1}{K}\sum_{k=0}^{K-1} H_{R,k}. \tag{3.55}$$

Problem (3.53)–(3.55) is a convex optimization problem and using the optimization techniques described in subsection 3.3.2, the optimal $P^*_{S,2k-1}$ and $P^*_{R,2k}$ can be obtained as

$$P^*_{S,2k-1} = \min\left\{\left[\frac{1}{\ln(2)(\eta_S + \frac{\eta_R\gamma_{S,2k-1}}{\gamma_{R,2k}})} - \frac{1}{\gamma_{S,2k-1}}\right]^+, B_{S,2k-1}\right\} \tag{3.56}$$

$$P^*_{R,2k} = \min\left\{\frac{\gamma_{S,2k-1}P^*_{S,2k-1}}{\gamma_{R,2k}}, B_{R,2k}\right\}, \tag{3.57}$$

where η_S and η_R are Lagrange multipliers associated with (3.54) and (3.55), respectively. The optimal η_S and η_R are computed offline using the same method as described in subsection 3.3.2 for link adaptive relaying before transmission starts.

When transmission begins, $P^*_{S,2k-1}$ and $P^*_{R,2k}$ are calculated using (3.56) and (3.57) with offline parameters η_S and η_R and online variables $\gamma_{S,2k-1}$, $\gamma_{R,2k}$, $B_{S,2k-1}$, and $B_{R,2k}$. For the $(K-1)$th and the Kth time slots, we ensure that either S or R uses up all of the stored energy.

Suboptimal Naive Power Allocation ("Naive" Scheme)

In this suboptimal "naive" approach, for each time slot, only the stored energies at hand determine the transmit power, i.e., this approach does not take into account the effect of the following time slots, and the transmitting node (S or R) uses up all of its available energy in each transmission interval. To be specific, for a particular time slot $k \in \{1, 2, \cdots, K/2\}$, $P^*_{S,2k-1} = \min\{B_{S,2k-1}, \frac{\gamma_{R,2k} B_{R,2k}}{\gamma_{S,2k-1}}\}$, and $P^*_{R,2k}$ follows directly from (3.42).

3.4.4 Complexity

In this subsection, we discuss the overheads entailed by the power allocation schemes proposed for conventional relaying in terms of computational cost and the required feedback. In the offline and the optimal online power allocation schemes, we solve convex optimization problems where the number of constraints is a function of K. The required computational cost to solve a convex optimization problem depends on the method used (e.g. bisection method, interior–point–method, etc.) and is polynomial in the size of the problem [75]. Therefore, the worst–case computational cost of the offline power allocation scheme for conventional relaying is polynomial in the number of time slots K [75]. We observe from (3.46) and (3.47) that the complexity of the optimal online power allocation scheme by stochastic DP increases exponentially with K. The complexities of the simplified versions of DP, i.e., DP–I_2 and DP–I_1, are linear in K. Moreover, the complexities of the naive and HR assisted

suboptimal online schemes are linear in K as well. The complexities of the proposed offline and online power allocation schemes are further investigated in terms of the required average execution time in Section V.

The required feedback information also contributes to the overhead of the proposed power allocation schemes. Like link adaptive relaying, S needs to know the instantaneous values of $\gamma_{S,2k-1}$, $\gamma_{R,2k}$, $H_{S,k}$, and $H_{R,k}$ along with the averages $\bar{\gamma}_S$, $\bar{\gamma}_R$, $H_{S,E}$, and $H_{R,E}$ for execution of the online power allocation algorithms. Furthermore, S has to convey $P^*_{R,k}$ to R.

3.5 Simulation Results

In this section, we evaluate the performance of the proposed offline and online power allocation schemes for the conventional and link adaptive relaying protocols. We assume that the (overall) average harvesting rate is $H_S = H_R = H_E$ (except in Fig. 3.9), and $H_{S,k}$ and $H_{R,k}$ independently take values from the set $\{0, H_E, 2H_E\}$, where all elements of the set are equiprobable. For Figs. 3.2–3.6, 3.10, and 3.11, we assume $H_E = 0.5$ Joule. We adopt $B_{S,max} = B_{R,max} = B_{max}$, where $B_{max} = 4$ Joules for Figs. 3.2, 3.3, 3.7, $B_{max} = 10$ Joules for Figs. 3.4–3.6, 3.9, 3.11, and $B_{max} = 100$ Joules for Fig. 3.8. We assume i.i.d. Rayleigh fading channels with $\bar{\gamma}_S = \bar{\gamma}_R = \bar{\gamma}$ for Figs. 3.2–3.5, 3.9, and 3.11 and i.n.d. Rayleigh fading channels for Figs. 3.6–3.8, and 3.10. We simulate 10^4 randomly generated realizations of the S–R and the R–D channels and the harvested energies at S and R to obtain the average throughput.

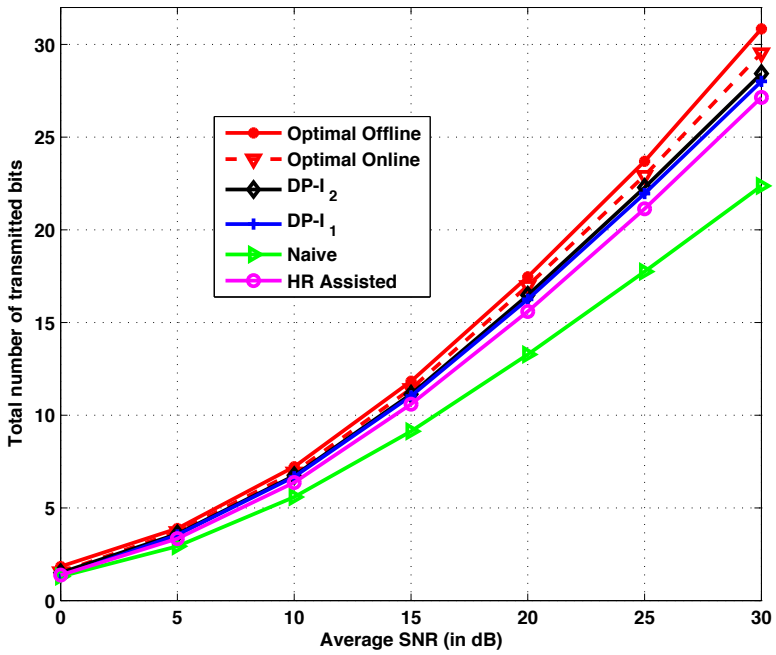

Figure 3.2: Conventional relaying: Total number of transmitted bits vs. average channel SNR $\bar{\gamma}$ for $K = 10$.

3.5.1 Performance of Different Power Allocation Schemes for Conventional Relaying

In this subsection, we show the performance of the proposed power allocation schemes for conventional relaying. In particular, the impact of the average channel SNR and the number of time slots on the total number of transmitted bits is studied.

Fig. 3.2 shows the total number of transmitted bits for the power allocation schemes proposed for conventional relaying vs. the average channel SNR, $\bar{\gamma}$, for $K = 10$. We observe that for all considered schemes, the total throughput increases as $\bar{\gamma}$ increases. We also notice that the offline scheme performs better than the online power allocation schemes for all $\bar{\gamma}$. This is due to the fact that in the optimal offline

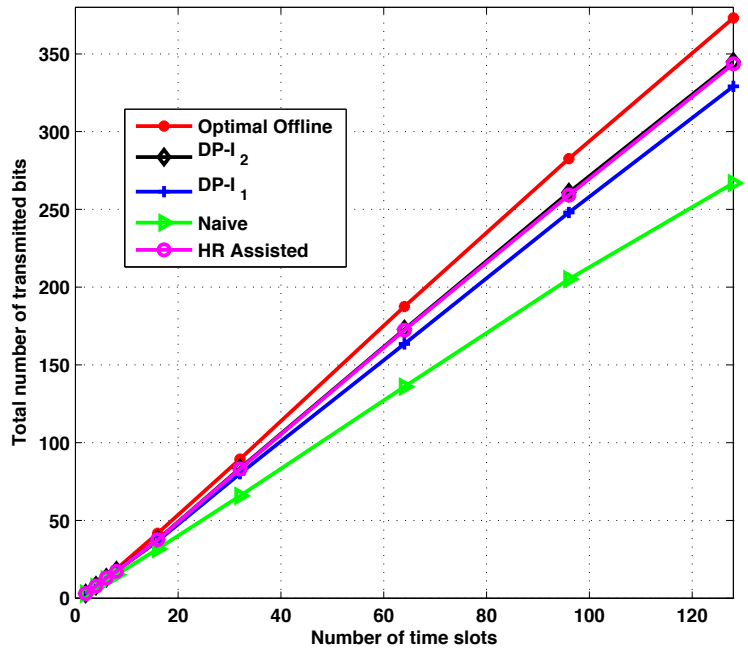

Figure 3.3: Conventional relaying: Total number of transmitted bits vs. number of time slots K for $\bar{\gamma} = 25$ dB.

scheme we assume that both causal and non–causal information regarding the CSI and the harvested energy are available whereas the online schemes are based only on causal information regarding the CSI and the harvested energy. Moreover, as expected, the optimal online scheme outperforms all considered suboptimal online schemes and performs close to the optimal offline scheme. The suboptimal online schemes DP–I_2 and DP–I_1 perform close to each other for all $\bar{\gamma}$. We note that both DP–I_2 and DP–I_1 outperform the HR assisted and the naive schemes.

In Fig. 3.3, we show the total number of transmitted bits for the power allocation schemes proposed for conventional relaying vs. the number of time slots K for $\bar{\gamma} = 25$ dB. We observe that the optimal offline method achieves the best perfor-

mance. Among the different suboptimal online schemes, DP–I_2 performs best. The HR assisted scheme provides a similar performance as DP–I_2 for large K. This is mainly due to the fact that the HR assisted scheme is based on the average harvesting rate which is more justified for large K. Moreover, we observe that the difference between the performances of DP–I_2 and DP–I_1 increases with increasing K. This shows that the consideration of the two next time slots instead of only the next time slot for calculation of the optimal transmit powers becomes more important for larger K.

3.5.2 Performance of Different Power Allocation Schemes for Link Adaptive Relaying

In this subsection, we show the impact of the average channel SNR and the number of time slots on the total number of transmitted bits for the different power allocation schemes proposed for link adaptive relaying.

Fig. 3.4 shows the total number of transmitted bits for link adaptive relaying vs. the average channel SNR $\bar{\gamma}$ for $K = 8$ and $K = 50$. Here, we consider the exhaustive search offline algorithm for $K = 8$, and the HR assisted online, the naive online, and the sBB offline power allocation schemes for both values of K. Recall that the optimal offline exhaustive search scheme is only effective for small K as the complexity increases exponentially with K. For $K = 8$, we observe that the exhaustive search and the sBB schemes have exactly the same performance for all considered $\bar{\gamma}$. This observation confirms that sBB scheme finds the global optimum solution of non–convex MINLP problems [91, 92]. The performance gap between the offline and the HR assisted online schemes is small at low $\bar{\gamma}$ and large at high $\bar{\gamma}$ for $K = 8$. Furthermore, the performance gap increases with $\bar{\gamma}$ for $K = 50$. For $K = 8$,

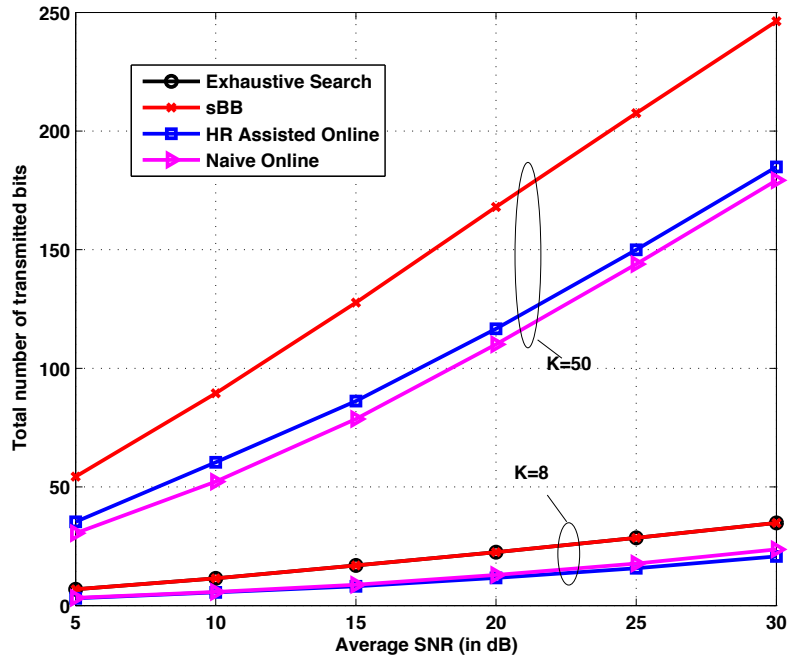

Figure 3.4: Link adaptive relaying: Total number of transmitted bits vs. average channel SNR $\bar{\gamma}$ for $K = 8$ and $K = 50$.

the naive online power allocation scheme has a small performance advantage over the HR assisted online algorithm for high $\bar{\gamma}$, whereas for $K = 50$, the HR assisted online algorithm shows better performance for all considered $\bar{\gamma}$.

3.5.3 Comparison Between Conventional and Link Adaptive Relaying

In this subsection, we compare the power allocation schemes proposed for conventional and link adaptive relaying. For offline power allocation, we compare the optimal schemes and for online power allocation, we compare the suboptimal schemes for conventional relaying with the HR assisted online scheme for link adaptive relaying. The optimal DP approach (for conventional relaying) is not included in the comparison

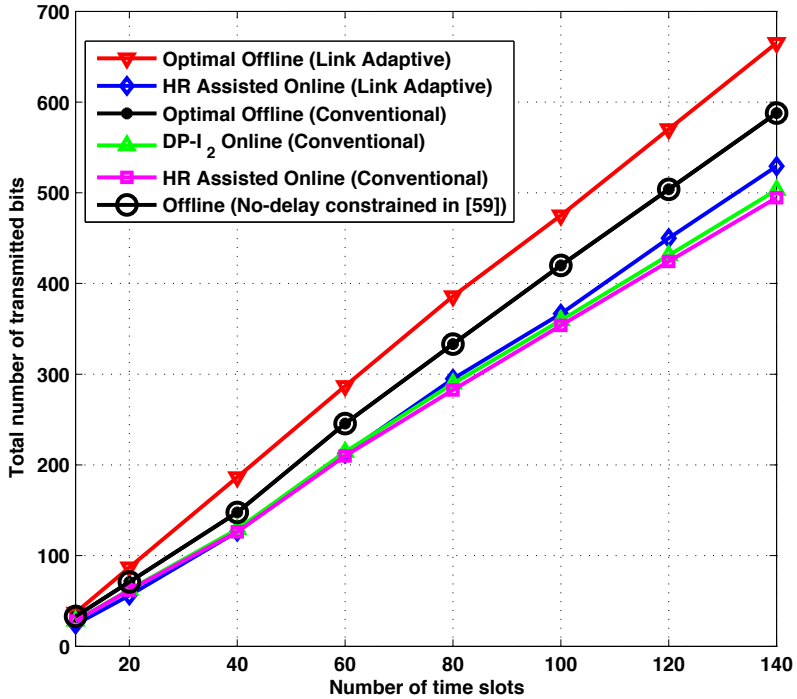

Figure 3.5: Comparison of conventional and link adaptive relaying: Total number of transmitted bits vs. number of time slots K for $\bar{\gamma}_S = \bar{\gamma}_R = \bar{\gamma} = 30$ dB.

because of its high complexity.

Total number of transmitted bits vs. K

Fig. 3.5 shows the total number of transmitted bits vs. the number of time slots, K for the offline and online power allocation schemes for conventional and link adaptive relaying. We assume symmetric S–R and R–D channels, i.e., $\bar{\gamma}_S = \bar{\gamma}_R = \bar{\gamma}$. We observe that link adaptive relaying significantly outperforms conventional relaying for offline power allocation. The performance gap increases with increasing K. This is mainly due to the fact that, for large K, we have more flexibility in selecting d_k, i.e., in selecting the S–R or R–D link for transmission to increase the system throughput.

In particular, for the offline case, the link adaptive relaying scheme can transmit 16 and 55 additional bits compared to conventional relaying for $K = 20$ and $K = 100$, respectively. For small K, the HR assisted online scheme for link adaptive relaying does not show a better performance than the online schemes for conventional relaying. However, for relatively large K, e.g. $K = 140$, the HR assisted online scheme for link adaptive relaying outperforms the DP–I_2 and HR assisted online schemes for conventional relaying by 26 and 34 bits, respectively. We note that the gain of link adaptive relaying over conventional relaying is the result of both power allocation and adaptive link selection since the power allocation affects the link selection and vice versa. Moreover, in Fig. 3.5, we have also included the performance of the no–delay constrained protocol in [59]. We observe that, because we assume a direct S–D link is not available, the performances of conventional relaying and the no–delay constrained protocol in [59] are identical for all considered values of K. This result was already shown in [59, Fig. 4] for non–fading channels and we arrive at the same result for fading channels.

In Fig. 3.6, we turn our attention to asymmetric links where we consider two scenarios for the average channel SNRs. Scenarios 1 and 2 are valid for $\bar{\gamma}_S = 20$ dB and $\bar{\gamma}_S = 10$ dB, respectively, where $\bar{\gamma}_R = 30$ dB in both cases. We compare the performance of the HR assisted online scheme for link adaptive relaying with that of the DP–I_2 and HR assisted schemes for conventional relaying. In contrast to Fig. 3.5, in Fig. 3.6, we observe that the HR assisted online scheme for link adaptive relaying outperforms the DP–I_2 (HR assisted) schemes even for small numbers of time slots, e.g. $K = 25$. Moreover, Fig. 3.6 clearly shows that the performance gains of the HR assisted online scheme for link adaptive relaying over the DP–I_2 (HR assisted) scheme for conventional relaying are significantly larger for asymmetric links compared to

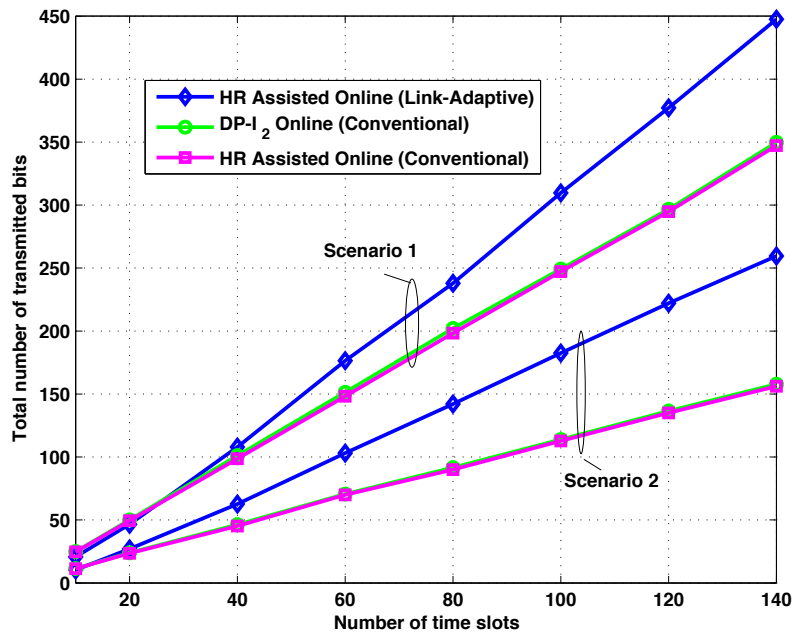

Figure 3.6: Comparison of online algorithms for conventional and link adaptive relaying: Total number of transmitted bits vs. number of time slots K for $\bar{\gamma}_S = 20$ dB (Scenario 1) and $\bar{\gamma}_S = 10$ dB (Scenario 2) with $\bar{\gamma}_R = 30$ dB.

symmetric links. The larger gains are caused by the flexibility introduced by the buffer at the relay. In the link adaptive scheme, the stronger link can be used less frequently since relatively large amounts of information can be transferred every time the link is used. Hence, the weaker link can be used more frequently to compensate for its poor link quality. In contrast, in conventional relaying, both links are used for the same amount of time regardless of their respective qualities.

Number of transmitted bits vs. H_E

Fig. 3.7 depicts the total number of transmitted bits for conventional and link adaptive relaying vs. the average harvesting rate, H_E, for $\bar{\gamma}_S = 10$ dB, $\bar{\gamma}_R = 30$ dB, and $K = 60$. We observe that the throughput increases with increasing H_E for all con-

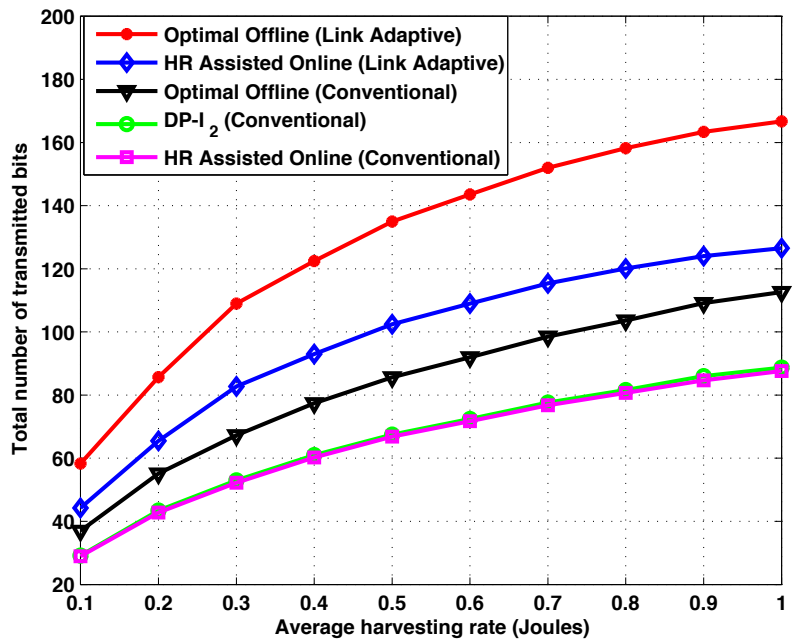

Figure 3.7: Comparison of conventional and link adaptive relaying: Total number of transmitted bits vs. H_E for $K = 60$, $\bar{\gamma}_S = 10$ dB, and $\bar{\gamma}_R = 30$ dB.

sidered power allocation schemes. We note that the slope of the throughput curves is large for small H_E and decreases with increasing H_E. This behavior is partially (apart from the behavior of the $\log(\cdot)$ function) due to the fact that the performance of all schemes is limited by the finite storage capability of the batteries. For large H_E, additional energy cannot be stored in the batteries and therefore the extra amount is wasted. We observe that the optimal offline and the HR assisted suboptimal online schemes for link adaptive relaying outperform the corresponding schemes for conventional relaying for all H_E.

In Fig. 3.8, we show the total number of transmitted bits vs. the average harvesting rate $H_S = H_R = H_E$ for $K = 1000$. Here, we study the performance of the HR assisted schemes for conventional and buffer–aided relaying for large K. We

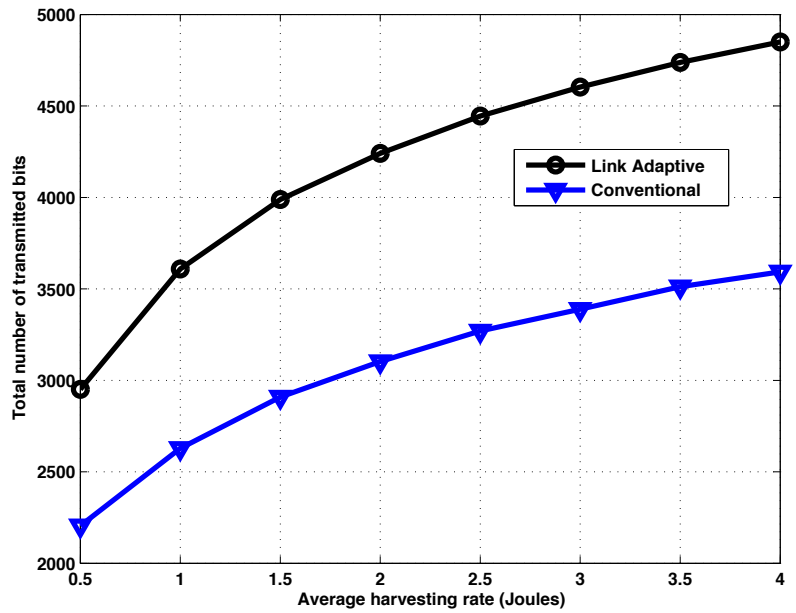

Figure 3.8: Comparison of the HR assisted online schemes for conventional and link adaptive relaying: Total number of transmitted bits vs. average harvesting rate for $K = 1000$, $\bar{\gamma}_S = 30$ dB, and $\bar{\gamma}_R = 15$ dB.

observe that, like for small K, buffer–aided link adaptive relaying also significantly outperforms conventional relaying for large K.

In Fig. 3.9, we show the performances of different power allocation schemes for both conventional and buffer–aided link adaptive relaying assuming that H_R changes over the time of transmission. In particular, we fix $H_S = 2$ Joules and linearly change H_R, from one transmission time interval to the next from a high value ($H_R = 2$ in $t1$) to a low value ($H_R = 0.25$ in $t5$) and then back to a high value ($H_R = 2$ in $t9$). Each transmission interval, $t1, t2, \cdots, t9$, lasts for $K = 50$ time slots. At the beginning of each transmission interval, ti, the proposed optimization schemes are executed and the total throughput during the $K = 50$ time slots is shown in Fig. 3.9. The change of H_R over time may model the impact that the change from cloudy weather ($t5$)

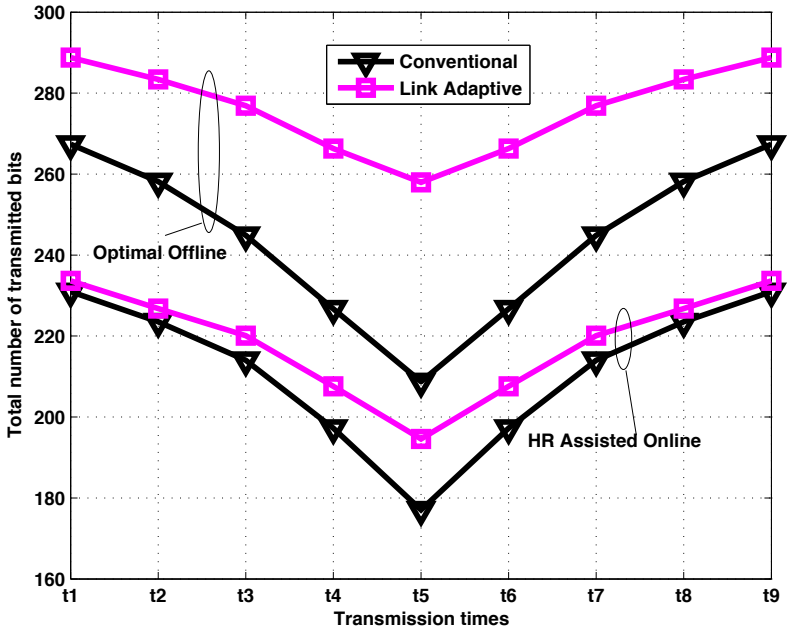

Figure 3.9: Total number of transmitted bits for offline and online power allocation schemes for conventional and link adaptive relaying when H_R changes over the time of transmission for $H_S = 2$ Joules, $K = 50$, and $\bar{\gamma}_S = \bar{\gamma}_R = 30$ dB.

to sunny weather ($t1$ and $t9$) has on a solar energy system. We observe that the throughput increases (decreases) with increasing (decreasing) H_R for both the offline and online power allocation schemes. Most importantly, the change in throughput is large for conventional relaying and small for link adaptive relaying. In fact, for link adaptive relaying, if the relay does not have enough energy to transmit data, the S–R link can be selected for transmission for several consecutive time slots and the received data at R is stored in the buffer and is forwarded to the destination at a later time. On the other hand, for conventional relaying, in each time slot, the source can only transmit the amount of data that the relay is able to forward to the destination. For this reason, the link adaptive protocol is able to cope better with sudden changes in the EH profile. Note that this behaviour is observed for both the

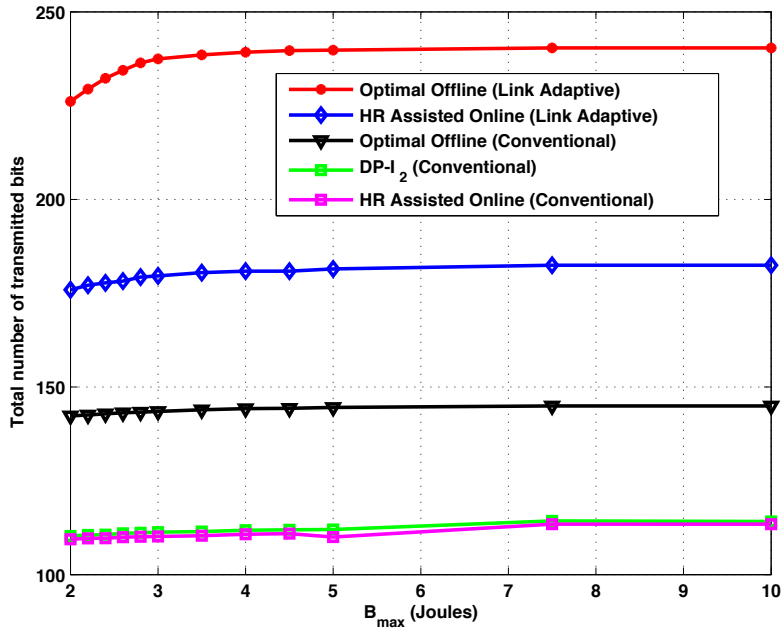

Figure 3.10: Comparison of conventional and link adaptive relaying: Total number of transmitted bits vs. B_{max} for $K = 100$, $\bar{\gamma}_S = 10$ dB, and $\bar{\gamma}_R = 30$ dB.

offline and the online schemes.

Total number of transmitted bits vs. B_{max}

In Fig. 3.10, we show the total number of transmitted bits for conventional and link adaptive relaying vs. B_{max} for $\bar{\gamma}_S = 10$ dB, $\bar{\gamma}_R = 30$ dB, and $K = 100$. We observe that for all considered power allocation schemes, the throughput first increases with increasing B_{max} but starting at a certain value of B_{max}, the throughput remains unchanged. This can be explained by the fact that for $H_E = 0.5$, small values of B_{max} limit the performance since the extra amount of harvested energy cannot be stored in the batteries. However, the constant throughput of all the schemes for large B_{max} indicates that, for the given parameters, increasing the storage capacities of the

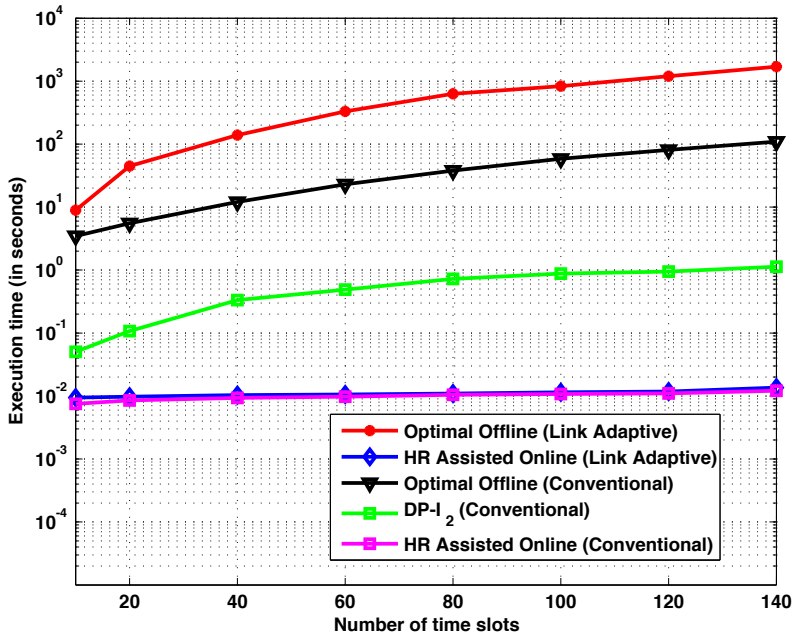

Figure 3.11: Comparison of execution times of conventional and link adaptive relaying: Execution time (in seconds) vs. number of time slots K for $\bar{\gamma} = 30$ dB.

batteries beyond a certain value does not improve the performance of the system. Therefore, Fig. 3.10 provides an indication for the required storage capacities of the batteries at S and R for different power allocation schemes to achieve a desired performance.

Execution time vs. K

In Fig. 3.11, we show the average execution time (in seconds) vs. the number of time slots, K, for all offline and online power allocation schemes for conventional and link adaptive relaying. We ran all the algorithms on the same computer system. In particular, all simulations were performed under MATLAB with the Intel(R) Core(TM) i7-2670QM (@2.20GHz 2.20GHz) processor. Therefore, it is reasonable to compare

the complexity of the algorithms based on their execution times. We observe that for both the offline and online schemes for both conventional and link adaptive relaying the execution time increases with K. Moreover, the required execution time for the sBB algorithm is higher than that for the offline scheme for conventional relaying for all K. The complexity of forming the look–up tables for the DP–I_2 scheme is not included in this analysis. Fig. 3.11 provides valuable information about the complexity–performance trade–off of the different proposed algorithms. For example, in case of conventional relaying, the HR assisted scheme is less complex than the DP–I_2 scheme with only a small performance degradation for sufficiently high average channel SNR and large K, see Fig. 3.3. Therefore, it is preferable to apply the HR assisted scheme compared to the DP–I_2 scheme. Moreover, although the worst case complexity of the sBB algorithm is exponential in K, from Fig. 3.11 we observe that its average complexity is comparable to that of the offline power allocation scheme for conventional relaying. Thus, for link adaptive relaying, we can conclude that the sBB algorithm is preferable over the exhaustive search method (which is not shown in Fig. 3.11 due to its very high execution time).

3.6 Conclusions

In this chapter, we considered the problem of transmit power allocation for single relay networks, where the source and the relay harvest the energy needed for transmission from the surrounding environment. Two different transmission strategies, namely conventional relaying and buffer–aided link adaptive relaying, were considered. We proposed optimal offline and optimal (conventional relaying) and several suboptimal online power allocation schemes maximizing the system throughput of the considered EH systems over a finite number of time slots. Simulation results showed

that the proposed suboptimal online schemes have a good complexity–performance trade–off. Moreover, we showed that, for both offline and online optimization, adopting the link adaptive protocol significantly improves the throughput compared to conventional relaying, especially for asymmetric link qualities, and buffer–aided link adaptive relaying is more robust to the changes in the EH profile than conventional relaying.

Chapter 4

Joint Power Allocation and Relay Selection in Energy Harvesting AF Relay Systems

4.1 Introduction

In Chapter 3, we have considered a single link EH DF relay system with two relaying protocols. In this chapter, we turn our attention to AF relay system. We consider a multi–relay network, where the source and the AF relays are EH nodes. Considering EH AF relays in this chapter helps us to compare relay selection strategies for systems powered by constant energy source, cf. Chapter 2 and energy harvester.

As mentioned in the Introduction of Chapter 3, a comprehensive performance analysis was provided in [81] for relay selection in an EH network. However, [81] derives the error rate expressions in a probabilistic manner, possibly with the consideration of large number of transmission time intervals. Moreover, as stated in Chapter 1, our focus in this thesis is to propose resource allocation schemes for a finite number of transmission time intervals for EH systems. The relay selection strategies described in [81] may not provide optimal results for finite number of time intervals for an EH relay network. Moreover, conventional relay selection methods

suitable for systems powered by constant energy sources [13, 98] cannot capture the fluctuating characteristics of the renewable energy over the time intervals, and hence cannot be applied in EH systems in a straight–forward manner. Therefore, in this chapter, we propose offline and online (real–time) joint relay selection and source and relay transmit power allocation schemes that maximize the end–to–end system throughput over a finite number of transmission intervals. The optimal relay selection policy depends on both the channel SNR and the amount of harvested energies stored at the batteries of the nodes.

The rest of this chapter is organized as follows. In Section 4.2, we discuss the considered system model. Sections 4.3 and 4.4 provide joint power allocation and relay selection schemes and simulation results, respectively. Section 4.5 concludes this chapter.

4.2 System Model

We consider an EH AF relay system with one source, S, one destination, D, and N half–duplex relays, R_n, $n \in \{1, 2, \cdots, N\}$. We assume that D is not an EH device and has continuous supply of power. S and R_n are EH devices and rely on the harvested energies to participate in signal transmission. The considered system model can be accommodated in different wireless communication systems, e.g., in wireless sensor networks, where an EH sensor node transmits data to the fusion centre via other EH sensor nodes [20]. In practice, a fusion centre can handle data from many sensor nodes and is powered by constant energy source. S and R_n are equipped with batteries with limited storage capabilities that can store at most $B_{S,max}$ and $B_{R_n,max}$ Joules of energy, respectively. We assume the transmission is organized in equal duration time intervals and each interval comprises two time slots of duration T. In

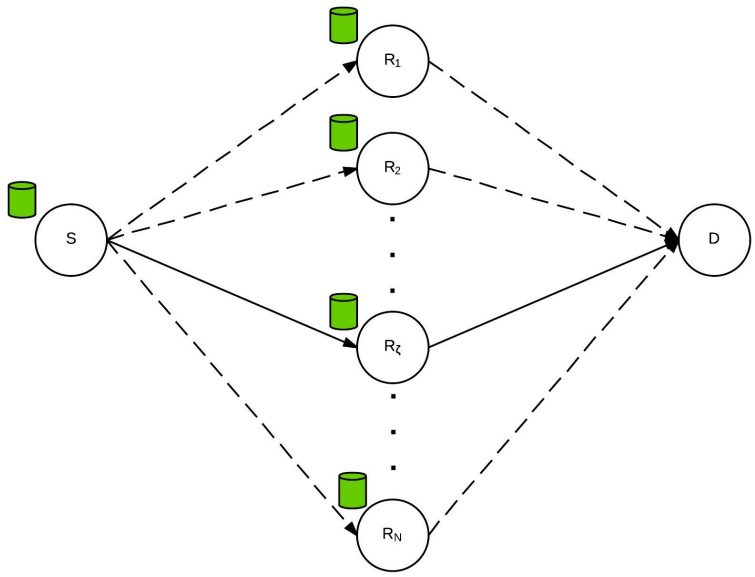

Figure 4.1: System model for a multi–relay communication network. Source, S, and relays, R_n, $n \in \{1, 2, \cdots, N\}$ are EH nodes. Solid line indicate the selected relay link.

the following, we set $T = 1$s. The total transmission time is equal to K intervals. We also assume that the transmitted packets contain Gaussian–distributed symbols and the transmission is impaired by AWGN. We define $\gamma_{SR_n,k}$ and $\gamma_{R_nD,k}$ as the channel SNRs of the S–R_n and R_n–D links in the kth interval, respectively. The transmit powers of S and R_n are denoted by $P_{S,k}$ and $P_{R_n,k}$, respectively. We assume the channels are quasi–static within each interval (block fading), are independent of each other, and may be non–identically distributed. However, $\gamma_{SR_n,k}$ ($\gamma_{R_nD,k}$) is identically distributed over the time intervals. For future reference, we introduce the average SNRs of the S–R_n and the R_n–D links as $\bar{\gamma}_{SR_n}$ and $\bar{\gamma}_{R_nD}$, respectively. In each time interval $k \in \{1, 2, \cdots, K\}$, a single relay, R_ζ, where $\zeta \in \{1, 2, \cdots, N\}$, is selected out of the N relays to forward the signals received from S to D. During the first time slot, S transmits and R_ζ receives, and during the second time slot, R_ζ transmits and

D receives. The end–to–end SNR, $\text{SNR}_{\text{eq},\zeta,k}$, at D is given by [74]

$$\text{SNR}_{\text{eq},\zeta,k} = \frac{P_{S,k}\gamma_{SR_\zeta,k}P_{R_\zeta,k}\gamma_{R_\zeta D,k}}{P_{S,k}\gamma_{SR_\zeta,k} + P_{R_\zeta,k}\gamma_{R_\zeta D,k} + 1} \tag{4.1}$$

Thus, the end–to–end (S–D) system throughput in interval k is given by $\frac{1}{2}\log_2(1 + \text{SNR}_{\text{eq},\zeta,k})$ bits/s/Hz. We also define $w_{n,k}$ as the relay selection variable which can be either 0 or 1. In particular, $w_{n,k} = 1$ ($w_{n,k} = 0$) indicates that R_n is selected (not selected) for transmission in time interval k.

Battery Dynamics: The battery energy of a node $\mathcal{N} \in \{S, R_1, R_2, \cdots, R_N\}$ in interval k is $B_{\mathcal{N},k}$. During transmission interval k, the transmit power of $\mathcal{N}$ is bounded by its battery energy, i.e., $0 \leq P_{\mathcal{N},k} \leq B_{\mathcal{N},k}$. We assume that the stored energy at $\mathcal{N}$ increases and decreases linearly provided the maximum storage capacity, $B_{\mathcal{N},max}$, is not exceeded, i.e.,

$$B_{\mathcal{N},k+1} = \min\{(B_{\mathcal{N},k} - P_{\mathcal{N},k} + H_{\mathcal{N},k}), B_{\mathcal{N},max}\}, \ \ \forall k. \tag{4.2}$$

In time interval k, the energy harvester at node $\mathcal{N}$ collects $H_{\mathcal{N},k} \leq B_{\mathcal{N},max}$ Joules of energy. $H_{\mathcal{N},k}$ is modelled as an ergodic random process with mean $H_{\mathcal{N}} \triangleq \mathcal{E}\{H_{\mathcal{N},k}\}$. $B_{\mathcal{N},1} = H_{\mathcal{N},0} \geq 0$ denotes the available energy at $\mathcal{N}$ before transmission starts.

4.3 Joint Power Allocation and Relay Selection

In this section, we present the proposed offline and online joint relay selection and power allocation algorithms.

4.3.1 Optimal Offline Optimization Algorithm

Our goal is to maximize the total number of transmitted bits (from S to D) delivered by a deadline of K intervals assuming offline knowledge of the full CSI and energy arrivals at S and R_n in each time interval. To this end, we formulate an offline optimization problem as

$$\max_{\mathcal{T}\succeq 0,\ w_{1,1},\cdots,w_{N,K}} \quad \sum_{k=1}^{K} \frac{1}{2}\log_2\left(1+\mathrm{SNR}_{\mathrm{eq},k}\right) \tag{4.3}$$

$$\text{s.t.} \quad \sum_{k=1}^{l}(P_{S,k}+\lambda_{S,k}) \leq \sum_{k=0}^{l-1} H_{S,k}, \ \ \forall l \tag{4.4}$$

$$\sum_{k=1}^{l}(w_{n,k}P_{R_n,k}+\lambda_{R_n,k}) \leq \sum_{k=0}^{l-1} H_{R_n,k}, \ \ \forall l, \ \ \forall n \tag{4.5}$$

$$\sum_{k=0}^{m} H_{S,k} - \sum_{k=1}^{m}(P_{S,k}+\lambda_{S,k}) \leq B_{S,max}, \ \forall m \tag{4.6}$$

$$\sum_{k=0}^{m} H_{R_n,k} - \sum_{k=1}^{m}(w_{n,k}P_{R_n,k}+\lambda_{R_n,k}) \leq B_{R_n,max}, \ \forall m, \ \forall n \tag{4.7}$$

$$\sum_{n=1}^{N} w_{n,k} = 1, \ \ \forall k \tag{4.8}$$

$$w_{n,k} \in \{0,1\}, \ \ \forall k, \ \forall n, \tag{4.9}$$

where $\mathrm{SNR}_{\mathrm{eq},k} \triangleq \sum_{n=1}^{N} \frac{w_{n,k}P_{S,k}P_{R_n,k}\gamma_{SR_n,k}\gamma_{R_nD,k}}{P_{R_n,k}\gamma_{R_nD,k}+P_{S,k}\gamma_{SR_n,k}+1}$ and $\mathcal{T} \triangleq \{P_{S,k},\ P_{R_1,k},\cdots,P_{R_N,k},\ \lambda_{S,k},\ \lambda_{R_1,k}\cdots,\lambda_{R_N,k} | k \in \{1,2,\cdots,K\}\}$. Also, $\forall l$, $\forall m$, $\forall n$, and $\forall k$ stand for $l \in \{1,2,\cdots,K\}$, $m \in \{1,2,\cdots,K-1\}$, $n \in \{1,2,\cdots,N\}$, and $k \in \{1,2,\cdots,K\}$, respectively. The slack variables $\lambda_{S,k}$ and $\lambda_{R_n,k}$ ensure that constraints (4.4)–(4.7) can be met for all realizations of $\gamma_{SR_n,k}$, $\gamma_{R_nD,k}$, $H_{S,k}$, and $H_{R_n,k}$. In particular, these slack variables represent the power (possibly) wasted in each transmission interval. Constraints (4.8) and (4.9) ensure that at a particular time interval k only one $w_{n,k}$ is equal to one, i.e., only one relay is selected. Constraints (4.4) and (4.5) ensure the causality of the

harvested energies at S and R_n, respectively. The (maximum) storage constraints for the batteries at both S and R_n are satisfied with constraints (4.6) and (4.7). To make the objective function of the optimization problem convex with respect to $P_{S,k}$ and $P_{R_n,k}$, we consider the following high SNR approximation:

$$\mathrm{SNR}_{\mathrm{eq},k} \approx \overline{\mathrm{SNR}}_{\mathrm{eq},k} \triangleq \sum_{n=1}^{N} \frac{w_{n,k} P_{S,k} P_{R_n,k} \gamma_{SR_n,k} \gamma_{R_n D,k}}{P_{R_n,k} \gamma_{R_n D,k} + P_{S,k} \gamma_{SR_n,k}}. \tag{4.10}$$

Problem (4.3)–(4.9) with $\mathrm{SNR}_{\mathrm{eq},k}$ replaced by $\overline{\mathrm{SNR}}_{\mathrm{eq},k}$ is a non–convex MINLP. The non–convexity arises due to the multiplicative form of $w_{n,k}$ and the power allocation variables of S and R_n in the objective function and the constraints. Due to the binary nature of $w_{n,k}$, the optimization problem in (4.3)–(4.9) can be recast as

$$\max_{\mathcal{T} \succeq 0,\ w_{1,1},\cdots,w_{N,K}} \quad \sum_{k=1}^{K} \frac{1}{2} \log_2 \left(1 + \overline{\overline{\mathrm{SNR}}}_{\mathrm{eq},k}\right) \tag{4.11}$$

$$\text{s.t.} \quad \sum_{k=1}^{l} (P_{R_n,k} + \lambda_{R_n,k}) \leq \sum_{k=0}^{l-1} H_{R_n,k}, \ \ \forall l, \ \ \forall n \tag{4.12}$$

$$\sum_{k=0}^{m} H_{R_n,k} - \sum_{k=1}^{m} (P_{R_n,k} + \lambda_{R_n,k}) \leq B_{R_n,max}, \ \forall m, \ \forall n \tag{4.13}$$

$$P_{R_n,k} \leq w_{n,k} \sum_{m=0}^{k-1} H_{R_n,m}, \ \ \forall k, \ \forall n \tag{4.14}$$

$$\text{Constraints (4.4), (4.6), (4.8), (4.9)} \tag{4.15}$$

where $\overline{\overline{\mathrm{SNR}}}_{\mathrm{eq},k} \triangleq \sum_{n=1}^{N} \frac{P_{S,k} P_{R_n,k} \gamma_{SR_n,k} \gamma_{R_n D,k}}{P_{R_n,k} \gamma_{R_n D,k} + P_{S,k} \gamma_{SR_n,k}}$. We note that constraint (4.14) relates the relay transmit power $P_{R_n,k}$ to the relay selection variable $w_{n,k}$. Specifically, when $w_{n,k} = 1$, i.e., relay R_n assists the source at time interval k, (4.12) and (4.13) are satisfied because (4.14) serves as an upper bound for $P_{R_n,k}$. On the other hand,

if $w_{n,k} = 0$, i.e., relay R_n is not selected to assist the source at time interval k, then constraint (4.14) automatically ensures that $P_{R_n,k} = 0$. Thus, the optimization problems in (4.3)–(4.9) with $\overline{\text{SNR}}_{\text{eq},k}$ and (4.11)–(4.15) are equivalent.

We observe that optimization problem (4.11)–(4.15) is a convex MINLP [75]. Furthermore, the continuous optimization variables, $\mathcal{T}$, can be linearly separated from the integer (binary) optimization variables $w_{n,k}$. Therefore, we can apply the GBD algorithm to solve this convex MINLP optimally [99, pp. 114–143]. GBD decomposes problem (4.11)–(4.15) into two sub–problems: a primal problem and a master problem. $P_{S,k}$, $P_{R_n,k}$, $\lambda_{S,k}$, and $\lambda_{R_n,k}$ are obtained by solving the primal problem for fixed values of $w_{n,k}$, which are obtained from the solution of the master problem. Solving the master problem gives $w_{n,k}$ for previously obtained $P_{S,k}$, $P_{R_n,k}$, $\lambda_{S,k}$, and $\lambda_{R_n,k}$ along with the corresponding Lagrange multipliers. GBD iteratively solves the primal problem and the master problem until their solutions converge. For the first iteration, a feasible initial value is adopted for the integer variables $w_{n,k}$. In the following, we describe the primal and master problems for a given iteration $i \in \{1, 2, \cdots, I\}$, where I is the number of iterations required for convergence of GBD.

Primal Problem (ith iteration): For the given optimal $w_{n,k}$ from iteration $i-1$, $w_{n,k}^{(i-1)*}$ (or a given initial $w_{n,k}^{(0)}$), we formulate the primal problem as follows

$$\max_{\mathcal{T} \succeq 0} \quad \sum_{k=1}^{K} \frac{1}{2} \log_2 \left(1 + \overline{\overline{\text{SNR}}}_{\text{eq},k}\right) \tag{4.16}$$

$$\text{s.t.} \quad \text{Constraints (4.4), (4.6), (4.12), (4.13)} \tag{4.17}$$

$$P_{R_n,k} \leq w_{n,k}^{(i-1)} \sum_{m=0}^{k-1} H_{R_n,m}, \ \forall k \text{ and } \forall n. \tag{4.18}$$

This is a convex optimization problem in $P_{S,k}$, $P_{R_n,k}$, $\lambda_{S,k}$, and $\lambda_{R_n,k}$ [75] and can

be solved optimally by any standard algorithm or solver, e.g., CVX [79]. Let $P_{S,k}^{(i)*}$, $P_{R_n,k}^{(i)*}$, $\lambda_{S,k}^{(i)*}$, and $\lambda_{R_n,k}^{(i)*}$ denote the optimal solutions at the ith iteration.

Master Problem (ith iteration): To formulate the master problem, we need the Lagrangian of the primal problem. The Lagrangian of the primal problem can be written as

$$\begin{aligned}
&\mathcal{L}(P_{S,k}, P_{R_n,k}, \lambda_{S,k}, \lambda_{R_n,k}, \xi_{S,l}, \xi_{R_n,l}, \eta_{S,m}, \eta_{R_n,m}, \alpha_{n,k}) = \\
&\sum_{k=1}^{K} \frac{1}{2} \log_2 \left(1+\sum_{n=1}^{N} \frac{P_{S,k} P_{R_n,k} \gamma_{SR_n,k} \gamma_{R_n D,k}}{P_{R_n,k} \gamma_{R_n D,k} + P_{S,k} \gamma_{SR_n,k}}\right) - \sum_{l=1}^{K} \xi_{S,l} \left(\sum_{k=1}^{l} (P_{S,k} + \lambda_{S,k}) - \sum_{k=0}^{l-1} H_{S,k}\right) \\
&- \sum_{n=1}^{N} \sum_{k=1}^{K} \alpha_{n,k} \left(P_{R_n,k} - w_{n,k} \sum_{m=0}^{k-1} H_{R_n,m}\right) - \sum_{n=1}^{N} \sum_{l=1}^{K} \xi_{R_n,l} \left(\sum_{k=1}^{l} (P_{R_n,k} + \lambda_{R_n,k})\right. \\
&\left. - \sum_{k=0}^{l-1} H_{R_n,k}\right) - \sum_{m=1}^{K} \eta_{S,m} \left(\sum_{k=0}^{m} H_{S,k} - \sum_{k=1}^{m} (P_{S,k} + \lambda_{S,k}) - B_{S,max}\right) - \sum_{n=1}^{N} \sum_{m=1}^{K} \eta_{R_n,m} \\
&\left(\sum_{k=0}^{m} H_{R_n,k} - \sum_{k=1}^{m} (P_{R_n,k} + \lambda_{R_n,k}) - B_{R_n,max}\right), \qquad (4.19)
\end{aligned}$$

where $\xi_{S,l}$, $\xi_{R_n,l}$, $\eta_{S,m}$, $\eta_{R_n,m}$, and $\alpha_{n,k}$ represent the Lagrange multipliers associated with constraints (4.4), (4.12), (4.6), (4.13), and (4.14), respectively. Let the optimal solution of the Lagrange multipliers of the primal problem be $\xi_{S,l}^*$, $\xi_{R_n,l}^*$, $\eta_{S,m}^*$, $\eta_{R_n,m}^*$, and $\alpha_{n,k}^*$. For a given $P_{S,k}^{(i)*}$, $P_{R_n,k}^{(i)*}$, $\lambda_{S,k}^{(i)*}$, $\lambda_{R_n,k}^{(i)*}$, $\xi_{S,l}^{(i)*}$, $\xi_{R_n,l}^{(i)*}$, $\eta_{S,m}^{(i)*}$, $\eta_{R_n,m}^{(i)*}$, and $\alpha_{n,k}^{(i)*}$, we formulate the master problem as follows

$$\max_{\beta_M \geq 0,\ w_{1,1},\cdots,w_{N,K}} \quad \beta_M \qquad (4.20)$$

$$\text{s.t.} \quad \beta_M \leq \mathcal{L}(P_{S,k}^{(j)*}, P_{R_n,k}^{(j)*}, \lambda_{S,k}^{(j)*}, \lambda_{R_n,k}^{(j)*}, \xi_{S,l}^{(j)*}, \xi_{R_n,l}^{(j)*}, \eta_{S,m}^{(j)*}, \eta_{R_n,m}^{(j)*}, \alpha_{n,k}^{(j)*}),\ j \in \{1,2,\cdots,i\} \qquad (4.21)$$

$$\text{Constraints (4.8), (4.9).} \qquad (4.22)$$

Now, problem (4.20)–(4.22) is a mixed integer linear problem (MILP) of $w_{n,k}$ and β_M and therefore it can be solved optimally by any standard optimization toolbox, e.g., MOSEK [100].

GBD Algorithm: At iteration i, the optimal solution of master problem (4.20)–(4.22) is $\beta_M^{(i)*}$, which is an upper bound for the optimum of problem (4.11)–(4.15). Moreover, at each iteration, the master problem has one additional constraint compared to those defined in the previous iteration. Thus, the newly obtained optimum of the master problem is always less than or equal to the previous one and therefore this upper bound is always non–increasing. On the other hand, the primal problem in (4.16)–(4.18) provides the solution for fixed integer variables and therefore, the optimum of the primal problem is always equal to or less than the optimum of the original problem in (4.11)–(4.15). Thus, the solution of the primal problem always gives a lower bound for the solution of the original problem. We set the lower bound at each iteration equal to the maximum of the lower bound of the previous iteration and the lower bound of the current iteration. At each iteration, we solve the primal problem with the given solution of the master problem from the previous iteration. Then, we solve the master problem with the given solution of the primal problem. This process continues and within a finite number of iterations, the GBD algorithm converges to the optimal solution due to the monotonicity of the upper and lower bounds [90]. We summarize the GBD algorithm in Algorithm 4.1.

We note that due its convexity, the primal problem can be solved in polynomial time whereas the master problem has non–polynomial complexity as it requires solving an integer problem. Nevertheless, since the GBD algorithm is executed offline, efficient commercial optimization software such as MOSEK can be used to solve the master problem efficiently [100].

Algorithm 4.1 : GBD Method

Initialization: $w_{n,k}^{(0)}$, convergence parameter, ϵ, $I \leftarrow \phi$ and $i \leftarrow 1$.
flag $\leftarrow 1$.
while flag $\neq 0$ **do**
    Solve primal problem (4.16)–(4.18) and obtain $P_{S,k}^{(i)*}$, $P_{R_n,k}^{(i)*}$, $\lambda_{S,k}^{(i)*}$, $\lambda_{R_n,k}^{(i)*}$, $\xi_{S,l}^{(i)*}$, $\xi_{R_n,l}^{(i)*}$, $\eta_{S,m}^{(i)*}$, $\eta_{R_n,m}^{(i)*}$, $\alpha_{n,k}^{(i)*}$ and the lower bound, $\mathrm{LB}^{(i)}$.
    $I \leftarrow I \cup \{i\}$.
    Solve master problem (4.20)–(4.22) and obtain $w_{n,k}^{(i)*}$ and the upper bound, $\mathrm{UB}^{(i)}$.
    if $|\mathrm{UB}^{(i)} - \mathrm{LB}^{(i)}| \leq \epsilon$ **then**
        flag $\leftarrow 0$.
    end if
    Set $i \leftarrow i + 1$.
end while

4.3.2 Suboptimal Online Optimization Algorithms

In practice, only causal information of channels and harvested energies is available. Therefore, the offline power allocation scheme is not readily applicable as the future CSI and the upcoming harvested energies are not known in advance. In principle, the optimal online algorithm may be implemented with stochastic DP. However, DP entails a high complexity due to the joint relay selection and power allocation. Thus, to avoid the high complexity of DP, we propose suboptimal HR assisted and naive online schemes.

HR Assisted Scheme

In this scheme, we jointly allocate the source and relay transmit powers and select the best relay based on the causal information of stored energies and channel SNRs as well as the average EH rates and the average channel SNRs. In particular, in order to ensure that source and relays have (with high probability) sufficient energy for transmission in their batteries without being overly conservative in the power

allocation, we limit the maximum transmit power based on the average energy HR $H_{\mathcal{N}}$, $\mathcal{N} \in \{S, R_1, \cdots, R_N\}$. This is straightforward for the source, where we impose $P_{S,k} \leq H_S$, as the source transmits in every time interval. In contrast, only one of the N available relays transmits in a given time interval. Thus, if we denote the probability of selecting relay n by f_n, the resulting relay power constraint is $w_{n,k}P_{R_n,k} \leq H_{R_n}/f_n$. An analytical expression for f_n is given by (2.23) in Chapter 2. Unfortunately, f_n does not only depend on the average channel SNRs but also on the transmit powers, which renders the overall problem highly non–convex. To avoid the complexity associated with this non–convexity, we approximate the source and relay transmit powers by H_S and NH_{R_n}, $n \in \{1, 2, \cdots, N\}$, respectively, which makes f_n independent of $P_{S,k}$ and $P_{R_n,k}$. Based on these considerations, the optimization problem for time interval k is formulated as

$$\max_{[P_{R_1,k},\cdots,P_{R_N,k}]\succeq 0,\ w_{1,k},\cdots,w_{N,k}} \quad \frac{1}{2}\log_2\left(1+\overline{\mathrm{SNR}}_{\mathrm{eq},k}\right) \tag{4.23}$$

$$\text{s.t.} \qquad P_{S,k} \leq B_{S,k},\ P_{S,k} \leq H_S, \tag{4.24}$$

$$w_{n,k}P_{R_n,k} \leq B_{R_n,k},\ w_{n,k}P_{R_n,k} \leq \tau H_{R_n}/f_n,\ \forall n \tag{4.25}$$

$$\sum_{n=1}^{N} w_{n,k} = 1,\ w_{n,k} \in \{0,1\},\ \forall n, \tag{4.26}$$

where τ is a scaling factor that can be optimized to further improve performance. As $\overline{\mathrm{SNR}}_{\mathrm{eq},k}$ in the objective function in (4.23) is an increasing function of $P_{S,k}$, the optimal $P_{S,k}$ can be obtained as

$$P^*_{S,k} = \min\left\{B_{S,k}, H_S\right\}. \tag{4.27}$$

Based on (4.27) and a change of variables, optimization problem (4.23)–(4.26) can be rewritten as

$$\max_{[P_{R_1,k},\cdots,P_{R_N,k}]\succeq 0,\ w_{1,k},\cdots,w_{N,k}} \frac{1}{2}\log_2\left(1+\overline{\overline{\mathrm{SNR}}}_{\mathrm{eq},k}\right) \tag{4.28}$$

$$\text{s.t.} \quad P_{R_n,k} \leq w_{n,k}\Gamma_{n,k},\ \ \forall n,\ \text{constraint (4.26)},\ \text{and}\ P_{S,k} = \min\left\{B_{S,k}, H_S\right\}, \tag{4.29}$$

where $\Gamma_{n,k} = \min\left\{B_{R_n,k}, \tau H_{R_n}/f_n\right\}$. For a given τ, problem (4.28), (4.29) is a convex MINLP and therefore, to solve it, we can use GBD by following the same procedure as for the offline optimization problem [90, pp. 114–143]. We note that problem (4.28), (4.29) is not a function of K, hence the complexity of the involved GBD algorithm is much lower than that of the GBD algorithm for the offline optimization problem. Moreover, for a given $w_{n,k}$, problem (4.28), (4.29) is convex in $P_{R_n,k}$ and the optimal $P_{R_n,k}$ is obtained as $P^*_{R_n,k} = w_{n,k}\Gamma_{n,k}$. Therefore, as an alternative to GBD, for each k, we can calculate the objective function in (4.28) with $P^*_{R_n,k}$ for all combinations of $w_{n,k}$, $n \in \{1, 2, \cdots, N\}$, and select the combination that gives the best result. For given channel and EH statistics, parameter τ can be optimized offline to maximize performance. However, we found that $\tau = 0.86$ gives high performance for a wide range of channel and EH parameters.

Naive Scheme

In this scheme, the source and the relays use their stored energies as their transmit powers in each time interval. Using these transmit powers, we calculate the equivalent SNRs for all links. Then, we select the relay which provides the maximum equivalent SNR among all the relays. The complexity of this scheme is linear in K.

4.3.3 Extension to Multiple Relay Selection

We extend the idea of single relay selection (and power allocation) scheme to multiple relay selection (and power) allocation scheme with necessary modifications in the optimization problems. We assume that when more than one relay is selected, the transmission happens over the orthogonal time slots. To select $N_S \leq N$ relays, we adopt $\sum_{k=1}^{K}(1/(N_S+1))\log_2(1+\overline{\overline{\mathrm{SNR}}}_{\mathrm{eq},k})$ and $(1/(N_S+1))\log_2(1+\overline{\overline{\mathrm{SNR}}}_{\mathrm{eq},k})$ in (4.11) and (4.28), respectively. Moreover, we incorporate $\sum_{n=1}^{N} w_{n,k} = N_S$ in (4.8) and (4.26). The offline and online optimization problems for joint multiple relay selection and power allocation can also be solved by GBD optimally. Moreover, when $N_S = N$, i.e., all relays participate in transmission, the offline and online optimization problems lead to convex optimization problems and hence can be solved optimally and efficiently.

4.4 Simulation Results

In this section, we evaluate the performance of the proposed offline and online joint relay selection and power allocation schemes for the considered AF relay system. In Figs. (4.2)–(4.4), we assume that the average HR is $H_S = H_{R_1} = \cdots = H_{R_N} = H_E =$ 0.5 Joule, and $H_{S,k}$ and $H_{R_n,k}$ independently take values from the set $\{0, H_E, 2H_E\}$, where all elements of the set are equiprobable. We adopt $B_{S,max} = B_{R_1,max} = \cdots = B_{R_N,max} = B_{max} = 100$ Joules and set $\tau = 0.86$. We consider exponentially distributed channel SNRs and show the performance of the proposed schemes for three different scenarios for N and the channel SNRs. We simulate 10^4 realizations of randomly generated S–R_n and R_n–D channel SNRs and harvested energies at S and R_n to obtain the average throughput. We consider three scenarios with three different values of N. In Scenario 1, we assume $N = 1$ and $\bar{\gamma}_{SR_1} = \bar{\gamma}_{R_1D} = \bar{\gamma}$ where $\bar{\gamma} = 10$ dB.

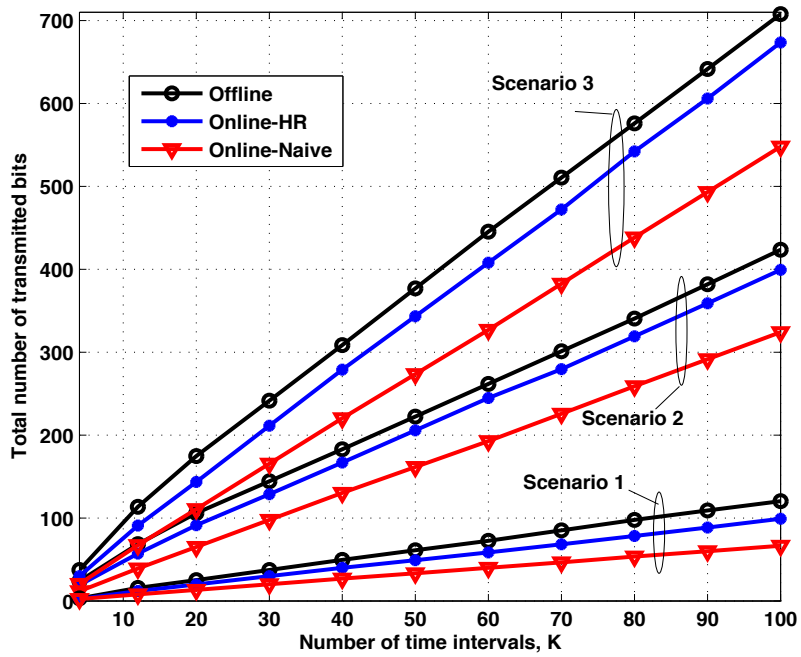

Figure 4.2: Total number of transmitted bits vs. number of time intervals K for $\bar{\gamma} = 10$ dB and average harvesting rate $H_E = 0.5$ Joule.

In Scenario 2, we assume $N = 3$ where the SNRs of the first link are the same as in Scenario 1 and for links 2 and 3, we assume $\bar{\gamma}_{SR_2} = \bar{\gamma}_{SR_3} = \bar{\gamma}_{R_2D} = \bar{\gamma}_{R_3D} = \bar{\gamma} + 10\,\text{dB}$. In Scenario 3, we assume $N = 5$ where the first 3 links are identical to the links of Scenario 2 and the SNRs of links 4 and 5 are $\bar{\gamma}_{SR_4} = \bar{\gamma}_{SR_5} = \bar{\gamma}_{R_4D} = \bar{\gamma}_{R_5D} = \bar{\gamma} + 20\,\text{dB}$. In Figs. 4.2 and 4.4, we consider all three scenarios, whereas Figs. 4.3 and 4.5 include only Scenario 3.

In Fig. 4.2, we show the total number of transmitted bits vs. the number of time intervals, K. From Fig. 4.2, we observe that the throughput increases with increasing K and increasing N for all considered joint power allocation and relay selection schemes. Furthermore, as expected, for each scenario, the optimal offline scheme is a performance upper bound for both online schemes. However, the HR assisted

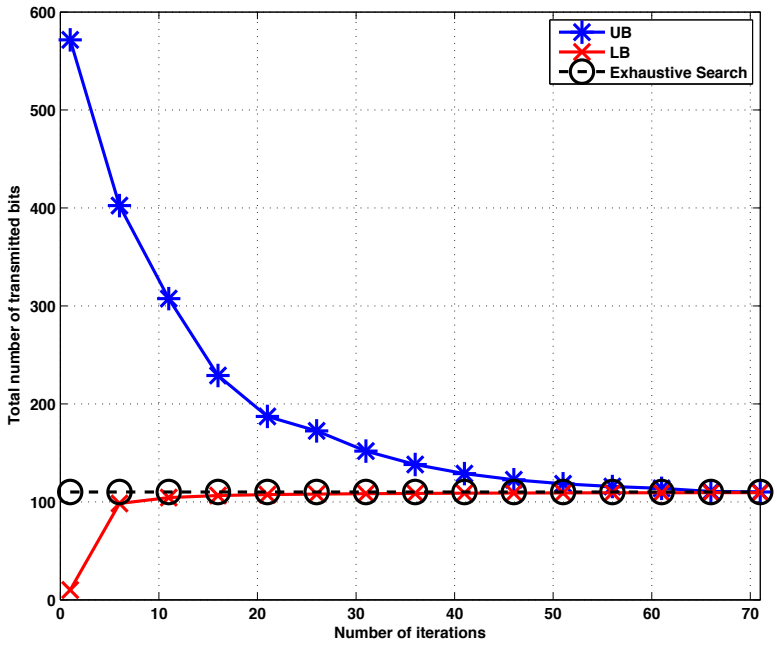

Figure 4.3: Convegence behavior of GBD vs. the number of iterations for $K = 10$, $\bar{\gamma} = 10$ dB, $N = 5$, and average harvesting rate $H_E = 0.5$ Joule.

scheme closely approaches the offline scheme and yields a significant gain compared to the naive scheme. This gain is caused by the more efficient use of the harvested energy by the HR assisted scheme compared to the naive scheme. In particular, the HR assisted scheme limits the source and relay transmit powers taking into account the statistical properties of the channels and the harvested energies. In contrast, the naive scheme spends in each time interval all energy stored in the batteries of the source and the selected relay.

In Fig. 4.3, we show the convergence behavior of GBD algorithm, which is adopted in the offline scheme. We assume $K = 10$ and consider only one realization of channel SNRs and harvested energies. The upper bound and the lower bound come from the solutions of the master and the primal problems, respectively. We observe

that with the number of iterations, the upper bound decreases and the lower bound increases and converge at the optimal solution. For the considered example in this figure, we see the convergence is reached at the 66th iteration. We also include the throughput performance of an exhaustive search method. In the exhaustive search method, we search over all the combinations of the relay selection variables, $w_{n,k}$ and select that combination which yields the best throughput. Note that for a given $w_{n,k}$, $n \in \{1, 2, \cdots, N\}$ and $k \in \{1, 2, \cdots, K\}$, problem (4.11)–(4.15) is convex and hence can be solved optimally and efficiently. We observe that the throughput obtained from GBD algorithm exactly matches with the throughput obtained from the exhaustive search method. This finding confirms that GBD algorithm finds the global optimum solution for convex MINLP [99].

In Fig. 4.4, we compare our proposed HR assisted scheme with a baseline scheme. In the baseline scheme, we assume that the relay, $\zeta \in \{1, 2, \cdots, N\}$ is selected according to the maximum bottleneck SNR of all the links as follows[16]:

$$\zeta = \underset{n \in \{1,\ldots,N\}}{\arg\max} \{\min\{\gamma_{SR_n,k}, \gamma_{R_nD,k}\}\}. \tag{4.30}$$

For the given relay selection policy in (4.30), we solve problem (4.28), (4.29) to obtain optimal power allocation policy. We observe that in Scenario 1, the proposed scheme and the baseline scheme show the identical results, as for $N = 1$, the relay is always selected for transmission. However, in Scenarios 2 and 3, we observe that the proposed scheme outperforms the baseline scheme. The baseline scheme does not take into the account the energy state of the batteries at the relays and selects the relay according to the CSI. Therefore, it is likely for the baseline scheme to select a relay that has a little amount of energy in its battery but has a better channel

[16]Note that this is the BRS scheme considered in Chapter 2.

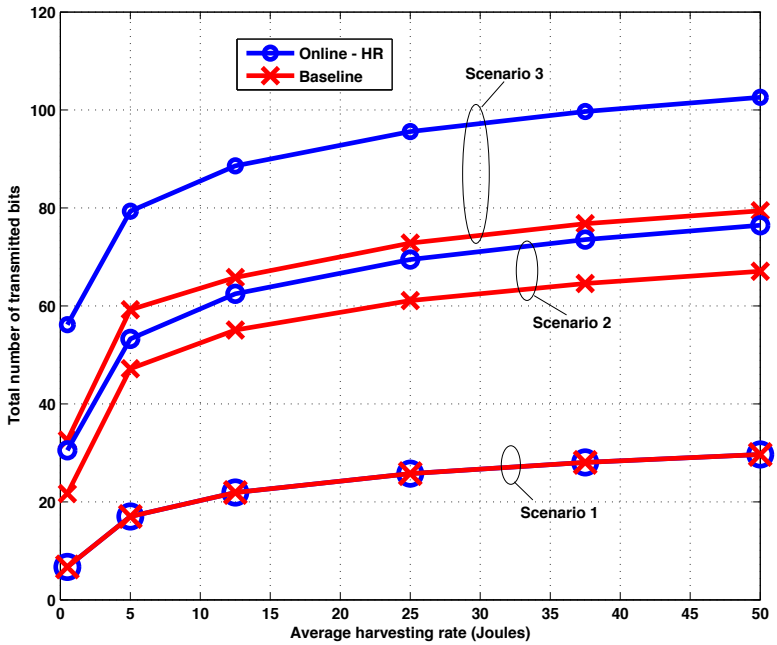

Figure 4.4: Total number of transmitted bits vs. average harvesting rate H_E for $K = 10$ and $\bar{\gamma} = 10$ dB.

condition for transmission. This policy of relay selection for EH nodes degrades the throughput performance. On the other hand, our proposed scheme considers both the channel condition and the battery states to perform joint relay selection and power allocation. This feature helps the proposed scheme to perform better than the baseline scheme. Moreover, we observe that the performance gain of the proposed scheme over the baseline scheme is large for Scenario 3 compared to Scenario 2 due to large number of relays participate in Scenario 3.

Fig. 4.5 shows the throughput (bits/sec) of the single and multiple relay selection schemes. Here, we assume $H_S = 1$ Joule, $H_{R_1} = 0.5$ Joule, $H_{R_2} = H_{R_3} = 0.7$ Joule, $H_{R_4} = H_{R_5} = 1$ Joule and adopt Scenario 3. We observe that the throughput degrades with the increasing number of selected relays. Selecting more than one relay

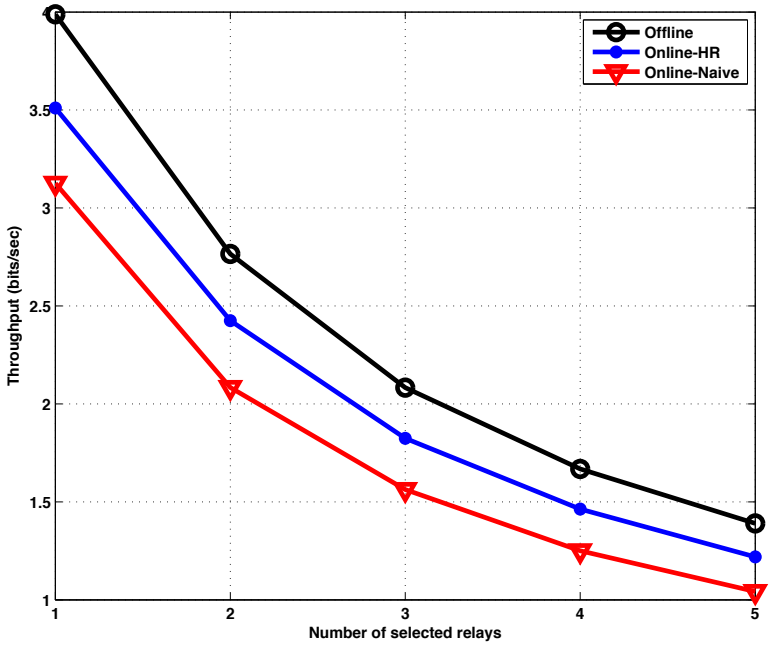

Figure 4.5: Throughput (bits/sec) vs. number of selected relays for $K = 30$, $\bar{\gamma} = 10$ dB, and $N = 5$.

requires large number of time slots for transmission and hence degrades the spectral efficiency. This observation was already known for contant energy source [67], but is new for EH systems.

4.5 Conclusion

In this chapter, we proposed offline and online joint relay selection and transmit power allocation schemes for EH AF relay system. Our offline optimization framework is based on GBD algorithm, which provides optimal results for convex MINLP. We proposed suboptimal but low–complexity HR assisted scheme, which performs close to the offline scheme. We compared the HR assisted scheme with a baseline scheme

and showed by simulations that the relay selection policy for EH system should exploit not only the CSI but also the energy state of the batteries for a better performance.

Chapter 5

Power Allocation for an Energy Harvesting Transmitter with Hybrid Energy Sources

5.1 Introduction

Green communication has attracted significant attention in academia and industry as the rapidly increasing energy consumption of the equipment in wireless communication systems has raised environmental concerns [8, 12]. In the literature, a number of power allocation schemes, which aim to provide a balance between energy consumption and performance, have been reported for different wireless communication systems [101]–[104]. Most of these works assume that the energies are supplied by a constant energy source and/or a rechargeable battery. As mentioned in the earlier chapters, recently EH has attracted considerable interest as an environmentally friendlier supply of energy for communication nodes compared to traditional sources of energy. The harvested energy is practically free of cost and can ensure a perpetual supply of energy.

In Chapters 3 and 4, we have assumed that EH is the only source of energy for the communication nodes. Furthermore, most of the works on communication

systems with EH capability [17, 18, 58, 59, 105, 106] analyze wireless communication systems that are powered solely by the EH nodes. However, from a practical point of view, to achieve both reliable and green communication, it is desirable to have a hybrid source of energy due to the intermittent nature of the harvested energy, cf. [107]. A hybrid energy source is a combination of a constant energy source, e.g., power grid, diesel generator etc., and an EH source which harvests energy from solar, wind, thermal, or electromechanical effects. The concept of hybrid energy sources has also drawn interest from industry. For instance, Huawei has already developed base stations for rural areas which draw their energy from both solar panels and diesel generators [108]. Motivated by these considerations, in this chapter, we consider a single communication link where the transmitter (e.g. a base station) is equipped with a hybrid energy source, cf. Fig. 5.1(a), which comprises a constant energy source and an energy harvester. The constant energy source is assumed to be fed by a costly and/or non–environmentally friendly generator, e.g., a diesel fuel power generator in a remote location or a nuclear power plant. In contrast, the harvested energy is green and stems from a sustainable source of energy.

In this chapter, our aim is to minimize the amount of energy drawn from the constant energy source, such that the harvested energy is efficiently utilized for transmitting a given number of data packets over a finite number of transmission intervals. We assume that there is a battery in the hybrid energy source to store the harvested energy. We consider a non–ideal battery which may leak a fraction of the stored energy over time. Thereby, the leakage depends on the charging and/or discharging effect, the chemical properties of the material, etc. [109, 110]. Note that our problem formulation is different from that in [17, 18, 58, 59, 105, 106] and [85, 109, 110], as [17, 18, 58, 59, 105, 106] and [85, 109, 110] consider throughput maximization and/or

transmission time minimization for communication systems employing EH sources only without exploiting a constant energy source. The solution of the optimization problem considered in this chapter provides insights regarding the optimal power allocation policy for communication systems with hybrid energy sources and thereby facilitates the design of reliable green communication systems.

We consider two scenarios for the arrival process of the data packets into the data queue at the transmitter. In Scenario 1, the data packets that have to be transmitted arrive before the transmission begins and no packets arrive during the transmission, cf. Fig. 5.1(b). In Scenario 2, the data packets may arrive during the course of transmission, cf. Fig. 5.1(c). For both scenarios, we derive offline and online (real–time) power allocation schemes that minimize the total amount of energy drawn from the constant energy source. We propose optimal online power allocation schemes for both considered scenarios using a stochastic DP approach. To avoid the high complexity inherent to DP, we also propose suboptimal online algorithms.

The remainder of this chapter is organized as follows. In Section 5.2, the system model for the EH system is presented. Offline and online power allocation schemes for Scenarios 1 and 2 are provided in Sections 5.3 and 5.4, respectively. In Section 5.5, the effectiveness of the proposed power allocation schemes is evaluated based on simulations. Section 5.6 concludes this chapter.

5.2 System Model

System Description: We consider a single communication link, where a transmitter (source), S, communicates with a receiver (destination), D, as shown in Fig. 5.1(a). We assume that S has a data queue with infinite capacity which can store data packets temporarily before their transmission. The energy required by S for signal

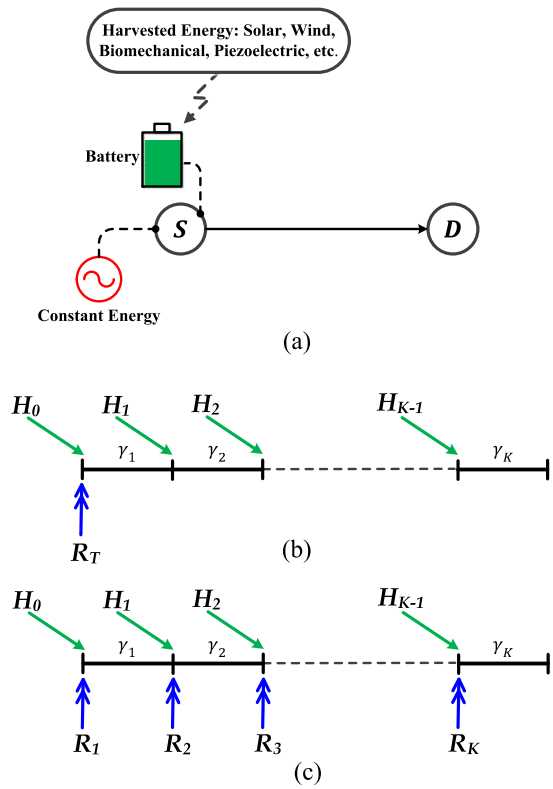

Figure 5.1: (a) System model for a communication link where the transmitter has a hybrid energy supply. (b) Illustration of Scenario 1 with K transmission intervals, channel SNRs γ_k, and harvested energies H_k, where $k \in \{1, 2, \cdots, K\}$. Here, R_T bits arrive before transmission begins. (c) Illustration of Scenario 2. Here, R_k bits arrive just before time interval, k.

transmission and processing is supplied by a hybrid source of energy. The hybrid source includes a constant energy source, possibly connected through a cable to the power grid, and an EH module which harvests energy from the surroundings. The harvested energy is stored in a battery that can store at most B_{max} Joules of energy. We consider a deadline of K transmission intervals and assume that data transmission is packet based. The duration of each transmission interval is T and without loss of generality, we assume $T = 1$s.

We consider two scenarios for packet arrivals. In Scenario 1, we assume that R_T

bits have arrived at S before the transmission starts and have to be transmitted in K transmission intervals, cf. Fig. 5.1(b). We assume that additional bits do not arrive during the transmission. On the other hand, in Scenario 2, we assume that R_k bits arrive immediately before transmission interval k, where $k \in \{1, 2, \cdots, K\}$, and all bits have to be transmitted by the end of the last transmission interval K, cf. Fig. 5.1(c).

Channel Model: We assume that the transmitted packets contain Gaussian distributed symbols and the transmission is impaired by AWGN. Let γ_k denote the channel SNR of the S–D link, which is assumed to be i.i.d. over the time intervals. For future reference, we introduce the average SNR of the S–D link as $\bar{\gamma}$. We denote total transmit power in interval $k \in \{1, 2, \cdots, K\}$ by $P_{E,k} + P_{H,k}$, where $P_{E,k}$ and $P_{H,k}$ are supplied by the constant energy source and the energy harvester, respectively. Furthermore, the total powers drawn from the constant energy source and the EH source are given by $\rho P_{E,k}$ and $\rho P_{H,k}$, respectively. Here, $\rho \geq 1$ is a constant that accounts for the inefficiency of the non–ideal power amplifier. For instance, if $\rho = 2$, 100 Watts of power are consumed in the power amplifier for every 50 Watts of power radiated in the radio frequency, and the efficiency of the power amplifier in this case is $\frac{1}{\rho} = 50\%$. We assume that the power required for signal processing at the transmitter, which is constant in each time interval, is supplied by the constant energy source and is excluded from the power allocation algorithm design.

Hybrid Energy Model: We assume that E_k is the maximum energy that can be drawn from the constant energy source in each interval, excluding the required constant signal processing power[17]. On the other hand, the energy harvester at S collects $H_k \leq B_{max}$ Joules of energy from its surroundings at the end of the

[17]We consider the general case where E_k may change from one transmission interval to the next. However, for the simulation results shown in Section 5.5, we assume a constant energy supply, i.e., $E_k = E$, $\forall k$.

kth interval. H_k is modeled as an ergodic random process with average EH rate $H_S \triangleq \mathcal{E}\{H_k\}$. Due to the inefficiency of the battery, a fraction of the stored harvested energy may be lost. We adopt the energy loss model from [111, 112] to incorporate the imperfections of the battery. We assume that a factor of $1-\mu$ of the stored harvested energy is leaked per time interval, where $0 \leq \mu < 1$ represents the efficiency of the battery per time interval. Similar to [18], we assume that the harvested energy stored in the battery increases and decreases linearly provided the maximum storage capacity B_{max} is not exceeded, i.e.,

$$B_{k+1} = \min\{\mu(B_k - \rho P_{H,k}) + H_k, B_{max}\}, \ \forall k, \tag{5.1}$$

where $B_1 = H_0 \geq 0$ denotes the available energy before transmission starts. Thus, B_k follows a first–order Markov process which depends only on the current state of the battery. Due to the finite storage capacity and the leakage of the battery, it is beneficial to draw the energy for packet transmission as quickly as possible from the battery so that more harvested energy can be stored in the future, and thus the amount of possibly wasted harvested energy is minimized.

5.3 Offline Power Allocation

In this section, we develop offline power allocation strategies for Scenarios 1 and 2. For offline power allocation, it is assumed that both the causal and the non–causal information regarding the channel SNR and the harvested energy are available a priori. For offline power allocation, Scenario 1 may be viewed as a special case of Scenario 2 by setting $R_1 = R_T$ and $R_k = 0$, where $k = 2, 3, \cdots, K$. Hence, we only formulate and describe the optimization problem for Scenario 2 in detail. We then

obtain the solution for Scenario 1 by setting $R_1 = R_T$ and $R_k = 0$, $k = 2, 3, \cdots, K$, see Section 5.3.2.

5.3.1 Offline Power Allocation for Scenario 2

We formulate the offline optimization problem for Scenario 2 as follows:

$$\min_{P_{E,k}\geq 0,\ P_{H,k}\geq 0,\ \lambda_{H,k}\geq 0} \quad \sum_{k=1}^{K} \rho P_{E,k} \tag{5.2}$$

$$\text{s.t.} \quad \sum_{k=1}^{q} \log_2(1+\gamma_k(P_{E,k}+P_{H,k})) \leq \sum_{k=1}^{q} R_k,\ \forall q \tag{5.3}$$

$$\sum_{k=1}^{K} \log_2(1+\gamma_k(P_{E,k}+P_{H,k})) = \sum_{k=1}^{K} R_k \tag{5.4}$$

$$\sum_{k=1}^{l} \rho\mu^{l-k} P_{H,k} \leq \sum_{k=0}^{l-1} \mu^{l-k-1}(H_k - \lambda_{H,k}),\ \forall l \tag{5.5}$$

$$\sum_{k=0}^{q} \mu^{q-k}(H_k - \lambda_{H,k}) - \sum_{k=1}^{q} \rho\mu^{q-k+1} P_{H,k} \leq B_{max},\ \forall q \tag{5.6}$$

$$\rho P_{E,k} \leq E_k, \qquad \forall k, \tag{5.7}$$

where $l \in \{1, 2, \cdots, K\}$, $q \in \{1, 2, \cdots, K-1\}$, and $k \in \{1, 2, \cdots, K\}$. Constraint (5.3) provides the flexibility to transmit the incoming data packets in future time intervals. Constraint (5.4) ensures that all the data packets are transmitted by a deadline of K transmission intervals. Constraint (5.5) stems from the causality constraint on the harvested energy and constraint (5.6) ensures that the harvested energy does not exceed the limited storage capacity of the battery. Thereby, $\lambda_{H,k}$ is a slack variable that ensures that problem (5.2)–(5.7) is always feasible. In particular, $\lambda_{H,k}$ represents the amount of harvested energy that is wasted in time interval k because of the limited

storage capacity of the battery[18]. The limitation on the amount of energy drawn from the constant energy source is reflected in constraint (5.7). Note that for a given time interval, for the constant energy supply, any extra amount of energy which is not used for transmission cannot be transferred to the next interval.

Problem (5.2)–(5.7) is not a convex optimization problem because of the non–convexity of constraint (5.3) and the non–affinity of constraint (5.4). We combine (5.3) and (5.4) and transform problem (5.2)–(5.7) into the following problem:

$$\min_{P_{E,k}\geq 0,\ P_{H,k}\geq 0,\ \lambda_{H,k}\geq 0} \quad \sum_{k=1}^{K} \rho P_{E,k} \tag{5.8}$$

$$\text{s.t.} \quad \sum_{k=l}^{K} \log_2(1+\gamma_k(P_{E,k}+P_{H,k})) \geq \sum_{k=l}^{K} R_k,\ \forall l \tag{5.9}$$

$$\text{Constraints (5.5)} - \text{(5.7)}, \tag{5.10}$$

where $l \in \{1, 2, \cdots, K\}$. However, constraint (5.9) is an equivalent representation of constraints (5.3) and (5.4), and hence problem (5.8)–(5.10) is equivalent to problem (5.2)–(5.7), i.e., both problems have the same optimal solution. Problem (5.8)–(5.10) is a convex optimization problem and thus can be solved optimally and efficiently [75]. We note that problem (5.8)–(5.10) is not always feasible. Assuming R_k, channel SNRs, γ_k, and harvested energies, H_k, are given for all time intervals, i.e., $k \in \{1, 2, \cdots, K\}$, a sufficient (but not necessary) condition for feasibility of problem (5.8)–(5.10) is

$$\sum_{k=1}^{K} \log_2(1+\frac{\gamma_k}{\rho}(E_k+H_k)) \geq \sum_{k=1}^{K} R_k. \tag{5.11}$$

[18]For example, if H_k is large (H_k is a random variable and cannot be controlled in the optimization problem) and B_{max} is small, then if $\lambda_{H,k}$ was omitted, constraint (5.6) would not be satisfied and problem (5.2)–(5.7) would become infeasible.

If the problem is not feasible, we can extend the number of transmission intervals to $K^* > K$ by following similar steps as in [17] to avoid infeasibility. Note that during time intervals $k' \in \{K+1, K+2, \cdots, K^*\}$, we have to assume that no additional data packets arrive at S to avoid the possibility of facing further infeasibility. It is worth mentioning that problem (5.8)–(5.10) is always feasible if $E_k \to \infty$, $\forall k$, i.e., when the constant energy supply is (practically) unlimited. In the following, we assume that problem (5.8)–(5.10) is feasible.

As problem (5.8)–(5.10) satisfies Slater's constraint qualification and is jointly convex in $P_{E,k}$, $P_{H,k}$, and $\lambda_{H,k}$, the duality gap between the dual optimum and the primal optimum is zero [75]. Therefore, we solve the problem by solving its dual. For this purpose, we first provide the Lagrangian of problem (5.8)–(5.10) which can be written as

$$\begin{aligned}\mathcal{L} =& \sum_{k=1}^{K} \rho P_{E,k} + \sum_{l=1}^{K} \alpha_l \left(\sum_{k=1}^{l} \rho \mu^{l-k} P_{H,k} - \sum_{k=0}^{l-1} \mu^{l-k-1} (H_k - \lambda_{H,k}) \right) \\ &+ \sum_{q=1}^{K-1} \xi_q \left(\sum_{k=0}^{q} \mu^{q-k} (H_k - \lambda_{H,k}) - \sum_{k=1}^{q} \rho \mu^{q-k+1} P_{H,k} - B_{max} \right) + \sum_{k=1}^{K} \beta_k \left(\rho P_{E,k} - E_k \right) \\ &- \sum_{l=1}^{K} \delta_l \left(\sum_{k=l}^{K} \log_2(1 + \gamma_k (P_{E,k} + P_{H,k})) - \sum_{k=l}^{K} R_k \right) \end{aligned} \tag{5.12}$$

where $\delta_l \geq 0$, $\alpha_l \geq 0$, $\xi_q \geq 0$, and $\beta_k \geq 0$ are the Lagrange multipliers associated with constraints (5.9), (5.5), (5.6), and (5.7), respectively. Note that the boundary conditions $P_{E,k} \geq 0$, $P_{H,k} \geq 0$, and $\lambda_{H,k} \geq 0$ are absorbed into the KKT conditions for deriving the optimal $P_{E,k}$, $P_{H,k}$, and $\lambda_{H,k}$. The dual of problem (5.8)–(5.10) can be stated as

$$\max_{\delta_l \geq 0,\ \alpha_l \geq 0,\ \xi_q \geq 0,\ \beta_k \geq 0} \quad \min_{P_{E,k} \geq 0,\ P_{H,k} \geq 0,\ \lambda_{H,k} \geq 0} \mathcal{L}. \tag{5.13}$$

Using standard optimization techniques and the KKT optimality conditions, the optimal $P_{E,k}$, $P_{H,k}$, and $\lambda_{H,k}$ can be obtained as

$$P^*_{E,k} = \left[\Xi_{E,k} - \frac{1}{\gamma_k} - P_{H,k}\right]^+, \tag{5.14}$$

$$P^*_{H,k} = \left[\Xi_{H,k} - \frac{1}{\gamma_k} - P_{E,k}\right]^+, \text{and} \tag{5.15}$$

$$\lambda^*_{H,k} = \left[\sum_{i=0}^{k-1} \mu^{k-i}(H_i - \lambda_{H,i}) - \sum_{i=1}^{k} \mu^{k-i+1}\rho P_{H,i} + H_k - B_{max}\right]^+, \tag{5.16}$$

respectively, where $[x]^+ = \max\{x, 0\}$ and $\lambda_{H,0} = 0$. The power allocation solutions in (5.14) and (5.15) can be interpreted as a form of water–filling, where $\Xi_{E,k} = \frac{\sum_{j=1}^{k}\delta_j}{\rho\ln(2)(1+\beta_k)}$ and $\Xi_{H,k} = \frac{\sum_{j=1}^{k}\delta_j}{\rho\ln(2)\left(\sum_{j=k}^{K}\alpha_j\mu^{j-k} - \sum_{j=k}^{K-1}\xi_j\mu^{j-k+1}\right)}$ are the water levels associated with $P^*_{E,k}$ and $P^*_{H,k}$, respectively. $P^*_{E,k}$ and $P^*_{H,k}$ depend on each other due to constraint (5.9).

From (5.15), we observe that when $B_{max} = \infty$, we have $\xi_q = 0$, $\forall q$, and in this case, the optimum water level for the EH source, $\Xi_{H,k}$, is monotonically non–decreasing. In this case, all harvested energy can be stored in the battery and thus $P^*_{H,k}$ can be more efficiently distributed over the time intervals to minimize the use of the constant energy source. However, when B_{max} is finite and if constraint (5.6) is satisfied with equality, i.e., at least one $\xi_q \neq 0$, $\forall q$, then the monotonicity of the optimum water level no longer holds. However, when constraint (5.6) is not satisfied with equality, the optimum water level is monotonically non–decreasing even for finite B_{max}. Furthermore, we observe from (5.14) that whenever constraint (5.7) is not satisfied with equality, i.e., $\beta_k = 0$, the optimum water level for the constant energy source, $\Xi_{E,k}$, is monotonically non–decreasing for increasing k.

We calculate the optimal Lagrange multipliers required in (5.14)–(5.16) via an iterative procedure [75]. We define t as the iteration index. For a given set of Lagrange

multipliers $(\delta(t), \alpha_l(t), \xi_q(t), \beta_k(t))$ and a given value of $P^*_{H,k}(t-1)$, we obtain $P^*_{E,k}(t)$ using (5.14) and then calculate $P^*_{H,k}(t)$ based on (5.15) by using $P^*_{E,k}(t)$ as $P_{E,k}$. We also calculate $\lambda^*_{H,k}(t)$ based on (5.16) by using $P^*_{H,k}(t)$ as $P_{H,k}$. The initial set of Lagrange multipliers $(\delta_l(1), \alpha_l(1), \xi_q(1), \beta_k(1))$ are chosen from the feasible set, i.e., $\delta_l(1) \geq 0,\ \alpha_l(1) \geq 0,\ \xi_q(1) \geq 0,\ \beta_k(1) \geq 0$. However, to calculate $P_{E,k}(1)$ for $t = 1$, $P_{H,k}(0) \geq 0$ is chosen such that (5.5) and (5.6) are satisfied. We update the Lagrange multipliers as follows:

$$\delta_l(t+1) = \left[\delta_l(t) - \Upsilon_1(t)\left(\sum_{k=l}^{K} \log_2(1+\gamma_k(P_{E,k}+P_{H,k})) - \sum_{k=l}^{K} R_k\right)\right]^+, \tag{5.17}$$

$$\alpha_l(t+1) = \left[\alpha_l(t) + \Upsilon_2(t)\left(\sum_{k=1}^{l} \rho\mu^{l-k} P^*_{H,k}(t) - \sum_{k=0}^{l-1} \mu^{l-k-1}(H_k - \lambda^*_{H,k}(t))\right)\right]^+, \tag{5.18}$$

$$\xi_q(t+1) = \left[\xi_q(t) + \Upsilon_3(t)\left(\sum_{k=0}^{q} \mu^{q-k}(H_k - \lambda^*_{H,k}(t)) - \sum_{k=1}^{q} \rho\mu^{q-k+1} P^*_{H,k}(t) - B_{max}\right)\right]^+, \tag{5.19}$$

$$\beta_k(t+1) = \left[\beta_k(t) + \Upsilon_4(t)\left(\rho P^*_{E,k}(t) - E_k\right)\right]^+, \tag{5.20}$$

where $l \in \{1, 2, \cdots, K\}$, $q \in \{1, 2, \cdots, K-1\}$, and $k \in \{1, 2, \cdots, K\}$. Here, $\Upsilon_n(t)$, $n \in \{1, \cdots, 4\}$, are positive step sizes. With the updated Lagrange multipliers, we solve $P^*_{E,k}(t+1)$ and $P^*_{H,k}(t+1)$ again and the same procedure continues until convergence. Note that due to the convexity of problem (5.8)–(5.10), the convergence to the optimal solution is guaranteed as long as the step sizes satisfy the infinite travel condition [75].

5.3.2 Offline Power Allocation for Scenario 1

For Scenario 1, $P^*_{E,k}$, $P^*_{H,k}$, and $\lambda^*_{H,k}$ are also given by (5.14), (5.15), and (5.16), respectively, but with $\delta_k = 0$ for $k \in \{2, 3, \cdots, K\}$, i.e., the water levels are given

by $\Xi_{E,k} = \frac{\delta_1}{\rho \ln(2)(1+\beta_k)}$ and $\Xi_{H,k} = \frac{\delta_1}{\rho \ln(2)\left(\sum_{j=k}^{K} \alpha_j \mu^{j-k} - \sum_{j=k}^{K-1} \xi_j \mu^{j-k+1}\right)}$. Furthermore, in (5.17), we have to set $R_1 = R_T$ and $R_k = 0$, $k = 2, 3, \cdots, K$. We note that the numerators of the optimum water levels $\Xi_{E,k}$ and $\Xi_{H,k}$ for Scenario 1 contain only one Lagrange multiplier, δ_1. Therefore, whenever constraint (5.7) is not satisfied with equality, i.e., $\beta_k = 0$, $\forall k$, the optimum water level of $P_{E,k}$ for Scenario 1 remains constant. However, B_{max} has the same impact on $P^*_{H,k}$ for Scenario 1 as for Scenario 2.

5.3.3 Complexity of the Proposed Offline Power Allocation Schemes

In the offline power allocation scheme, we solve a convex optimization problem where the number of constraints is a function of K. The required computational cost to solve a convex optimization problem is polynomial in the size of the problem [75]. Therefore, for both considered scenarios, the worst–case computational cost of the proposed offline power allocation scheme is polynomial in the number of time intervals K [75].

5.4 Online Power Allocation

In practice, only causal information of channels and harvested energies is available for power allocation. Therefore, the offline power allocation scheme is not readily applicable as in a given time interval k, the future CSI and the upcoming harvested energy are not known in advance. In this section, for both considered scenarios, we propose an optimal and a suboptimal, less complex online power allocation schemes. For the online schemes, the random data arrivals in Scenario 2 during transmission

play an important role[19]. Since this feature is not present in Scenario 1, to improve the clarity of our chapter, we describe the online power allocation schemes for Scenarios 1 and 2 separately.

5.4.1 Optimal Online Power Allocation

For optimal online power allocation, we employ a stochastic DP approach [18, 23] which exploits the causal information regarding the channel SNRs, the harvested energies, and their pdfs. For Scenario 2, the causal information regarding the incoming data bits and the pdf of the data bit arrival process also have to be known. Note that the pdfs of the channel SNR, the harvested energy, and the incoming data bits can be obtained via long–term measurements.

Scenario 1

Let $\boldsymbol{c}_k^{(1)} \triangleq (\gamma_k, H_{k-1}, B_k, D_{k-1}^{(1)}, T_k)$ denote the state of the system in time interval k which includes channel SNR γ_k, incoming harvested energy H_{k-1}, stored harvested energy B_k, the total number of remaining bits to be transmitted over the following time intervals $D_{k-1}^{(1)}$, and the remaining number of time intervals T_k. $D_{k-1}^{(1)}$ is calculated at the end of time interval $(k-1)$. Our aim is to minimize the amount of energy drawn from the constant energy source over K intervals and we assume the initial state $\boldsymbol{c}_1^{(1)} = (\gamma_1, H_0, B_1, D_0^{(1)}, T_1)$ is known. We define a policy $p^{(1)} = \{P_{E,k}(\boldsymbol{c}_k^{(1)}), P_{H,k}(\boldsymbol{c}_k^{(1)}), \forall \boldsymbol{c}_k^{(1)}, k = 1, 2, \cdots, K\}$, as feasible if the constraints $[P_{E,k}(\boldsymbol{c}_k^{(1)}), P_{H,k}(\boldsymbol{c}_k^{(1)})] \succeq 0$ and $\rho P_{E,k}(\boldsymbol{c}_k^{(1)}) \leq E_k$, $\rho P_{H,k}(\boldsymbol{c}_k^{(1)}) \leq B_k$ are satisfied for all

[19]For example, for optimal power allocation, different system state definitions and Bellman's equations result for Scenarios 1 and 2 [18]. Therefore, neither of the optimal online schemes be directly considered as a special case of the other.

k. Moreover,

$$D_k^{(1)} = D_{k-1}^{(1)} - \log_2(1 + \gamma_k(P_{E,k} + P_{H,k})) \tag{5.21}$$

for $k \in \{1, 2, \cdots, K\}$ and $D_0^{(1)} = R_T$. The objective function to be minimized can be reformulated as [18]

$$W(p^{(1)}) = \sum_{k=1}^{K} \mathcal{E}\{\rho P_{E,k} | \boldsymbol{c}_1^{(1)}, p^{(1)}\}, \tag{5.22}$$

where the expectation is with respect to the channel SNR and the harvested energy. In particular, for a given $\boldsymbol{c}_1^{(1)}$, the minimum amount of energy drawn from the constant energy source can be obtained as

$$W^* = \min_{p^{(1)} \in \mathcal{P}} W(p^{(1)}), \tag{5.23}$$

where $\mathcal{P}$ denotes the space of all feasible policies. In general, the optimization of $P_{E,k}$ and $P_{H,k}$ cannot be performed independently in each time interval because of the EH constraints. Therefore, to obtain W^*, we adopt a stochastic DP approach by using Bellman's equations [18].

To this end, we denote the minimum energy drawn from the constant energy source in time interval k as $J_k^{(1)}(E_k, B_k, D_{k-1}^{(1)})$. For a given $\boldsymbol{c}_1^{(1)}$, the total minimum energy W^* is given by $J_1^{(1)}(E_1, B_1, D_0^{(1)})$, which can be recursively obtained from $J_K^{(1)}(E_K, B_K, D_{K-1}^{(1)})$, $J_{K-1}^{(1)}(E_{K-1}, B_{K-1}, D_{K-2}^{(1)})$, $\cdots$, $J_2^{(1)}(E_2, B_2, D_1^{(1)})$ [18]. For the

last time interval K, we have

$$J_K^{(1)}(E_K, B_K, D_{K-1}^{(1)}) = \min_{\substack{P_{E,K}\geq 0,\ P_{H,K}\geq 0 \\ \rho P_{E,K}\leq E_K \\ \rho P_{H,K}\leq B_K \\ \log_2(1+\gamma_K(P_{E,K}+P_{H,K}))\geq D_{K-1}^{(1)}}} \rho P_{E,K} \tag{5.24}$$

and for time interval $k \in \{1, 2, \cdots, K-1\}$, we have $J_k^{(1)}(E_k, B_k, D_{k-1}^{(1)}) =$

$$\min_{\substack{P_{E,k}\geq 0,\ P_{H,k}\geq 0 \\ \rho P_{E,k}\leq E_k \\ \rho P_{H,k}\leq B_k}} \rho P_{E,k} + \bar{J}_{k+1}^{(1)}(E_{k+1}, \mu(B_k - \rho P_{H,k}), D_{k-1}^{(1)} - \log_2(1+\gamma_k(P_{E,k}+P_{H,k}))), \tag{5.25}$$

where $\bar{J}_{k+1}^{(1)}(E_{k+1}, \mu(B_k - \rho P_{H,k}), D_{k-1}^{(1)} - \log_2(1+\gamma_k(P_{E,k}+P_{H,k}))) =$

$$\mathcal{E}_{\tilde{\gamma}_{k+1},\tilde{H}_k}\Big\{ J_{k+1}^{(1)}(E_{k+1}, \min\{\mu(B_k - \rho P_{H,k}) + \tilde{H}_k, B_{max}\}, D_{k-1}^{(1)} - \log_2(1+\gamma_k(P_{E,k}+P_{H,k})))\Big\}. \tag{5.26}$$

Here, $\tilde{\gamma}_{k+1}$ represents the random SNR in the $(k+1)$th interval where the SNR γ_k in the kth interval is known. Similarly, $\tilde{H}_k$ denotes the random harvested energy in the kth time interval where the harvested energy H_{k-1} in the $(k-1)$th interval is known and E_k is assumed to be known for all time intervals. The pdfs of the channel SNR and the harvested energy have to be known for evaluation of (5.26). It can be shown that the cost functions in (5.24) and (5.25) are jointly convex in $P_{E,k}$ and $P_{H,k}$. Therefore, (5.24) and (5.25) are convex optimization problems and can be solved efficiently and optimally [75]. Note that (5.25) and (5.26) may not be feasible for all $\tilde{\gamma}_{k+1}$ and $\tilde{H}_k$. We discard the results corresponding to those $\tilde{\gamma}_{k+1}$ and $\tilde{H}_k$ which provide infeasible solutions and only consider those $\tilde{\gamma}_{k+1}$ and $\tilde{H}_k$ which provide feasible results in (5.25) and (5.26).

Using (5.24) and (5.25), $P^*_{E,k}$ and $P^*_{H,k}$, $k \in \{1, 2, \cdots, K\}$, can be obtained for different possible values of γ_k and B_k. The results are stored in a look–up table. This is done before transmission starts. When transmission starts, for a given realization of γ_k and B_k, in time interval k, those values of $P^*_{E,k}$ and $P^*_{H,k}$ that correspond to that realization are taken from the look–up table. If (5.25) is not feasible for a given γ_k and B_k in an interval k due to an insufficient available amount of energy for transmitting the required number of data bits, the transmitter transmits as many bits as possible using the available power, i.e., $P^*_{H,k} = \frac{B_k}{\rho}$ and $P^*_{E,k} = \frac{E_k}{\rho}$. If (5.24) is not feasible for a given γ_K and B_K, then the transmitter extends the transmission deadline from K to $K^* > K$ to ensure that all the bits are transmitted by the K^*th interval.

Scenario 2

We follow similar steps as for Scenario 1 and employ a stochastic DP approach also for Scenario 2. However, different from Scenario 1, the main challenge here is how to incorporate the random nature of the data bit arrival process to account for the effect of data arrivals in future time intervals.

Let $\boldsymbol{c}^{(2)}_k \triangleq (\gamma_k, H_{k-1}, B_k, R_k, D^{(2)}_{k-1}, T_k)$ denote the state for time interval k, where

$$D^{(2)}_k = D^{(2)}_{k-1} - \log_2(1 + \gamma_k(P_{E,k} + P_{H,k})) + R_{k+1} \tag{5.27}$$

represents the total number of remaining bits to be transmitted over the following time intervals which is calculated at the end of a given time interval $(k-1)$. In particular, $D^{(2)}_0 = R_1$. Note that unlike Scenario 1, the number of bits R_k which arrive immediately before interval k, is now considered as one of the state elements for Scenario 2. We assume the initial state $\boldsymbol{c}^{(2)}_1 = (\gamma_1, H_0, B_1, R_1, D^{(2)}_0, T_1)$ is known. We define a policy $p^{(2)} = \{P_{E,k}(\boldsymbol{c}^{(2)}_k), P_{H,k}(\boldsymbol{c}^{(2)}_k), \forall \boldsymbol{c}^{(2)}_k, k = 1, 2, \cdots, K\}$, as feasible if

the constraints $[P_{E,k}(\boldsymbol{c}_k^{(2)}), P_{H,k}(\boldsymbol{c}_k^{(2)})] \succeq 0$ and $\rho P_{E,k}(\boldsymbol{c}_k^{(2)}) \leq E_k$, $\rho P_{H,k}(\boldsymbol{c}_k^{(2)}) \leq B_k$ are satisfied for all k. For a given $\boldsymbol{c}_1^{(2)}$, the minimum energy drawn from the constant energy source can be obtained as

$$W^* = \min_{p^{(2)} \in \mathcal{P}} \sum_{k=1}^{K} \mathcal{E}\{\rho P_{E,k} | \boldsymbol{c}_1^{(2)}, p^{(2)}\}, \tag{5.28}$$

where the expectation is taken also with respect to the incoming data packets in addition to the channel SNR and the harvested energy. We use again Bellman's equations to obtain W^* for Scenario 2 and hence denote the minimum energy drawn from the constant energy source in time interval k as $J_k^{(2)}(E_k, B_k, D_{k-1}^{(2)})$ [18]. For a given $\boldsymbol{c}_1^{(2)}$, the total minimum energy $W^* = J_1^{(2)}(E_1, B_1, D_0^{(2)})$ can be recursively obtained from $J_K^{(2)}(E_K, B_K, D_{K-1}^{(2)})$, $J_{K-1}^{(2)}(E_{K-1}, B_{K-1}, D_{K-2}^{(2)})$, $\cdots$, $J_2^{(2)}(E_2, B_2, D_1^{(2)})$. For the last time interval K, we have

$$J_K^{(2)}(E_K, B_K, D_{K-1}^{(2)}) = \min_{\substack{P_{E,K} \geq 0,\ P_{H,K} \geq 0 \\ \rho P_{E,K} \leq E_K \\ \rho P_{H,K} \leq B_K \\ \log_2(1+\gamma_K(P_{E,K}+P_{H,K})) \geq D_{K-1}^{(2)}}} \rho P_{E,K} \tag{5.29}$$

and for time interval k, we obtain $J_k^{(2)}(E_k, B_k, D_{k-1}^{(2)}) =$

$$\min_{\substack{P_{E,k} \geq 0,\ P_{H,k} \geq 0 \\ \rho P_{E,k} \leq E_k \\ \rho P_{H,k} \leq B_k}} \rho P_{E,k} + \bar{J}_{k+1}^{(2)}(E_{k+1}, \mu(B_k - \rho P_{H,k}), D_{k-1}^{(2)} - \log_2(1 + \gamma_k(P_{E,k} + P_{H,k}))), \tag{5.30}$$

where $\bar{J}_{k+1}^{(2)}(E_{k+1}, \mu(B_k - \rho P_{H,k}), D_{k-1}^{(2)} - \log_2(1 + \gamma_k(P_{E,k} + P_{H,k}))) =$

$$\mathcal{E}_{\tilde{\gamma}_{k+1}, \tilde{H}_k, \tilde{R}_{k+2}} \Big\{ J_{k+1}^{(2)}(E_{k+1}, \min\{\mu(B_k - \rho P_{H,k}) + H_k, B_{max}\}, \\ D_{k-1}^{(1)} - \log_2(1 + \gamma_k(P_{E,k} + P_{H,k})) + \tilde{R}_{k+2}) \tag{5.31}$$

Here, $\tilde{R}_{k+2}$ represents the random incoming data bits at the source just before the $(k+2)$th interval. It can be shown that the cost functions in (5.29) and (5.30) are jointly convex in $P_{E,k}$ and $P_{H,k}$ [75]. A possible infeasibility of (5.30) and (5.31) can be handled by following the same procedure as in case of Scenario 1. Furthermore, using (5.29) and (5.30), $P^*_{E,k}$ and $P^*_{H,k}$, $k \in \{1, 2, \cdots, K\}$, are obtained for different possible values of γ_k, B_k, and R_k offline and the results are stored in look–up tables and used during the course of transmission.

5.4.2 Suboptimal Online Power Allocation

In the proposed DP–based optimal online power allocation algorithm, for a given transmission interval k, we take into account the average effect of all succeeding time intervals, cf. (5.26) and (5.31). Due to the recursive nature of DP, the computational cost of this approach increases exponentially with increasing K. For this reason, in the following, we propose a suboptimal but efficient online power allocation scheme, which performs close to the optimal DP approach with reduced complexity. To this end, we assume that the average SNR $\bar{\gamma}$ is known along with the causal information of the channel SNRs, harvested energies, and the data arrivals (for Scenario 2). As the optimal offline algorithm results in water–filling solutions for $P^*_{E,k}$ and $P^*_{H,k}$, our objective is to design an online algorithm which adaptively sets the required number of data bits to be transmitted according to the current CSI. How the target number of data bits to be transmitted is obtained is summarized in the following property.

Property 1 *Suppose P' is the power that a transmitter can use to send a required amount of data either in the current time interval k or in the next time interval $k+1$. Assuming that the transmitter only has causal information of the channel SNR, the gain of allocating P' in interval k instead of in interval $k+1$ can be lower bounded*

by $\log_2\left(\frac{\gamma_k}{\bar{\gamma}}\right)$.

Proof 2 *The expected gain in allocating P' in the current time interval k over future time interval $k+1$ is given by*

$$\Delta G = \log_2(1+\gamma_k P') - \mathcal{E}_{\tilde{\gamma}_{k+1}}\left\{\log_2(1+\tilde{\gamma}_{k+1}P')\right\}. \tag{5.32}$$

Using Jensen's inequality $\mathcal{E}_{\tilde{\gamma}_{k+1}}\left\{\log_2(1+\tilde{\gamma}_{k+1}P')\right\} \leq \log_2(1+\bar{\gamma}P')$ in (5.32) yields

$$\Delta G \geq \log_2(1+\gamma_k P') - \log_2(1+\bar{\gamma}P') \approx \log_2\left(\frac{\gamma_k}{\bar{\gamma}}\right) \tag{5.33}$$

where the approximation holds for sufficiently large P'.

The significance of using the lower bound of ΔG in (5.33) for the proposed suboptimal online power allocation algorithm will become apparent in the problem formulations for Scenarios 1 and 2 in the following. Note that exploiting ΔG in its original form in the suboptimal online power allocation would result in a non–convex optimization problem, which would be difficult to solve.

Scenario 1

Based on the findings in Property 1, we formulate the optimization problem for a given time interval $k \in \{1, 2, \cdots, K-1\}$ as follows

$$\min_{P_{E,k}\geq 0,\ P_{H,k}\geq 0} \quad \rho P_{E,k} \tag{5.34}$$

$$\text{s.t.} \qquad \log_2(1+\gamma_k(P_{E,k}+P_{H,k})) \geq \lfloor \vartheta_k^{(1)} \rfloor \tag{5.35}$$

$$\rho P_{H,k} \leq B_k, \tag{5.36}$$

$$\rho P_{H,k} \geq \min\left\{(1-\mu)B_k, \frac{2^{\lfloor \vartheta_k^{(1)} \rfloor}-1}{\gamma_k}\right\}, \tag{5.37}$$

$$\rho P_{E,k} \leq E_k, \tag{5.38}$$

where $\vartheta_k^{(1)} = \max\left\{0, \min\left\{\frac{D_{k-1}^{(1)}}{T_k} + \log_2\left(\frac{\gamma_k}{\bar{\gamma}}\right), D_{k-1}^{(1)}\right\}\right\}$ and $\lfloor\cdot\rfloor$ denotes a floor operation. If problem (5.34)–(5.38) is not feasible in an interval k due to an insufficient available amount of energy for transmitting the required number of data bits, constraint (5.35) is relaxed and the transmitter transmits as many bits as possible using the available power, i.e., $P_{H,k}^* = \frac{B_k}{\rho}$ and $P_{E,k}^* = \frac{E_k}{\rho}$. Let us assume that optimization problem (5.34)–(5.38) is always feasible for all time intervals $k \in \{1, 2, \cdots, K-1\}$ for power allocation algorithm design. The right hand side of (5.35) incorporates the adaptive transmission of data packets based on the channel condition. In particular, based on Property 1, for a given interval k, if the channel SNR is better than the average channel SNR, i.e., $\gamma_k > \bar{\gamma}$, in addition to the average data rate $\frac{D_{k-1}^{(1)}}{T_k}$, we allow the transmission of an extra $\log_2\left(\frac{\gamma_k}{\bar{\gamma}}\right) > 0$ data bits. However, if the channel SNR is worse than the average channel SNR, i.e., $\gamma_k < \bar{\gamma}$, we transmit less than the average data rate $\frac{D_{k-1}^{(1)}}{T_k}$ since $\log_2\left(\frac{\gamma_k}{\bar{\gamma}}\right) < 0$. We note that (5.35) implicitly includes a cost associated with missing the deadline as $\vartheta_k^{(1)}$ is inversely proportional to the remaining number of time intervals, T_k. However, for the Kth time interval, the right hand side of (5.35) is replaced by $D_{K-1}^{(1)}$. This means that in the last time interval, all the remaining data packets are transmitted irrespective of the channel condition provided that a sufficient amount of energy can be drawn from the constant energy source and the stored harvested energy. Furthermore, in the right hand side of (5.37), the term $(1-\mu)B_k$ incorporates the effect of μ on $P_{H,k}$ in the optimization problem. For example, if μ is very small i.e., most of the stored harvested energy is lost due to leakage, (5.37) forces $P_{H,k}$ to use up all stored energy completely in

the current time interval so that the losses in future time intervals are minimized. Moreover, $\frac{2^{\vartheta_k^{(1)}}-1}{\gamma_k}$ in (5.37) further avoids the possible waste of the harvested energy in the current time interval. For example, in some cases, using $\rho P_{H,k} \geq (1-\mu)B_k$ might result in $\log_2(1+\gamma_k(P^*_{E,k}+P^*_{H,k})) > \vartheta_k^{(1)}$ which would lead to a waste of energy. This is avoided by adopting $\min\left\{(1-\mu)B_k, \frac{2^{\vartheta_k^{(1)}}-1}{\gamma_k}\right\}$ as the lower bound for $P_{H,k}$. This choice efficiently reduces the loss of harvested energy in the current and future time intervals. If problem (5.34)–(5.38) is not feasible for time interval K, then the transmitter extends the transmission deadline from K to $K^* > K$ to ensure that all the bits are transmitted by the K^*th interval.

Problem (5.34)–(5.38) is a convex optimization problem and can be solved optimally and efficiently [75]. The Lagrangian of problem (5.34)–(5.38) is given by

$$\mathcal{L}'_1 = \rho P_{E,k} - \delta'_k\left(\log_2(1+\gamma_k(P_{E,k}+P_{H,k})) - \vartheta_k^{(1)}\right) - B_k) + \xi'_k((1-\mu)B_k - \rho P_{H,k}) + \alpha'_k(\rho P_{H,k} + \beta'_k(\rho P_{E,k} - E_k), \quad (5.39)$$

where δ'_k, α'_k, ξ'_k, and β'_k represent the Lagrange multipliers associated with (5.35), (5.36), (5.37), and (5.38), respectively. The dual of problem (5.34)–(5.38) can be stated as

$$\max_{\delta'_k\geq 0,\ \alpha'_k\geq 0,\ \xi'_k\geq 0,\ \beta'_k\geq 0} \quad \min_{P_{E,k}\geq 0,\ P_{H,k}\geq 0} \mathcal{L}'_1. \quad (5.40)$$

Using standard optimization procedures and KKT optimality conditions, the optimal

$P_{H,k}$ and $P_{E,k}$ can be obtained as

$$P_{E,k}^{*} = \left[\frac{\delta_k'}{\rho \ln(2)(1+\beta_k')} - \frac{1}{\gamma_k} - P_{H,k}\right]^{+} \text{ and} \tag{5.41}$$

$$P_{H,k}^{*} = \left[\frac{\delta_k'}{\rho \ln(2)(\alpha_k' - \xi_k')} - \frac{1}{\gamma_k} - P_{E,k}\right]^{+}, \tag{5.42}$$

respectively. We observe that the optimal solutions for $P_{E,k}$ and $P_{H,k}$ depend only on causal information regarding the instantaneous channel SNR and harvested energy and also on the average SNR, $\bar{\gamma}$, through the Lagrange multipliers. Moreover, (5.41) and (5.42) have a water–filling structure. Similar to the offline power allocation algorithm, the optimal Lagrange multipliers in (5.41), (5.42) can be obtained iteratively.

Scenario 2

The suboptimal online power allocation for Scenario 2 can also be obtained from problem (5.34)–(5.38) after replacing $\vartheta_k^{(1)}$ by $\vartheta_k^{(2)}$, where $\vartheta_k^{(2)} = \max\left\{0, \min\left\{\left(D_{k-1}^{(2)} + \log_2\left(\frac{\gamma_k}{\bar{\gamma}}\right)\right), D_{k-1}^{(2)}\right\}\right\}$. Hence, for Scenario 2, $P_{E,k}^{*}$ and $P_{H,k}^{*}$ are also given by (5.41) and (5.42), respectively, but with δ_k' and ξ_k' being replaced by δ_k'' and ξ_k'', respectively. δ_k'' and ξ_k'' represent the Lagrange multipliers associated with (5.35) and (5.37), where $\vartheta_k^{(1)}$ is replaced by $\vartheta_k^{(2)}$. Similar to Scenario 1, the optimal solutions of $P_{E,k}$ and $P_{H,k}$ for Scenario 2 depend on the causal knowledge of the instantaneous channel SNR, harvested energy, and the average SNR, $\bar{\gamma}$, through the Lagrange multipliers. Moreover, the optimal solutions of $P_{E,k}$ and $P_{H,k}$ for Scenario 2 are also influenced by the number of data bits that have just arrived through the Lagrange multipliers.

5.4.3 Complexity of the Proposed Online Power Allocation Schemes

The complexity of the optimal DP based online power allocation scheme increases exponentially with K. For the suboptimal online scheme, we solve a convex optimization problem for each time interval and the size of each convex problem does not depend on K. Hence, the complexity of the suboptimal online scheme is linear in K.

5.5 Simulation Results

In this section, we evaluate the performance of the proposed power allocation schemes for Scenarios 1 and 2. We assume that in each time interval H_k, $k \in \{0, 1, \cdots, K-1\}$, independently takes a value from the set $\{0, H_S, 2H_S\}$, where all elements of the set are equiprobable. For all presented simulation results, $B_{max} = 50$ Joules and $\rho = 2.5$, which corresponds to a power amplifier efficiency of 40%[20]. In Figs. 5.3–5.10, we assume $E_1 = E_2 = \cdots = E_K = 40$ Joules whereas in Fig. 5.2, we assume $E_1 = E_2 = \cdots = E_K = 8$ Joules. As we consider a small duration for each time interval ($T = 1$s), the battery efficiency per interval is high [112]. Thus, we assume $\mu = 0.99$ for all the figures except for Fig. 5.9. The channel SNR follows an exponential distribution with means $\bar{\gamma} = 10$ dB for Fig. 5.2, and $\bar{\gamma} = 25$ dB for Figs. 5.3–5.10. For Scenario 2, R_k follows a uniform distribution with mean R_{avg}. For the simulation results in Figs. 5.3–5.8 and 5.10, 10^4 randomly generated realizations of the channel SNRs, harvested energies, and incoming data packets (for Scenario 2) are considered to obtain the average consumed powers. The total powers drawn from the constant energy source and the harvested energy are denoted as $P_{E,Tot} = \sum_{k=1}^{K} \rho P_{E,k}$ and

[20] We consider a class A/B power amplifier with a moderate efficiency [113].

$P_{H,Tot} = \sum_{k=1}^{K} \rho P_{H,k}$, respectively.

For comparison, we consider two baseline schemes for offline optimization in Figs. 5.3–5.5. In baseline scheme 1, we minimize the total consumed power, i.e., the sum of the powers drawn from the constant energy source and the energy harvester. The offline optimization problems for baseline scheme 1 are obtained by adopting $\sum_{k=1}^{K} \rho(P_{H,k} + P_{E,k})$ as objective function in (5.2) for Scenarios 1 and 2, respectively. The objective of baseline scheme 1 is to minimize the total consumed energy rather than the consumed non–renewable energy. In baseline scheme 2, we define the number of data bits to be transmitted in each interval k as $\lfloor R_T/K \rfloor$ and R_k for Scenarios 1 and 2, respectively. In each interval k, at first we draw power from the harvested energy and if the harvested energy cannot satisfy the bit rate requirement, then we draw power from the constant energy source. It is worth mentioning that baseline scheme 1 follows a common approach for power minimization in the existing wireless communication systems whereas baseline scheme 2 is a naive and basic policy that prioritizes consuming renewable energy first.

5.5.1 Behavior of Offline Power Allocation Over Time Intervals k

In Fig. 5.2, we show the optimum power levels of $P_{E,k}$ and $P_{H,k}$ for the offline and suboptimal online power allocation schemes for Scenario 1 as functions of the time intervals k. In addition, we also show the inverse channel SNR $\frac{1}{\gamma_k}$ and H_k as well as the water levels of $P_{E,k}$ and $P_{H,k}$ for the offline scheme. $H_S = 2$, $R_T = 40$, and $K = 10$ are adopted in this figure.

For the optimal offline power allocation scheme, we observe that the water level of $P_{E,k}$, $\Xi_{E,k}$, does not remain constant over the time intervals. As E_k is not large

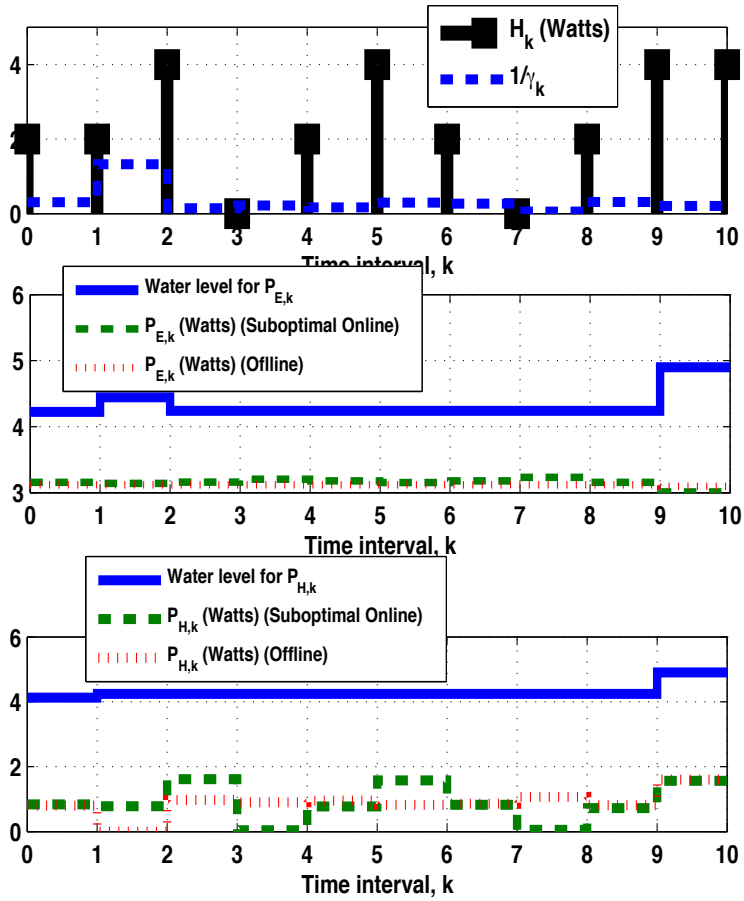

Figure 5.2: Harvested energy H_k, fading level, water level, and optimal $P_{E,k}$ for Scenario 1 vs. time interval k for $K = 10$ and $H_S = 2$ Joules.

enough, Lagrange multiplier β_k, associated with constraint (5.7), can be non–zero and this causes $\Xi_{E,k}$ to vary with k. For all time intervals, $\Xi_{E,k} - P^*_{H,k}$ is larger than the inverse channel SNR and thus $P^*_{E,k} > 0$. We also observe that the water level of $P_{H,k}$, $\Xi_{H,k}$ is monotonically non–decreasing. As B_{max} is sufficiently large for the considered case, (5.6) is not met with equality and thus $\xi_k = 0$, for $k \in \{1, 2, \cdots, 9\}$. This forces $\Xi_{H,k}$ either to remain constant or to increase. In time interval $k = 2$, $\Xi_{H,k} - P^*_{E,k}$ is less than the inverse channel SNR and therefore $P^*_{H,k} = 0$. In the rest of the time intervals, $\Xi_{H,k} - P^*_{E,k}$ is greater than the inverse channel SNR and therefore

$P^*_{H,k} > 0$. We observe for the suboptimal online power allocation scheme that due to the lack of non–causal information, this scheme cannot make full use of the harvested energy and thereby increases the power drawn from the constant energy source. For instance, we observe that in $k = 2$, although the inverse channel SNR is high, the suboptimal online scheme draws more power from the harvested energy than the optimal offline scheme and therefore cannot exploit the good channel condition (low $1/\gamma_k$) in $k = 4$ due to the lack of stored harvested energy in the battery. Moreover, compared to the offline scheme, the suboptimal online scheme consumes more energy from the constant energy source in $k \in \{4, 5\}$. Also, although no energy is harvested at the end of interval $k = 7$, the offline scheme still draws energy from the battery to transmit data bits in $k = 8$ to exploit the good channel condition. On the other hand, suboptimal online scheme cannot draw harvested energy at the beginning of $k = 8$, because it has already used up the stored harvested energy in $k < 7$. As the offline scheme has non–causal knowledge about the channel SNR and the harvested energy, this scheme can adjust the power levels in all the intervals to minimize the total power consumption from the constant energy source.

5.5.2 Comparison of the Proposed Offline Schemes with the Baseline Schemes

Fig. 5.3 shows $P_{E,Tot}$ and $P_{H,Tot}$ vs. the HR H_S for Scenario 1, where $R_T = 75$ bits and $K = 10$. The upper and lower subfigures compare the proposed scheme with baseline schemes 1 and 2, respectively. We observe that $P_{E,Tot}$ decreases with increasing H_S for the proposed and the baseline schemes. Since we minimize the power drawn from the constant power source and the amount of data to be transmitted is constant, as the harvesting rate increases, more harvested energy is available for

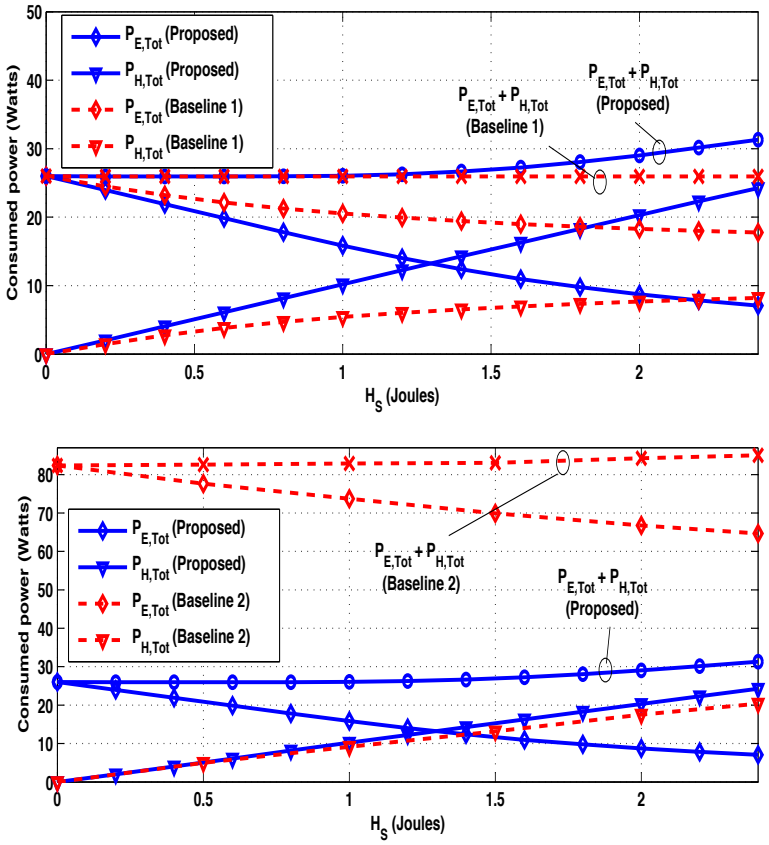

Figure 5.3: Consumed power for Scenario 1 vs. H_S for $K = 10$ and $R_T = 75$ bits. Only offline schemes are considered.

use which results in increased consumption of harvested energy and decreased consumption from the constant power source. We observe that the $P_{E,Tot}$ ($P_{H,Tot}$) curve of the proposed scheme always remains below (above) the $P_{E,Tot}$ ($P_{H,Tot}$) curves of both baseline schemes, and that the gap between the schemes increases as the HR H_S increases. As expected, for $H_S = 0$ Joule, i.e., when there is no harvested energy, the proposed scheme and baseline scheme 1 yield the same $P_{E,Tot}$ and $P_{H,Tot} = 0$. However, for $H_S = 0$ Joule, the proposed scheme and baseline scheme 2 yield different

$P_{E,Tot}$. As baseline scheme 2 has to transmit a fixed number of data bits in each time interval irrespective of the channel conditions, it is less flexible and consumes a large amount of power from the constant energy source. In particular, for $H_S = 1.5$ Joules, we observe that adopting the proposed scheme allows to save 7 Watts and 55 Watts of power drawn from the constant energy source compared to baseline schemes 1 and 2, respectively.

We have also included the total powers consumed by the proposed and the baseline schemes in Fig. 5.3. We observe that for baseline scheme 1, the increase of $P_{H,Tot}$ with increasing H_S exactly compensates the decrease of $P_{E,Tot}$ with increasing H_S, and therefore, the total consumed power does not change with H_S. Intuitively, as baseline scheme 1 minimizes the total consumed energy, H_S has no impact on the total power consumption. On the other hand, for the proposed scheme, for large H_S, $P_{H,Tot}$ increases faster with H_S than $P_{E,Tot}$ decreases with H_S. As a result, the total consumed power increases with H_S after a certain threshold. The reason for the higher total power consumption is the increase in power drawn from the energy harvester to decrease the consumption from the constant energy source. Similar to the proposed scheme, the total power consumption of baseline scheme 2 is also influenced by H_S and increases with increasing H_S.

In Figs. 5.4 and 5.5, we compare the performance of the proposed and the baseline offline schemes for Scenarios 1 and 2 as functions of the amount of transmitted data. In particular, Fig. 5.4 shows $P_{E,Tot}$ and $P_{H,Tot}$ vs. R_T for Scenario 1 whereas in Fig 5.5 we present $P_{E,Tot}$ and $P_{H,Tot}$ vs. $R_{avg}K$ for Scenario 2 where $R_{avg} = (1/K)\sum_{k=1}^{K} R_k$. For both scenarios, we adopt $H_S = 6.75$ Joules and $K = 10$. We observe that the transmit powers, $P_{E,Tot}$ and $P_{H,Tot}$, increase with increasing R_T (R_{avg}) because the larger the amount of data that has to be transmitted, the higher the required transmit

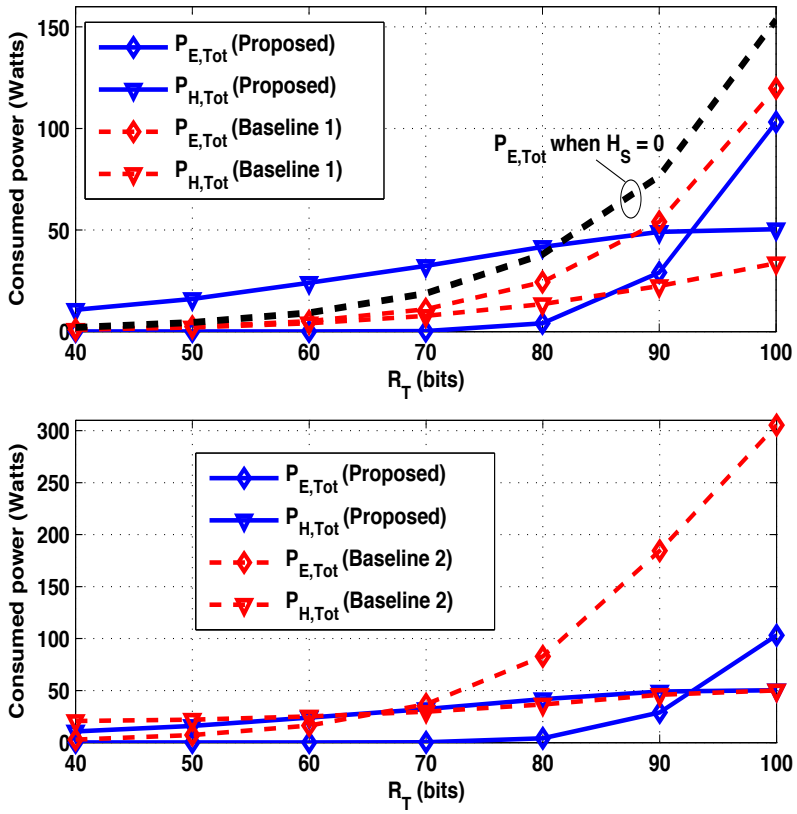

Figure 5.4: Consumed power for Scenario 1 vs. R_T for $K = 10$ and $H_S = 6.75$ Joules. Only offline schemes are considered.

power. However, the rate of increase is not the same for $P_{E,Tot}$ and $P_{H,Tot}$. The rate with which $P_{E,Tot}$ increases is small for low R_T (R_{avg}), because for low R_T (R_{avg}), the consumed power is mainly drawn from the energy harvester. On the other hand, for large R_T (R_{avg}), $P_{E,Tot}$ increases rapidly as the harvested energy alone is not sufficient to supply the required power completely. Moreover, for large R_T (R_{avg}), $P_{H,Tot}$ saturates because the maximum energy that the energy harvester can provide is limited by $\sum_{k=1}^{K} H_k$. We observe again that in both scenarios our proposed schemes are more efficient in reducing $P_{E,Tot}$ than baseline schemes 1 and 2, respectively. For comparison, we also show $P_{E,Tot}$ for the proposed and baseline scheme 1 for

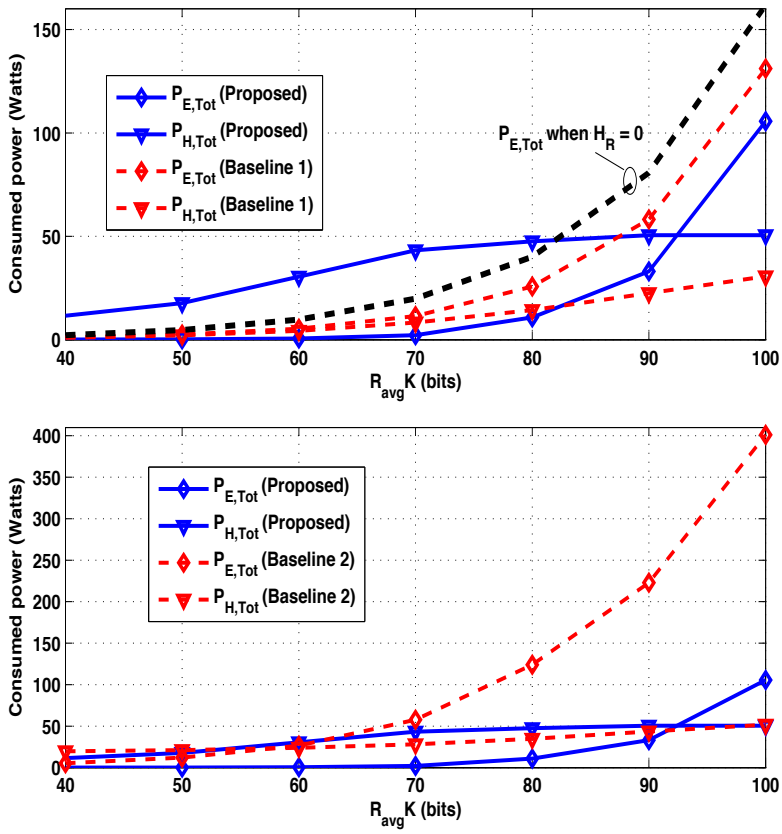

Figure 5.5: Consumed power for Scenario 2 vs. $R_{avg}K$ for $K = 10$ and $H_S = 6.75$ Joules. Only offline schemes are considered.

$H_S = 0$ Joule (i.e., no energy harvester) and observe that both schemes yield identical results as expected. Besides, $P_{E,Tot}$ for $H_S = 0$ Joule is always larger than $P_{E,Tot}$ for $H_S = 6.75$ Joules as without the supplement of the energy harvester, the constant energy source has to supply all the required power. Moreover, a comparison of the powers consumed in Scenario 1 and Scenario 2 reveals that Scenario 1 requires a (slightly) lower $P_{E,Tot}$ than Scenario 2. This can be explained by the fact that knowing the amount of data to be transmitted before the transmission starts provides more flexibility to allocate the transmit powers over the transmission intervals than when the data packets arrive during the course of transmission.

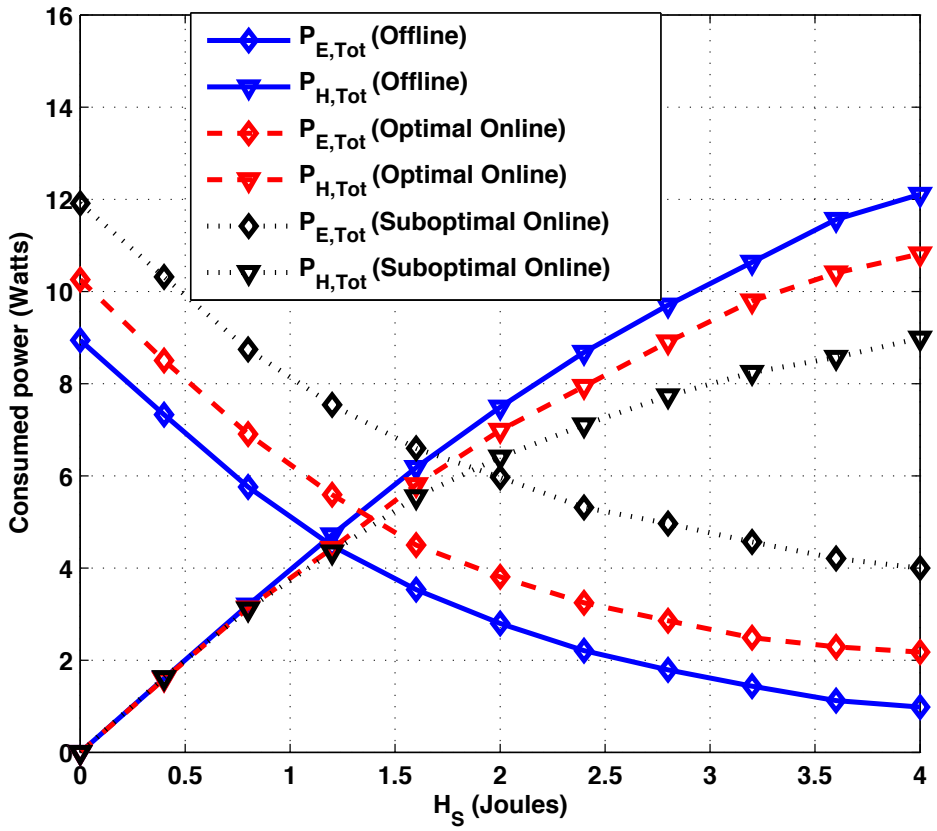

Figure 5.6: Consumed power for Scenario 1 vs. H_S for $K = 4$ and $R_T = 30$ bits.

5.5.3 Comparison of the Proposed Offline and Online Schemes

Fig. 5.6 shows $P_{E,Tot}$ and $P_{H,Tot}$ vs. the HR H_S for Scenario 1 for all considered power allocation schemes. We assume $R_T = 30$ bits and $K = 4$. We observe that $P_{E,Tot}$ ($P_{H,Tot}$) decreases (increases) with H_S for all power allocation schemes. As expected the offline power allocation scheme performs better than the online power allocation schemes for all H_S. Moreover, the optimal DP based online scheme outperforms the suboptimal online scheme because DP makes optimal use of the statistical properties

of the channel SNR and the harvested energy. We observe that the performance gaps between the offline scheme and the online schemes increase with increasing H_S. Having non–causal knowledge regarding the channel SNR and the harvested energy helps more in minimizing $P_{E,Tot}$ for high H_S than for low H_S. However, for low H_S, the gap between the offline and online schemes for $P_{H,Tot}$ is very small as all the harvested energies are used up for low H_S regardless of the non–causal information (of the channel SNR and the harvested energy) for the considered R_T. On the contrary, for high H_S, the offline scheme makes efficient use of H_S whereas the online schemes may under–utilize the harvested energy and result in a lower $P_{H,Tot}$. It is worth mentioning that a similar behavior can be observed for Scenario 2 (not shown here).

Fig. 5.7 shows $P_{E,Tot}$ and $P_{H,Tot}$ vs. the HR H_S for Scenario 1, for the offline and suboptimal online power allocation schemes for $K = 40$ and $R_T = 300$ bits. The optimal DP based online power allocation scheme has not been implemented here because of its inherent high computational cost for large K. We observe that the performance gap between the offline and suboptimal online power allocation schemes increases with increasing H_S as also observed in Fig. 5.6. However, the performance gap between the offline $P_{E,Tot}$ and the suboptimal online $P_{E,Tot}$ is larger in Fig. 5.7 compared to Fig. 5.6 for all H_S. In fact, exploiting non–causal knowledge of the channel SNR and the incoming harvested energy is more beneficial for large K than for small K. Note that a similar behavior can be observed for Scenario 2 (not shown).

In Fig. 5.8, we show $P_{E,Tot}$ and $P_{H,Tot}$ vs. H_S for Scenarios 1 and 2 for the suboptimal online power allocation scheme. Here, we assume $K = 100$ and $R_T = \sum_{k=1}^{K} R_k = 500$ bits. We observe that Scenario 1 requires a lower $P_{E,Tot}$ than Scenario 2 for all considered H_S. The random arrival of data packets in Scenario 2 introduces additional restrictions for power allocation compared to Scenario 1, where the amount

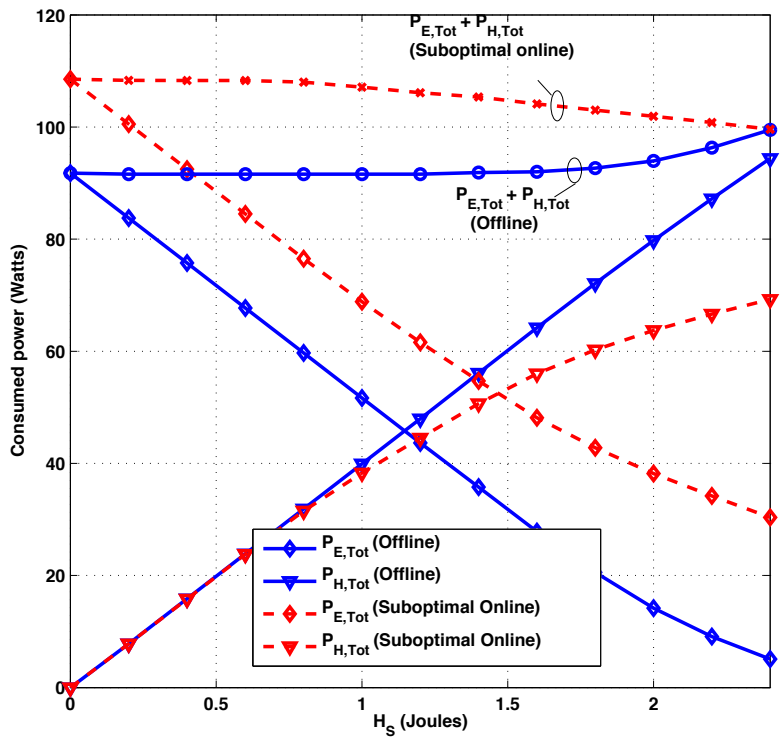

Figure 5.7: Consumed power for Scenario 1 vs. H_S for $K = 40$ and $R_T = 300$ bits.

of data to be transmitted is known before transmission starts. Hence, the observations made for Scenarios 1 and 2 for the offline scheme in Figs. 5.4 and 5.5 also translate to the suboptimal online scheme. On the other hand, since for the considered example $R_T = \sum_{k=1}^{K} R_k = 500$ bits have to be transmitted in only 100 time intervals, the harvested energy is completely used in both scenarios for all considered values of H_S. Thus, we observe in Fig. 5.8 no significant difference for $P_{H,Tot}$ between Scenarios 1 and 2.

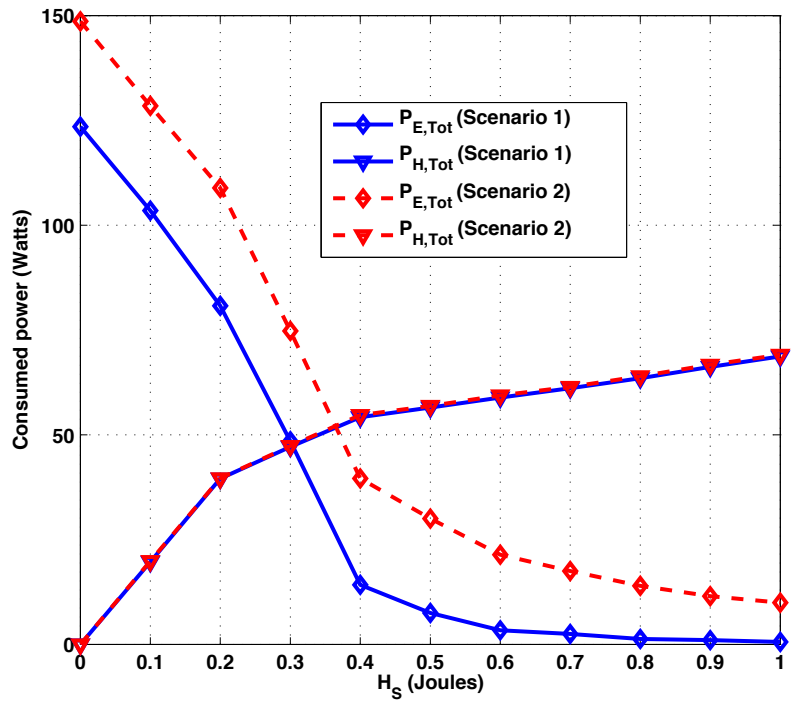

Figure 5.8: Consumed power for Scenarios 1 and 2 vs. H_S for $K = 100$ and $R_T = \sum_{k=1}^{K} R_k = 500$ bits.

5.5.4 Effect of μ on the Proposed Schemes

In Fig. 5.9, we show $\rho P_{H,k}$ vs. time interval k for the optimal offline and suboptimal online power allocation schemes for $K = 9$, $H_S = 2$ Joules, $\bar{\gamma} = 25$ dB, $R_T = 50$ bits, and three different values of μ, namely $\mu = \{0, 0.5, 1.0\}$. We assume $[\gamma_1\, \gamma_2\, \cdots\, \gamma_9] = [104.02\ 23.86\ 219.11\ 145.77\ 190.44\ 107.76\ 119.56\ 623.05\ 102.54]$ for all the considered μ. We observe that when $\mu = 0$, i.e., when the battery cannot store the harvested energy at all, the offline and suboptimal online schemes use up all of the harvested energy immediately (right after its arrival) in the current time interval to avoid any possible loss of the harvested energy. Increasing μ helps the

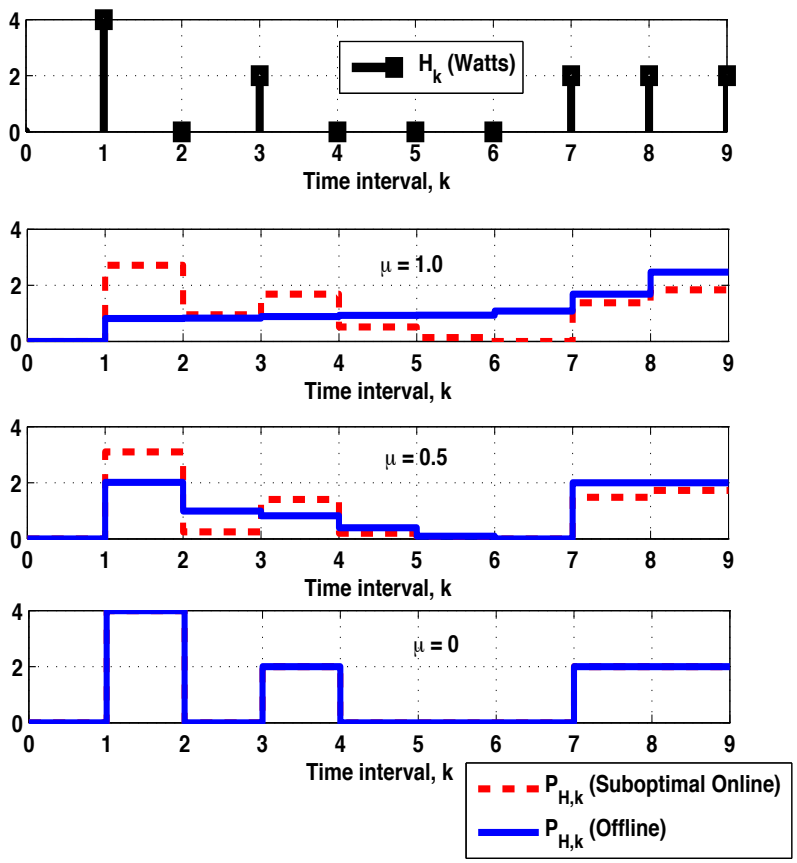

Figure 5.9: $P_{H,k}$ for Scenario 1 vs. k for $K = 9$ and $H_S = 2$ Joules.

offline and suboptimal online schemes to store the harvested energy if necessary, and to use it when the channel is better. This property is observed for $\mu = 0.5$ and $\mu = 1.0$. In Table 5.1, we show $P_{H,Tot}$ obtained for the considered offline and suboptimal online power allocation schemes for $\sum_{k=0}^{8} H_k = 10$ Joules and the value of μ assumed in Fig. 5.9. We observe that for $\mu = 0.5$ and $\mu = 1$, the offline scheme consumes more harvested energy than the suboptimal online scheme. However, for $\mu = 0$, all the harvested energy is used by both the considered schemes as any stored harvested energy would be completely lost.

Table 5.1: $P_{H,Tot}$ obtained for the parameters used for Fig. 5.9 for offline and suboptimal online power allocation schemes.

μ	Offline (Joules)	Suboptimal online (Joules)
1.0	9.93	9.21
0.5	8.32	8.16
0	10	10

5.5.5 Impact of Various EH Profiles

In Fig. 5.10, we show the impact of different EH profiles on $P_{E,Tot}$ and $P_{H,Tot}$ for Scenario 1 as a function of R_T. We assume $K = 50$ and consider offline power allocation. Two cases, denoted as Case A and Case B, are considered here to show the impact of two different EH profiles on the consumed powers. Case A assumes an EH profile, where the energy is harvested in every third time interval, whereas Case B considers another EH profile, where the energy is harvested in every time interval. In both cases, the average EH rate is 5 Joules/interval and the channel SNR changes in every time interval. We observe from Fig. 5.10 that the $P_{E,Tot}$ ($P_{H,Tot}$) curve for Case B is always below (above) the $P_{E,tot}$ ($P_{H,Tot}$) curve for Case A. In Case A, the energy is harvested at a slower rate than in Case B, i.e., in Case A there is less flexibility for power allocation. Thus, more energy is consumed from the constant energy source for Case A to transmit the required amount of data bits.

5.6 Conclusions

In this chapter, we optimized the power allocation for a point–to–point communication system with a hybrid energy source. The hybrid energy source includes a constant energy source (non–renewable) and an energy harvester (renewable). The

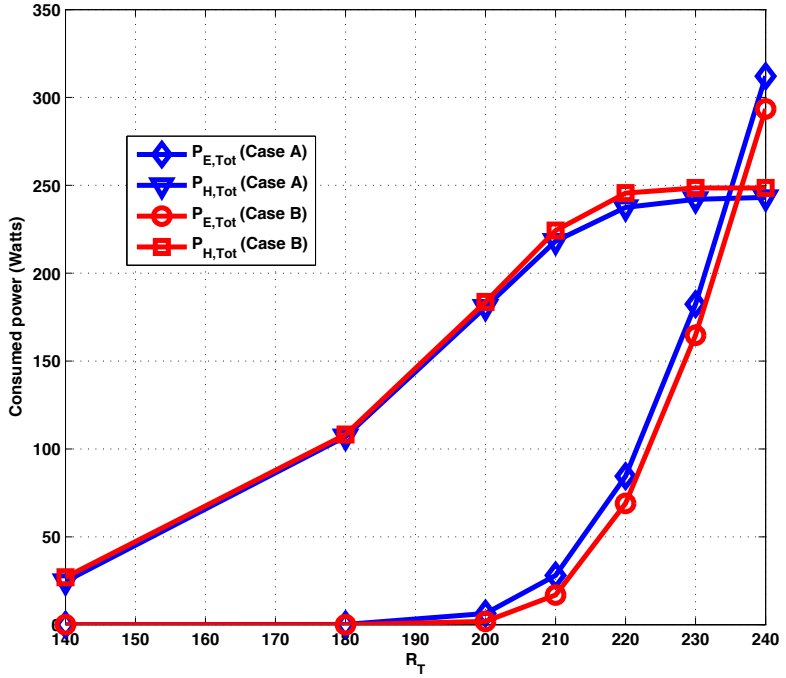

Figure 5.10: Consumed power for Scenario 1 vs. R_T for $K = 50$ and two different EH profiles.

harvested energy is stored in a battery which is modeled as a storage system with leakage. We proposed to minimize the amount of power drawn from the constant energy source to make full use of the harvested energy. We presented optimal offline, optimal online, and suboptimal online power allocation schemes for two different data arrival scenarios. We used stochastic DP to implement the optimal online power allocation scheme. Because of the inherently high complexity of DP, a low–complexity suboptimal online power allocation scheme was also proposed. A comparison of the proposed power allocation schemes with baseline schemes revealed that the proposed schemes significantly reduce the power drawn from the constant energy source and utilize the harvested energy more efficiently. Moreover, simulation results revealed that if the data to be transmitted arrives randomly over the transmission intervals,

the power consumption from the constant energy source is always higher than if the data arrives before transmission starts.

Chapter 6

Conclusions and Future Work

In Section 6.1 of this final chapter, we briefly review our results and highlight the contributions of this thesis to the literature. In Section 6.2, we propose directions for future research.

6.1 Summary of Results

This thesis focused on resource allocation schemes for different cooperative and non–cooperative communication systems. We considered systems that are impaired by Gaussian and non–Gaussian noises and powered by constant energy sources and energy harvesters. The main results of each chapter are summarized as follows:

In Chapter 2, we derived closed–form asymptotic error rate expressions for best relay selection (BRS) and partial relay selection (PRS) in an AF relay network. Our derived expressions are valid for i.n.d. Rayleigh fading and noises with finite moments. We used the derived error rate expressions to develop general power allocation frameworks for BRS and PRS with energy consumption constraints. Furthermore, we considered a relay subset selection scheme to reduce the CSI feedback overhead. We used computer simulations to show the accuracy of the derived error rate expressions and the effectiveness of the proposed power allocation schemes.

In Chapter 3, we considered a single source–relay–destination link that used EH at the source and the relay. We considered conventional and buffer–aided link adap-

tive relaying protocols and proposed optimal offline and optimal (for link adaptive relaying) and suboptimal online resource allocation schemes for both protocols. The offline scheme for conventional relaying was formulated as a convex optimization problem and hence could be solved optimally and efficiently. On the other hand, the offline scheme for link adaptive relaying results in a non–convex MINLP, which was optimally solved by the sBB method with relatively lower computational cost than the exhaustive search method. We formulated the optimal online scheme for conventional relaying by stochastic dynamic programming (DP). We did not formulate the optimal online scheme for link adaptive relaying, because it would have incurred a large computational cost. Our proposed suboptimal online schemes achieved a good performance–complexity trade–off. Simulation results revealed that link adaptive relaying has significantly better throughput than conventional relaying, at the expense of a higher complexity.

In Chapter 4, we jointly optimized the relay selection and power allocation for an AF relay network that used EH nodes for the source and the relays. We proposed optimal offline and suboptimal but low–complexity online resource allocation schemes. The offline scheme was initially formulated as a non–convex MINLP, which was then converted into a convex MINLP and optimally solved by the GBD algorithm. We avoided formulating the optimal online scheme using DP due to its high computational cost, but eventually proposed a low–complexity but suboptimal online scheme. Simulation results revealed that the suboptimal online scheme yields significantly more throughput gain than a naive scheme and performs close to the offline scheme.

In Chapter 5, we considered a point–to–point communication system that used a hybrid energy supply for its source. The hybrid energy supply consisted of a constant energy source and an energy harvester. We considered two scenarios for

the data arrival process. In the first scenario, all the data packets arrived before the transmission began. In the second scenario, the data packets may have arrived during the data transmission. Our objective was to minimize the amount of energy drawn from the constant energy source and thus efficiently utilize the harvested energy. We proposed optimal offline, optimal online, and suboptimal but low–complexity online schemes for both data arrival processes. We compared our proposed schemes with baseline schemes via simulations and observed that our proposed schemes performed much better than the baseline schemes in terms of reducing the energy consumption from the constant energy source.

6.2 Future Works

In the following, we propose some ideas for future research that are based on the results of this thesis.

6.2.1 Performance Analysis of Relay Selection Schemes Impaired by α–stable noise

A broad class of non–Gaussian phenomena that is encountered in practice can be characterized by α–stable distributions [114]. α–stable noise has heavier tails than the Gaussian distribution. Examples of α–stable noise include underwater acoustic signals, low–frequency atmospheric noise, and some types of man–made impulsive noise. The characteristic component α, $0 \leq \alpha \leq 2$, defined in the pdf of α–stable noise, controls the heaviness of the tails of the pdf. For instance, a small positive value of α indicates severe impulsiveness, whereas $\alpha = 2$ indicates the Gaussian distribution as its special case. The performance analysis in Chapter 2 is valid for the noises with

finite moments. However, our analysis in Chapter 2 cannot be applied to α–stable noise, because it does not have finite moments. Developing new techniques to analyze α–stable noise for AF relay selection systems would be an interesting direction for future research.

6.2.2 Intelligent Resource Allocation for EH Systems

The proposed offline and online resource allocation schemes for EH systems in Chapters 3–5 require non–causal or statistical information regarding the channel SNR, the harvested energy, and the data arrival process. Assuming non–causal information in the offline optimization framework is too optimistic in practice unless the underlying processes are deterministic or highly predictable. These assumptions are relaxed in the online optimization framework, which exploits statistical information about the system parameters. However, in many practical systems, the statistical properties may change over time or not be available. In both cases, learning based algorithms can be employed to identify the characteristics of the channel SNR and the energy and data arrival processes. In [115], a single source–destination link is considered and the Q–learning method is used to identify the energy and data arrival processes. The identified processes and collected information provided the bases for the resource allocation schemes that were proposed to maximize the expected sum of the transmitted data over the lifetime of the source. In the future, researchers could tackle the interesting challenge of exploiting machine–learning methods for EH cooperative communication systems in order to identify the EH characteristics of the communication nodes, their incoming data arrival process, and the channel SNRs of all the involved links. Moreover, the performance and the complexity of different machine–learning methods applicable to EH systems could also be investigated.

6.2.3 Wireless Information and Power Transfer in Relay Networks

Researchers have recently been very interested in the simultaneous transfer of information and RF energy in different communication systems [54], [116]–[118]. The simultaneous transfer of information and energy ensures that RF signals are utilized in transmitting both data and energy at the same time, and thus potentially offers great advantages to end users. However, as the information reception and RF EH have different power sensitivities, it is vital that receivers are carefully designed to successfully receive energy and information [119]. Time–sharing and power–splitting receivers are the receivers most commonly discussed in the literature [53]. It would therefore be interesting for researchers to study the behavior of wireless information and power transfers in different relay networks, e.g., in conventional relaying, buffer–aided link adaptive relaying, multi–relay networks, etc. Analyzing the performance of different receivers for different relay networks and comparing their performances would also be interesting.

6.2.4 Resource Allocation for a Multi–hop Conventional and Buffer–Aided Link Adaptive EH Relaying Protocols

Multi–hop[21] communication provides better throughput and lower error rate performance compared to single–hop communication [120]–[123]. In Chapter 3, we considered a two–hop system and demonstrated that buffer–aided link adaptive relaying protocol performs better than conventional relaying. Consequently, another interesting direction for future research would be to extend the contributions made in Chapter 3 to the multi–hop scenario. However, such an extension would be non–trivial,

[21] Here, "multi–hop" refers to more than two hops.

because the new optimization problem for the multi–hop link adaptive protocol is more involved in that the number of link selection (integer) variables is large and the computational cost is therefore very high. Hence, research should focus on the performance–complexity trade–off of the multi–hop link adaptive EH systems.

Bibliography

[1] J. A. Paradiso, and T. Starner, "Energy Scavenging for Mobile and Wireless Electronics," *IEEE Pervasive Computing*, vol. 4, no. 1, pp. 18–27, 2005.

[2] "Powercast," *[Online]: http://www.powercastco.com.*

[3] D. S. Michalopoulos, and G. K. Karagiannidis, "PHY-Layer Fairness in Amplify and Forward Cooperative Diversity Systems," *IEEE Trans. Commun.*, vol. 52, pp. 130–135, Feb. 2004.

[4] *[Online]: http://rtcmagazine.com/articles/view/101631.*

[5] *[Online]: http://news.dice.com/2011/08/24/scientists-create-energy-harvesting-lcd-screens/.*

[6] *[Online]: http://xncroft.com/projects/energyshoes.html.*

[7] A. R. Mishra, *Fundamentals of Cellular Network Planning and Optimisation: 2G/2.5G/3G... Evolution to 4G.* John Wiley and Sons, 2004.

[8] Z. Hasan, H. Boostanimehr, and V. K. Bhargava, "Green Cellular Networks: A Survey, Some Research Issues and Challenges," *IEEE Communications Surveys and Tutorials*, vol. 13, no. 4, pp. 524–540, 2011.

[9] D. Qiao, S. Choi, and K. G. Shin, "Interference Analysis and Transmit Power Control in IEEE 802.11a/h Wireless LANs," *IEEE/ACM Trans. Netw.*, vol. 15, pp. 1007–1020, Oct. 2007.

[10] G. Song and Y. Li, "Cross-layer Optimization for OFDM Wireless Networks-part II: Algorithm Development," *IEEE Trans. on Wireless Commun.*, vol. 4, pp. 625–634, Mar. 2005.

[11] T. M. Cover and J. A. Thomas, *Elements of Information Theory (Wiley Series in Telecommunications and Signal Processing).* Wiley-Interscience, 2006.

[12] G. P. Fettweis and E. Zimmermann, "ICT Energy Consumption - Trends and Challenges," in *Proc. of IEEE Intern. Conf. on Acoustics, Speech and Signal Process.*, Sep. 2008.

[13] S. Mallick, R. Devarajan, M. M. Rashid, and V. K. Bhargava, "Resource Allocation for Selective Relaying Based Cellular Wireless System with Imperfect CSI," *IEEE Trans. Commun.*, vol. 61, pp. 1822–1834, May 2013.

[14] W. Cho, R. Cao, and L. Yang, "Optimum Resource Allocation for Amplify–and–Forward Relay Networks With Differential Modulation," *IEEE Trans. Signal Processing*, vol. 56, pp. 5680–5691, Nov. 2008.

[15] D. W. K. Ng and R. Schober, "Cross–Layer Scheduling for OFDMA Amplify-and-Forward Relay Networks," *IEEE Trans. on Veh. Technol.*, vol. 59, pp. 1443–1458, Mar. 2010.

[16] A. Nasri, R. Schober, and I. F. Blake, "Performance and Optimization of Amplify-and-Forward Cooperative Diversity Systems in Generic Noise and Interference," *IEEE Trans. Wireless Commun.*, vol. 10, pp. 1132–1143, Apr. 2011.

[17] O. Ozel, K. Tutuncuoglu, J. Yang, S. Ulukus, and A. Yener, "Transmission with Energy Harvesting Nodes in Fading Wireless Channels: Optimal Policies," *IEEE J. Select. Areas Commun.*, vol. 29, pp. 1732–1743, Sep. 2011.

[18] C. K. Ho and R. Zhang, "Optimal Energy Allocation for Wireless Communications with Energy Harvesting Constraints," *IEEE Trans. Signal Processing*, vol. 60, pp. 4808–4818, Sep. 2012.

[19] A. Kansal, J. Hsu, S. Zahedi, and M. B. Srivastava, "Power Management in Energy Harvesting Sensor Networks," *ACM Trans. Embed. Comput. Syst.*, vol. 6, pp. 1–35, Sep. 2007.

[20] V. Sharma, U. Mukherji, V. Joseph, and S. Gupta, "Optimal Energy Management Policies for Energy Harvesting Sensor Nodes," *IEEE Trans. on Wireless Commun.*, vol. 9, pp. 1326–1336, Apr. 2010.

[21] H. Li, N. Jaggi, and B. Sikdar, "Relay Scheduling for Cooperative Communications in Sensor Networks with Energy Harvesting," *IEEE Trans. on Wireless Commun.*, vol. 10, pp. 2918–2928, Sep. 2011.

[22] Z. A. Eu, H. P. Tan, and W. K. G. Seah, "Wireless Sensor Networks Powered by Ambient Energy Harvesting: An Empirical Characterization," in *Proc. of IEEE ICC*, May 2010.

[23] D. P. Bertsekas, *Dynamic Programming and Optimal Control Vol. 1.* Belmont, MA: Athens Scientific, 1995.

[24] A. Nasri, A. Nezampour, and R. Schober, "Adaptive L_p–Norm Diversity Combining in Non-Gaussian Noise and Interference," *IEEE Trans. on Wireless Commun.*, vol. 8, pp. 4230–4240, Aug. 2009.

[25] D. Middleton, "Statistical-physical Models of Man–made Radio Noise–Parts I and II," *U.S. Dept. Commerce Office Telecommun.*, Apr. 1974 and 1976.

[26] C. Tellambura, "Cochannel Interference Computation for Arbitrary Nakagami Fading," *IEEE Trans. Veh. Technol.*, vol. 48, pp. 487–489, Mar. 1999.

[27] C. Tepedelenlioglu and P. Gao, "On Diversity Reception Over Fading Channels with Impulsive Noise," *IEEE Trans. on Veh. Technol.*, vol. 454, pp. 2037–2047, Nov. 2005.

[28] R. Schober, Y. Ma, L. Lampe, and P. Mathiopoulos, "Diversity Combining for Coherent and Differential M-PSK in Fading and Class-A Impulsive Noise," *IEEE Trans. Wireless Commun.*, vol. 4, pp. 1425–1432, Jul. 2005.

[29] P. Gao and C. Tepedelenlioglu, "Space–Time Coding Over Fading Channels With Impulsive Noise," *IEEE Trans. on Wireless Commun.*, vol. 6, pp. 220–229, 2007.

[30] A. Nezampour, A. Nasri, R. Schober, and Y. Ma, "Asymptotic BEP and SEP of Quadratic Diversity Combining Receivers in Correlated Ricean Fading, Non–Gaussian Noise, and Interference," *IEEE Trans. Commun.*, vol. 57, pp. 1039–1049, Apr. 2009.

[31] M. Dohler, R. W. Heath Jr., A. Lozano, C. Papadias, and R. A. Valenzuela, "Is the PHY Layer Dead?" *IEEE Commun. Magazine*, vol. 49, pp. 159–165, Apr. 2011.

[32] Q. Shan, S. Bhatti, I. A. Glover, R. Atkinson, I. E. Portugues, and R. Rutherford, "Noise Amplitude Distribution of Impulsive Noise from Measurements in a Power Substation," in *Proc. of 44th International Universities Power Engineering Conference (UPEC)*, Sep. 2009, pp. 1–5.

[33] J. G. Gonzales, *Robust Techniques for Wireless Communications in Non–Gaussian Environments.* PhD Dissertation, University of Delaware, Fall 1997.

[34] H. M. Hall, "A new Model for Impulsive Phenomena: Application to Atmospheric–Noise Communication Channels," *Technical Reports 3412-8 and 7050-7, Stanford Electronics Labrotaries, Stanford University, Palo Alto, California*, Aug. 1966.

[35] C. L. Nikias and M. Shao, *Signal Processing with Alpha–stable Distributions and Applications.* New York: Wiley, 1995.

[36] M. Simon and M. Alouini, *Digital Communications over Fading Channels.* John Wiley & Sons, 2005.

[37] G. Turin, "The Characteristic Function of Hermitian Quadratic Forms in Complex Normal Random Variables," *Biometrica*, pp. 199–201, Jun. 1960.

[38] "Wolfram Mathworld." *[Online]: http://mathworld.wolfram.com/Gamma Function.html.*

[39] A. K. Anhari and L. Lampe, "Performance Analysis for BICM Transmission over Gaussian Mixture Noise Fading Channels," *IEEE Trans. Commun.*, vol. 58, pp. 1962–1972, Jul. 2010.

[40] J. Mitra and L. Lampe, "Convolutionally Coded Transmission over Markov-Gaussian Channels: Analysis and Decoding Metrics," *IEEE Trans. Commun.*, vol. 58, pp. 1939–1949, Jun. 2010.

[41] C. Keller and M. Pursley, "Clipped Diversity Combining for Channels with Partial-Band Interference - Part I: Clipped-Linear Combining," *IEEE Trans. Commun.*, vol. 35, pp. 1320–1328, Dec. 1987.

[42] J. Cui and A. Sheikh, "Outage Probability of Cellular Radio Systems Using Maximal Ratio Combining in the Presence of Multiple Interferers," *IEEE Trans. Commun.*, vol. 47, pp. 1121–1124, Aug. 1999.

[43] X. Zhang and N. Beaulieu, "Outage Probability of MRC With Unequal-Power Cochannel Interferers in Correlated Rayleigh Fading," *IEEE Commun. Letters*, vol. 10, pp. 7–9, Jan. 2006.

[44] D. Tse and P. Viswanath, *Fundamentals of Wireless Communications*. Cambridge, UK: Cambridge University Press, 2005.

[45] T. Voigt, H. Ritter, and J. Schiller, "Utilizing Solar Power in Wireless Sensor Networks," *Proc. of IEEE International Conference on Local Computer Networks*, pp. 416–422, Oct. 2003.

[46] D. Krüger, C. Buschmann, and S. Fischer, "Solar Powered Sensor Network Design and Experimentation," in *Proc. of International Symposium on Wireless Communication Systems*, Sep. 2009, pp. 11–15.

[47] T. Y. Kheng, "Analysis, Design and Implementation of Energy Harvesting Systems for Wireless Sensor Nodes," *Thesis: National University of Singapore*, 2010.

[48] *[Online]: http://www.nrel.gov/wind/.*

[49] L. Varshney, "Transporting Information and Energy Simultaneously," in *Proc. of IEEE Intern. Sympos. on Inf. Theory*, Jul. 2008, pp. 1612–1616.

[50] P. Grover and A. Sahai, "Shannon Meets Tesla: Wireless Information and Power Transfer," in *Proc. of IEEE Intern. Sympos. on Inf. Theory*, Jun. 2010, pp. 2363–2367.

[51] R. J. M. Vullers, R. V. Schaijk, I. Doms, C. V. Hoof, and R. Mertens, "Micropower Energy Harvesting," *Elsevier Solid-State Circuits*, vol. 53, no. 7, pp. 684–693, Jul. 2009.

[52] H. Jabbar, Y. S. Song, and T. T. Jeong, "RF Energy Harvesting System and Circuits for Charging of Mobile Devices," *IEEE Trans. Consumer Electron.*, vol. 56, pp. 247–253, Feb. 2010.

[53] A. A. Nasir, X. Zhou, S. Durrani, and R. A. Kennedy, "Relaying Protocols for Wireless Energy Harvesting and Information Processing," *[Online]: http://arxiv.org/abs/1212.5406.*

[54] X. Zhou, R. Zhang, and C. K. Ho, "Wireless Information and Power Transfer: Architecture Design and Rate–Energy Tradeoff," *IEEE Trans. on Wireless Commun. (in press).*

[55] C. Mikeka and H. Arai, "Development of a Batteryless Sensor Transmitter," *Proc. of IEEE Radio and Wireless Symposium*, pp. 68–71, Jan. 2010.

[56] W. Yu and X. Qian, "Design of 3KW Wind and Solar Hybrid Independent Power Supply System for 3G Base Station," in *Proc. of International Symposium on Knowledge Acquisition and Modeling*, Nov. 2009, pp. 289–292.

[57] J. Yang and S. Ulukus, "Transmission Completion Time Minimization in an Energy Harvesting System," in *Proc. of Information Sciences and Systems (CISS)*, Mar. 2010, pp. 1–6.

[58] ——, "Optimal Packet Scheduling in an Energy Harvesting Communication System," *IEEE Trans. Commun.*, vol. 60, pp. 220–230, Jan. 2012.

[59] C. Huang, R. Zhang, and S. Cui, "Throughput Maximization for the Gaussian Relay Channel with Energy Harvesting Constraints," *IEEE J. Select. Areas Commun.*, vol. 31, pp. 1469–1479, Aug. 2013.

[60] O. Ozel and S. Ulukus, "On the Capacity Region of the Gaussian MAC with Batteryless Energy Harvesting Transmitters," in *Proc. of IEEE Globecom*, Dec. 2012.

[61] J. A. Paradiso and M. Feldmeier, "A Compact, Wireless, Self–Powered Pushbutton Controller," in *Proc. of ACM Ubicomp*, Oct. 2001, pp. 299–304.

[62] I. Krikidis, G. Zheng, and B. Ottersten, "Harvest–Use Cooperative Networks with Half/Full-Duplex Relaying," in *Proc. of IEEE WCNC*, Apr. 2013.

[63] A. Bletsas, A. Khisti, D. P. Reed, and A. Lippman, "A Simple Cooperative Diversity Method Based on Network Path Selection," *IEEE J. Select. Areas Commun.*, vol. 24, pp. 659–672, Mar. 2006.

[64] E. Beres, and R. Adve, "Selection Cooperation in Multi–Source Cooperative Networks," *IEEE Trans. on Wireless Commun.*, vol. 7, pp. 118–127, Jan. 2008.

[65] J. N. Laneman, and G. W. Wornell, "Distributed Space–Time–Coded Protocols for Exploiting Cooperative Diversity in Wireless Networks," *IEEE Trans. Inform. Theory*, vol. 49, pp. 2415–2425, Oct. 2003.

[66] J. Boyer, D. D. Falconer, and H. Yanikomeroglu, "Cooperative Connectivity Models for Wireless Relay Networks," *IEEE Trans. Wireless Commun.*, vol. 6, pp. 1992–2000, Jun. 2007.

[67] T. Q. Duong, V. N. Q. Bao, and H. J. Zepernick, "On the Performance of Selection Decode–and–Forward Relay Networks over Nakagami–M Fading Channels," *IEEE Commun. Letters*, vol. 13, pp. 172–174, Mar. 2009.

[68] I. Krikidis, J. Thompson, S. McLaughlin, and N. Goertz, "Amplify–and–Forward with Partial Relay Selection," *IEEE Commun. Letters*, vol. 12, pp. 235–237, Apr. 2008.

[69] H. Ding, J. Ge, and Z. Jiang, "Asymptotic Performance Analysis of Amplify–and–Forward with Partial Relay Selection in Rician Fading," *IEEE Electronics Letters*, vol. 46, pp. 248–250, Feb. 2010.

[70] C. K. Lo, S. Vishwanath, and R. W. Heath, "Relay Subset Selection in Wireless Networks Using Partial Decode-and-Forward Transmission," *IEEE Trans. Veh. Technol.*, vol. 58, pp. 692–704, Feb. 2009.

[71] E. Beres and R. Adve, "Optimal Relay-Subset Selection and Time-Allocation in Decode-and-Forward Cooperative Networks," in *Proc. of IEEE Globecom*, Nov. 2009, pp. 1–5.

[72] Y. Zhao, R. Adve and T. J. Lim, "Improving Amplify–and–Forward Relay Networks: Optimal Power Allocation versus Selection," *IEEE Trans. Wireless Commun.*, vol. 6, pp. 3114–3123, Aug. 2007.

[73] B. Maham and A. Hjorungnes, "Minimum Power Allocation in SER Constraint Relay Networks," in *Proc. of IEEE VTC*, May 2008, pp. 2431–2435.

[74] M. Hasna, and M. S. Alouini, "End–to–End Performance of Transmission Systems with Relays Over Rayleigh–Fading Channels," *IEEE Trans. Wireless Commun.*, vol. 2, pp. 1126–1131, Nov. 2003.

[75] S. Boyd and L. Vandenberghe, *Convex Optimization.* Cambridge, UK: Cambridge University Press, 2004.

[76] I. Gradshteyn, and I. Ryzhik, *Table of Integrals, Series and Products.* Academic Press, New York, 2000.

[77] I. Ahmed, A. Nasri, D. Michalopoulos, R. Schober, and R. K. Mallik, "Relay Subset Selection and Fair Power Allocation for Best and Partial Relay Selection in Generic Noise and Interference," *[Online]: www.ece.ubc.ca/∼imtiazah/TechReport.pdf.*

[78] S. Boyd, S. Kim, L. Vandenberghe, and A. Hassibi, "A Tutorial on Geometric Programming," *Optimization and Engineering*, vol. 8, pp. 67–127, 2007.

[79] M. Grant and S. Boyd, "CVX: Matlab Software for Disciplined Convex Programming," *[Online]: http://www.cvxr.com/cvx/*, Apr. 2011.

[80] M. O. Hasna and M. A. Alouini, "Harmonic Mean and End-to-End Performance of Transmission Systems With Relays," *IEEE Trans. Commun.*, vol. 52, pp. 130–135, Feb. 2004.

[81] B. Medepally and N. B. Mehta, "Voluntary Energy Harvesting Relays and Selection in Cooperative Wireless Networks," *IEEE Trans. on Wireless Commun.*, vol. 9, pp. 3543–3553, Nov. 2010.

[82] J. Yang, O. Ozel, and S. Ulukus, "Broadcasting with an Energy Harvesting Rechargeable Transmitter," *IEEE Trans. on Wireless Commun.*, vol. 11, pp. 571–583, Feb. 2012.

[83] C. Huang, R. Zhang, and S. Cui, "Outage Minimization in Fading Channels under Energy Harvesting Constraints," in *Proc. of IEEE ICC*, Jun. 2012.

[84] K. Tutuncuoglu and A. Yener, "Cooperative Energy Harvesting Communications with Relaying and Energy Sharing," in *Proc. of Information Theory Workshop*, Sep. 2013.

[85] B. Gurakan, O. Ozel, J. Yang, and S. Ulukus, "Energy Cooperation in Energy Harvesting Communications," *IEEE Trans. Commun.*, vol. 61, pp. 4884–4898, Dec. 2013.

[86] A. Host–Madsen and J. Zhang, "Capacity Bounds and Power Allocation for Wireless Relay Channels," *IEEE Trans. Inform. Theory*, vol. 51, pp. 2020–2040, jun 2005.

[87] J. N. Laneman, D. N. C. Tse, and G. W. Wornell, "Cooperative Diversity in Wireless Networks: Efficient Protocols and Outage Behaviour," *IEEE Trans. Inform. Theory*, vol. 50, pp. 3062–3080, Dec. 2004.

[88] A. Ikhlef, D. S. Michalopoulos, and R. Schober, "Max-Max Relay Selection for Relays with Buffers," *IEEE Trans. on Wireless Commun.*, vol. 11, pp. 1124 – 1135, Mar. 2012.

[89] N. Zlatanov, R. Schober, and P. Popovski, "Buffer-Aided Relaying with Adaptive Link Selection," *IEEE J. Select. Areas Commun.*, vol. 31, pp. 1530–1542, Aug. 2013.

[90] N. B. Mehta, V. Sharma, and G. Bansal, "Performance Analysis of a Cooperative System with Rateless Codes and Buffered Relays," *IEEE Trans. on Wireless Commun.*, vol. 10, pp. 1069–1081, Apr. 2011.

[91] E. M. B. Smith and C. C. Pantelides, "A Symbolic Reformulation/Spatial Branch–and–Bound Algorithm for the Global Optimization of Non–Convex MINLPs," *Elsevier Journal of Computers and Chemical Engineering*, vol. 23, pp. 457–478, May. 1999.

[92] P. Belotti, J. Lee, L. Liberti, F. Margot, and A. Waechter, "Branching and Bounds Tightening Techniques for Non–Convex MINLP," *Optimization Methods and Software*, vol. 24, pp. 597–634, Aug. 2009.

[93] "Couenne, an exact solver for nonconvex MINLPs," *[Online]:https://projects.coin-or.org/Couenne*.

[94] N. Zlatanov and R. Schober, "Buffer-Aided Relaying with Adaptive Link Selection - Fixed and Mixed Rate Transmission," *IEEE Trans. Inform. Theory*, vol. 59, pp. 2816–2840, May 2013.

[95] D. W. K. Ng, E. S. Lo, and R. Schober, "Energy-Efficient Resource Allocation in OFDMA Systems with Hybrid Energy Harvesting Base Station," *IEEE Trans. on Wireless Commun.*, vol. 12, pp. 3412–3427, Jul. 2013.

[96] D. W. K. Ng and R. Schober, "Spectral Efficient Optimization in OFDM Systems with Wireless Information and Power Transfer," in *Proc. of IEEE EUSIPCO*, Sep. 2013.

[97] R. Corless, G. Gonnet, D. Hare, D. Jeffrey, and D. Knuth, "On the Lambert W Function," *Advances in Computational Mathematics*, vol. 5, pp. 329–359, 1996.

[98] K. T. Phan, D. H. N. Nguyen, and T. Le-Ngoc, "Joint Power Allocation and Relay Selection in Cooperative Networks," in *Proc. of IEEE Globecom*, Dec. 2009.

[99] C. A. Floudas, "Nonlinear and Mixed–Integer Optimization: Fundamentals and Applications," *Oxford University Press*, 1995.

[100] "MOSEK Software," *[Online]: http://www.mosek.com.*

[101] L. Ruan and V. K. N. Lau, "Power Control and Performance Analysis of Cognitive Radio Systems under Dynamic Spectrum Activity and Imperfect Knowledge of System State," *IEEE Trans. Wireless Commun.*, vol. 8, pp. 4616–4622, Sep. 2009.

[102] Z. Hasan, G. Bansal, E. Hossain, and V. Bhargava, "Energy-Efficient Power Allocation in OFDM- Based Cognitive Radio Systems: A Risk Return model," *IEEE Trans. Wireless Commun.*, vol. 8, pp. 6078–6088, Dec. 2009.

[103] W. L. Huang and K. B. Letaief, "Cross-Layer Scheduling and Power Control Combined With Adaptive Modulation for Wireless Ad Hoc Networks," *IEEE Trans. Commun.*, vol. 55, pp. 728–739, Apr. 2007.

[104] S. Gao, L. Qian, and D. R. Vaman, "Energy Efficient Adaptive Modulation in Wireless Cognitive Radio Adhoc Networks," in *Proc. of IEEE SECON*, Jun. 2008, pp. 1–8.

[105] K. Tutuncuoglu and A. Yener, "Optimum Transmission Policies for Battery Limited Energy Harvesting Nodes," *IEEE Trans. Wireless Commun.*, vol. 11, pp. 1180–1189, Mar. 2012.

[106] I. Ahmed, A. Ikhlef, R. Schober, and R. K. Mallik, "Power Allocation for Conventional and Buffer-Aided Link Adaptive Relaying Systems with Energy Harvesting Nodes," *IEEE Trans. on Wireless Commun.*, pp. 1182–1195, Mar. 2014.

[107] E. O. Torres, L. A. Milner, and Gabriel A. Rincón-Mora, "Hybrid Supplies for Wireless Micro-Systems," *The Electromechanical Society's INTERFACE*, vol. 17, pp. 57–60, 2008.

[108] "Green Energy Solution by Huawei," *[Online]:http://www.huawei.com/en/solutions/go-greener/hw-076723-green-hybrid-powercube.htm.UdxZdxbRkRk.*

[109] K. Tutuncuoglu and A. Yener, "Communicating Using an Energy Harvesting Transmitter: Optimum Policies Under Energy Storage Losses," *[Online]: http://arxiv.org/abs/1208.6273.*

[110] S. Reddy and C. R. Murthy, "Profile Based Load Scheduling in Wireless Energy Harvesting Sensors for Data Rate Maximization," in *Proc. of IEEE ICC*, 2010, pp. 1–5.

[111] R. Shigeta, Y. Kawahara, and T. Asami, "Demo: Capacitor Leakage Aware Duty Cycle Control for Energy Harvesting Wireless Sensor Networks," in *Proc. of the 9th ACM Conf. on Embedded Networked Sensor Systems*, 2011, pp. 387–388.

[112] T. Zhu, Z. Zhong, Y. Gu, T. He, and Z. L. Zhang, "Leakage-aware Energy Synchronization for Wireless Sensor Networks," in *Proc. of the 7th International Conference on Mobile Systems, Applications, and Services*, 2009, pp. 319–332.

[113] Q. Wang, M. Hempstead, and W. Yang, "A Realistic Power Consumption Model for Wireless Sensor Network Devices," in *Proc. of the Third Annual IEEE Commun. Society Conf. on Sensor, Mesh and Ad Hoc Commun. and Networks*, vol. 1, Sep. 2006, pp. 286–295.

[114] G. A. Tsihrintzis and C.L. Nikias, "Performance of optimum and suboptimum receivers in the presence of impulsive noise modeled as an alpha-stable process," *IEEE Trans. Commun.*, vol. 43, pp. 904–914, Feb. 1995.

[115] P. Blasco, D. Gündüz, and M. Dohler, "A Learning Theoretic Approach to Energy Harvesting Communication System Optimization," *IEEE Trans. on Wireless Commun.*, vol. 12, pp. 1872–1882, Apr. 2013.

[116] D. W. K. Ng, E. S. Lo, and R. Schober, "Wireless Information and Power Transfer: Energy Efficiency Optimization in OFDMA Systems," *IEEE Trans. on Wireless Commun.*, vol. 12, pp. 6352–6370, Dec. 2013.

[117] D. W. K. Ng, L. Xiang, and R. Schober, "Multi-Objective Beamforming for Secure Communication in Systems with Wireless Information and Power Transfer," in *Proc. of the IEEE PIMRC*, Jun. 2013.

[118] D. W. K. Ng and R. Schober, "Resource Allocation for Secure Communication in Systems with Wireless Information and Power Transfer," in *Proc. of IEEE Globecom*, Dec. 2013.

[119] R. Zhang and C. K. Ho, "MIMO Broadcasting for Simultaneous Wireless Information and Power Transfer," *IEEE Trans. on Wireless Commun*, vol. 12, pp. 1989–2001, May 2013.

[120] J. Boyer, D. D. Falconer, and H. Yanikomeroglu, "Multi–hop Diversity in Wireless Relaying Channels," *IEEE Trans. Commun.*, vol. 52, pp. 1820–1830, Oct. 2004.

[121] O. Oyman, N. J. Laneman, and S. Sandhu, "Multi–hop Relaying for Broadband Wireless Mesh Networks: From Theory to Practice," *IEEE Commun. Magazine*, vol. 45, pp. 2551–2557, Sep. 2009.

[122] G. Amarasuriya, C. Tellambura and M. Ardakani, "Performance Bounds for AF Multi–Hop Relaying over Nakagami Fading," in *Proc. of IEEE WCNC*, Apr. 2010.

[123] C. Conne, M. Ju, H. Song and I. Kim, "SER Analysis and PDF Derivation for Multi–Hop Amplify–and–Forward Relay Systems," *IEEE Trans. Commun.*, vol. 58, pp. 2413–2424, Aug. 2010.

[124] H. P. Hsu, *Theory and Problems of Probability, Random Variables, and Random Processes*. Schaum's Outline Series.

[125] "Wolfram Mathworld." *[Online]: http://functions.wolfram.com/Hypergeo/-metricFunctions/ Hypergeometric2F1/06/01/05/01/02*.

Appendix A

Exploiting [16, Eq. (33) and (37)], for BRS the MGF of Δ_{k_s} can be expressed as

$$\Phi^{B}_{\Delta_{k_s}}(s) = \mathcal{E}_{a_{k_s},\theta_{k_s}}\left\{e^{-s\Delta_{k_s}}\right\} = \sum_{\xi=0}^{\infty} s^{2\xi}(2d)^{2\xi} \sum_{i+j=\xi} \frac{\beta_i\beta_j}{2i!2j!}\Psi^{ij}_{k_s}, \tag{A.1}$$

where $\beta_i \triangleq \Gamma(i+1/2)/(\sqrt{\pi}\Gamma(i+1))$ and

$$\Psi^{ij}_{k_s} \triangleq \mathcal{E}_{\gamma_{1k_s}\gamma_{2k_s}\bar{n}_{1k_s}\bar{n}_{2k_s}}\left\{\Omega^{ij}_{k_s}(d^2 s)|\bar{n}_{1k_s}|^{2i}|\bar{n}_{2k_s}|^{2j}\right\} \tag{A.2}$$

with

$$\Omega^{ij}_{k_s}(s) \triangleq \frac{e^{-s\frac{\gamma_{1k_s}\gamma_{2k_s}}{\gamma_{1k_s}+\gamma_{2k_s}}}\gamma_{1k_s}^{2j+i}\gamma_{2k_s}^{2i+j}}{\left(\gamma_{1k_s}+\gamma_{2k_s}\right)^{2i+2j}}. \tag{A.3}$$

Since the channel gains and the noise samples are mutually independent, $\Psi^{ij}_{k_s}$ can be expanded as

$$\Psi^{ij}_{k_s} = \sum_{k=1}^{N} \mathcal{E}_{\gamma_{1k}\gamma_{2k}}\left\{\Omega^{ij}_{k}(d^2 s)\right\}\mathcal{E}_{\bar{n}_{1k}\bar{n}_{2k}}\left\{|\bar{n}_{1k}|^{2i}|\bar{n}_{2k}|^{2j}\right\}. \tag{A.4}$$

Using the results in [124, Solved Problem 4.25], the joint probability density function (pdf) of γ_{1k} and γ_{2k} can be expressed as

$$p(x,y) = \begin{cases} p_{\gamma_{1k}}(x)p_{\gamma_{2k}}(y)\prod\limits_{\substack{m=1\\m\neq k}}^{N} P_{z_m}(x), & x \leq y \\ p_{\gamma_{1k}}(x)p_{\gamma_{2k}}(y)\prod\limits_{\substack{m=1\\m\neq k}}^{N} P_{z_m}(y), & x > y \end{cases} \tag{A.5}$$

where $z_m = \min\{\gamma_{1m}, \gamma_{2m}\}$, $p_{\gamma_{1k}}(\gamma_{1k}) = \bar{\gamma}_{1k}^{-1} e^{-\gamma_{1k}/\bar{\gamma}_{1k}}$ and $p_{\gamma_{2k}}(\gamma_{2k}) = \bar{\gamma}_{2k}^{-1} e^{-\gamma_{2k}/\bar{\gamma}_{2k}}$ are Rayleigh pdfs, and $P_{z_m}(\cdot)$ denotes the cdf of z_m. Since we are interested in the high SNR behavior, we replace the cdf of z_m with its first order Taylor series expansion $P_{z_m}(z) \doteq \frac{\bar{\gamma}_{1m}+\bar{\gamma}_{2m}}{\bar{\gamma}_{1m}\bar{\gamma}_{2m}} z$. Based on this approximation, $\mathcal{E}_{\gamma_{1k}\gamma_{2k}}\left\{\Omega_k^{ij}(d^2 s)\right\}$ in (A.4) can be written as

$$\mathcal{E}_{\gamma_{1k}\gamma_{2k}}\left\{\Omega_k^{ij}(s)\right\} = \Psi_{Ak}^{ij}(s) + \Psi_{Bk}^{ij}(s), \tag{A.6}$$

$$\text{where} \quad \Psi_{Ak}^{ij}(s) = \int_{\gamma_{1k}=0}^{\infty} \int_{\gamma_{2k}=0}^{\gamma_{1k}} C_{\gamma,\bar{\gamma}}^{i,j,k} \gamma_{2k}^{N-1} d\gamma_{1k} d\gamma_{2k} \tag{A.7}$$

$$\text{and} \quad \Psi_{Bk}^{ij}(s) = \int_{\gamma_{1k}=0}^{\infty} \int_{\gamma_{2k}=\gamma_{1k}}^{\infty} C_{\gamma,\bar{\gamma}}^{i,j,k} \gamma_{1k}^{N-1} d\gamma_{1k} d\gamma_{2k} \tag{A.8}$$

with

$$C_{\gamma,\bar{\gamma}}^{i,j,k} = \frac{e^{-s\frac{\gamma_{1k}\gamma_{2k}}{\gamma_{1k}+\gamma_{2k}}} \gamma_{1k}^{2j+i} \gamma_{2k}^{2i+j} e^{-\frac{\gamma_{1k}}{\bar{\gamma}_{1k}}} e^{-\frac{\gamma_{2k}}{\bar{\gamma}_{2k}}}}{(\gamma_{1k}+\gamma_{2k})^{2i+2j} \bar{\gamma}_{1k}\bar{\gamma}_{2k} \prod_{m=1, m\neq k}^{N} \left(\frac{\bar{\gamma}_{1m}\bar{\gamma}_{2m}}{\bar{\gamma}_{1m}+\bar{\gamma}_{2m}}\right)}. \tag{A.9}$$

Applying the transformation of variables, $\gamma_{1k} = r^2 \cos^2\phi$ and $\gamma_{2k} = r^2 \sin^2\phi$, the definition $N_{\bar{\gamma}} \triangleq (\bar{\gamma}_{1k}\bar{\gamma}_{2k} \prod_{m=1,m\neq k}^{N} \frac{\bar{\gamma}_{1m}\bar{\gamma}_{2m}}{\bar{\gamma}_{1m}+\bar{\gamma}_{2m}})^{-1}$, and the definition of the Gamma function, $\Gamma(t) = \int_0^\infty x^{t-1} e^{-x} dx$, in $\Psi_{Ak}^{ij}(s)$ of (A.8) leads to

$$\Psi_{Ak}^{ij}(s) = 2N_{\bar{\gamma}}\Gamma(i+j+N+1) \int_0^{\pi/4} \frac{\left(\sin^2\phi\right)^{2i+j+N-\frac{1}{2}} \left(\cos^2\phi\right)^{2j+i+\frac{1}{2}}}{\left(s\cos^2\phi\sin^2\phi + \frac{\cos^2\phi}{\bar{\gamma}_{1k}} + \frac{\sin^2\phi}{\bar{\gamma}_{2k}}\right)^{i+j+N+1}} d\phi. \tag{A.10}$$

Splitting the integration limit in (A.10) into two intervals $[0, \epsilon]$ and $[\epsilon, \pi/4]$ yields

$$\Psi_{Ak}^{ij}(s) = 2N_{\bar{\gamma}}\Gamma(i+j+N+1)(\mathrm{I}_{Ak} + \mathrm{II}_{Ak}), \tag{A.11}$$

where I_{Ak} and II_{Ak} correspond to the integrals from 0 to ϵ and from ϵ to $\pi/4$, respectively. For $\epsilon \to 0$, $\sin\phi \to \phi$, and $\cos\phi \to 1$, which leads to

$$\mathrm{I}_{Ak} = \int_0^{\epsilon} \frac{\left(\phi^2\right)^{2i+j+N-\frac{1}{2}} \bar{\gamma}_{1k}^{i+j+N+1}}{\left(\left(s+\frac{1}{\bar{\gamma}_{2k}}\right)\phi^2\bar{\gamma}_{1k}+1\right)^{i+j+N+1}} d\phi. \tag{A.12}$$

Using [76, 3.194.1], (A.12) can be written as

$$\mathrm{I}_{Ak} = \frac{\epsilon^{2(2i+j+N)}\bar{\gamma}_{1k}^{i+j+N+1}}{2(2i+j+N)}\, {}_2\mathcal{F}_1(2i+j+N, i+j+N+1; \\ 2i+j+N+1; -(s+1/\bar{\gamma}_{2k})\bar{\gamma}_{1k}\epsilon^2), \tag{A.13}$$

where ${}_2\mathcal{F}_1(\cdot,\cdot;\cdot;\cdot)$ denotes the Gaussian hypergeometric function. Exploiting the asymptotic behavior of ${}_2\mathcal{F}_1(\cdot,\cdot;\cdot;z)$ for $z \to \infty$ [125], (A.13) can be rewritten as

$$\mathrm{I}_{Ak} = \frac{1}{2(2i+j+N)s^{i+j+N+1}} \left[\frac{\Gamma(1-i)\Gamma(2i+j+N+1)(\bar{\gamma}_{1k}s)^{-(i-1)}}{\Gamma(i+j+N+1)} \right. \\ \left. + \frac{(2i+j+N)\epsilon^{2(i-1)}}{i-1}\right] + o\left(\bar{\gamma}_{1k}^{-(i-1)^+}\right). \tag{A.14}$$

On the other hand, assuming $\epsilon \to 0$ and $\bar{\gamma}_{1k}, \bar{\gamma}_{2k} \to \infty$, II_{Ak} can be stated as

$$\mathrm{II}_{Ak} = \frac{1}{s^{i+j+N+1}} \int_{\epsilon}^{\pi/4} \left(\sin^2\phi\right)^{i-\frac{3}{2}} \left(\cos^2\phi\right)^{j-N-\frac{1}{2}} d\phi. \tag{A.15}$$

Due to the symmetry of $\Psi_{Ak}^{ij}(s)$ and $\Psi_{Bk}^{ij}(s)$ in (A.8), an asymptotic expression similar to (A.10) can also be developed for $\Psi_{Bk}^{ij}(s)$. This leads to

$$\Psi_{Bk}^{ij}(s) = 2N_{\bar{\gamma}}\Gamma(i+j+N+1)(\mathrm{I}_{Bk}+\mathrm{II}_{Bk}), \tag{A.16}$$

where

$$\mathrm{I}_{Bk} = \frac{1}{2(2j+i+N)s^{i+j+N+1}}\left[\frac{\Gamma(1-j)\Gamma(2j+i+N+1)(\bar{\gamma}_{2k}s)^{-(j-1)}}{\Gamma(i+j+N+1)} + \frac{(2j+i+N)\epsilon^{2(j-1)}}{j-1}\right] + o\left(\bar{\gamma}_{2k}^{-(j-1)^+}\right) \quad \text{(A.17)}$$

and II_{Bk} is independent of $\bar{\gamma}_{1k}$ and $\bar{\gamma}_{2k}$.

Based on (A.10) and (A.14)–(A.17), we evaluate now $\mathcal{E}_{\gamma_{1k}\gamma_{2k}}\{\Omega_k^{ij}(s)\}$ in (A.6) for four different cases.

Case 1: When $i = 0$ and $j = 0$,

$$\mathcal{E}_{\gamma_{1k}\gamma_{2k}}\left\{\Omega_k^{ij}(s)\right\} = \frac{(N-1)!}{\prod\limits_{\substack{m=1\\m\neq k}}^{N}\left(\frac{\bar{\gamma}_{1m}\bar{\gamma}_{2m}}{\bar{\gamma}_{1m}+\bar{\gamma}_{2m}}\right)s^N}\left(\frac{1}{\bar{\gamma}_{1k}}+\frac{1}{\bar{\gamma}_{2k}}\right) + o\left(\bar{\gamma}_c^{-1}\right), \quad \text{(A.18)}$$

where $\bar{\gamma}_c \triangleq \prod_{k=1}^{N}\min\{\bar{\gamma}_{1k}\bar{\gamma}_{2k}\}$.

Case 2: When $i \neq 0$ and $j = 0$, we get

$$\mathcal{E}_{\gamma_{1k}\gamma_{2k}}\left\{\Omega_k^{ij}(s)\right\} = \frac{(i+N-1)}{\bar{\gamma}_{1k}\prod\limits_{\substack{m=1\\m\neq k}}^{N}\left(\frac{\bar{\gamma}_{1m}\bar{\gamma}_{2m}}{\bar{\gamma}_{1m}+\bar{\gamma}_{2m}}\right)s^{i+N}} + o\left(\bar{\gamma}_c^{-1}\right). \quad \text{(A.19)}$$

Case 3: When $i = 0$ and $j \neq 0$, we have

$$\mathcal{E}_{\gamma_{1k}\gamma_{2k}}\left\{\Omega_k^{ij}(s)\right\} = \frac{(j+N-1)}{\bar{\gamma}_{2k}\prod\limits_{\substack{m=1\\m\neq k}}^{N}\left(\frac{\bar{\gamma}_{1m}\bar{\gamma}_{2m}}{\bar{\gamma}_{1m}+\bar{\gamma}_{2m}}\right)s^{j+N}} + o\left(\bar{\gamma}_c^{-1}\right). \quad \text{(A.20)}$$

Case 4: When $i \neq 0$ and $j \neq 0$, we obtain

$$\mathcal{E}_{\gamma_{1k}\gamma_{2k}}\left\{\Omega_k^{ij}(s)\right\} = o\left(\bar{\gamma}_c^{-2}\right). \quad \text{(A.21)}$$

Combining (A.1), (A.4), (A.18)–(A.21), using $\mathcal{E}_{\bar{n}_{1k}\bar{n}_{2k}}\{|\bar{n}_{1k}|^{2i}|\bar{n}_{2k}|^{2j}\} = m_{1k}(i)m_{2k}(j)$, where $m_{1k}(i) \triangleq \mathcal{E}\{|\bar{n}_{1k}|^{2i}\}$ and $m_{2k}(i) \triangleq \mathcal{E}\{|\bar{n}_{2k}|^{2i}\}$, and exploiting the identity $s^{2\xi}\beta_\xi(\xi!)^2 = 2\xi!$, we obtain (2.11).

Appendix B

For PRS–S, relay selection depends only on the instantaneous S–R SNRs. Thus, the joint pdf of γ_{1k} and γ_{2k} is given by

$$p(x,y) = p_{\gamma_{1k}}(x)p_{\gamma_{2k}}(y)\prod_{\substack{i=1\\ i\neq k}}^{N} P_{\gamma_{1i}}(x) = p_{\gamma_{1k}}(x)p_{\gamma_{2k}}(y) \times \sum_{\substack{u_1=0\\ k\neq 1}}^{1}\sum_{\substack{u_2=0\\ k\neq 2}}^{1}\cdots\sum_{\substack{u_N=0\\ k\neq N}}^{1}(-1)^{\sum_{i=1,i\neq k}^{N} u_i} e^{-\gamma_{1k}\sum_{i=1,i\neq k}^{N}\frac{u_i}{\bar{\gamma}_{1i}}}, \quad \text{(B.1)}$$

where $P_{\gamma_{1i}}(z) = 1 - e^{-\frac{z}{\bar{\gamma}_{1i}}}$. Eqs. (A.1)–(A.4) are also valid for PRS–S and based on (B.1), $\mathcal{E}_{\gamma_{1k}\gamma_{2k}}\left\{\Omega_k^{ij}(s)\right\}$ in (A.4) can be written as

$$\mathcal{E}_{\gamma_{1k}\gamma_{2k}}\left\{\Omega_k^{ij}(s)\right\} = \sum_{\substack{u_1=0\\ k\neq 1}}^{1}\cdots\sum_{\substack{u_N=0\\ k\neq N}}^{1}(-1)^{\sum_{\substack{i=1\\ i\neq k}}^{N} u_i}\int_{\gamma_{1k}=0}^{\infty}\int_{\gamma_{2k}=0}^{\infty}\frac{e^{-s\frac{\gamma_{1k}\gamma_{2k}}{\gamma_{1k}+\gamma_{2k}}}\gamma_{1k}^{2j+i}\gamma_{2k}^{2i+j}}{(\gamma_{1k}+\gamma_{2k})^{2i+2j}} \times \frac{e^{-\gamma_{1k}\left(\frac{1}{\bar{\gamma}_{1k}}+\sum_{i=1,\,i\neq k}^{N}\frac{u_i}{\bar{\gamma}_{1i}}\right)}e^{-\frac{\gamma_{2k}}{\bar{\gamma}_{2k}}}}{\bar{\gamma}_{1k}\bar{\gamma}_{2k}}d\gamma_{1k}d\gamma_{2k}. \quad \text{(B.2)}$$

Applying $\gamma_{1k} = r^2\cos^2\phi$, $\gamma_{2k} = r^2\sin^2\phi$, and the definition of the Gamma function in (B.2) yields

$$\mathcal{E}_{\gamma_{1k}\gamma_{2k}}\left\{\Omega_k^{ij}(s)\right\} = \sum_{\substack{u_1=0\\ k\neq 1}}^{1}\cdots\sum_{\substack{u_N=0\\ k\neq N}}^{1}\frac{(-1)^{\sum_{i=1,i\neq k}^{N} u_i}2\Gamma(i+j+2)}{\bar{\gamma}_{1k}\bar{\gamma}_{2k}}\left(\mathrm{I}_k+\mathrm{II}_k+\mathrm{III}_k\right), \quad \text{(B.3)}$$

where

$$\mathrm{I}_k + \mathrm{II}_k + \mathrm{III}_k = \int_0^{\pi/2} \frac{\left(\sin^2\phi\right)^{2i+j+\frac{1}{2}}\left(\cos^2\phi\right)^{2j+i+\frac{1}{2}}}{\left(s\cos^2\phi\sin^2\phi + \frac{\cos^2\phi}{\bar{\gamma}_t} + \frac{\sin^2\phi}{\bar{\gamma}_{2k}}\right)^{i+j+2}} d\phi, \tag{B.4}$$

with $\bar{\gamma}_t \triangleq \frac{1}{\bar{\gamma}_{2k}} + \sum_{i=1, i\neq k}^{N} \frac{u_i}{\bar{\gamma}_{2i}}$. Next, we spit the integral in (B.4) into the three parts I_k, II_k, and III_k corresponding to the three integration intervals $[0, \epsilon)$, $[\epsilon, \pi/2 - \epsilon)$, and $[\pi/2 - \epsilon, \pi/2]$, respectively. For $\epsilon \to 0$ we can show that

$$\mathrm{I}_k = \frac{\Gamma(1-i)\Gamma(2i+j+2)\bar{\gamma}_t^{1-i}}{2(2i+j+1)\Gamma(i+j+2)s^{2i+j+1}} + o\left(\bar{\gamma}_t^{-(i-1)^+}\right) \tag{B.5}$$

$$\mathrm{III}_k = \frac{\Gamma(1-j)\Gamma(2j+i+2)\bar{\gamma}_{2k}^{1-j}}{2(2j+i+1)\Gamma(i+j+2)s^{2j+i+1}} + o\left(\bar{\gamma}_{2k}^{-(j-1)^+}\right). \tag{B.6}$$

Furthermore, for $\bar{\gamma}_{1k}, \bar{\gamma}_{2k} \to \infty$, II_k can be neglected due to its independence of $\bar{\gamma}_{1k}$ and $\bar{\gamma}_{2k}$. $\Phi^{PS}_{\Delta_{k_s}}(s)$ in (2.15) can be obtained by evaluating $\mathcal{E}_{\gamma_{1k}\gamma_{2k}}\left\{\Omega_k^{ij}(s)\right\}$ for the four different cases $(i = 0, j = 0)$, $(i = 0, j \neq 0)$, $(i \neq 0, j = 0)$, and $(i \neq 0, j \neq 0)$ based on (B.3), (B.5), and (B.6), and applying this result in (A.1) and (A.4), cf. Appendix A.

Appendix C

Some research works that are not directly related to this dissertation but have been published/submitted/under preparation during my time as a Ph.D. student at UBC are as follows:

- I. Ahmed, R. Schober, and R. K. Mallik, "Asymptotic Performance of L_p–Norm MIMO Detection," in *Proc. of IEEE VTC*, September 2010, Ottawa, Canada.
- I. Ahmed, A. Nasri, R. Schober, and R. K. Mallik, "Asymptotic Performance of Generalized Selection Combining in Generic Noise and Fading," *IEEE Trans. on Commun.*, vol. 60, pp. 916-922, May 2012.
- I. Ahmed, A. Ikhlef, D. W. K. Ng, and R. Schober, "Optimal Resource Allocation for Energy Harvesting Two-way Relay Systems with Channel Uncertainty," in *Proc. of IEEE GlobalSIP*, December 2013, Austin, Texas, USA.
- I. Ahmed, A. Ikhlef, D. W. K. Ng, and R. Schober, "Power Allocation for a Hybrid Energy Harvesting Relay System with Imperfect Channel and Energy State Information," in *Proc. of IEEE WCNC*, 2014, Istanbul, Turkey.
- I. Ahmed, D. W. K. Ng, A. Ikhlef, R. Schober, V. Wong, and L. Lampe, "Resource Allocation and Wireless Energy Transfer for a Two-Way Relay System with Channel and Energy State Uncertainty," *to be submitted.*
- I. Ahmed, A. Nezampour, R. Schober, and R. K. Mallik, "Asymptotic Performance Analysis of L_p–Norm MIMO Detection," *to be submitted.*

- I. Ahmed, D. W. K. Ng, R. Schober, and L. Lampe, "Joint Relay Selection and Power Allocation for Energy Harvesting Relay System with Wireless Energy Transfer," *under preparation.*